Henrique Miguel Aljustrel da Costa

Licenciatura em Engenharia Química e Bioquímica

Sensing humidity with multicomponent hybrid gel films and characterization of an optimized gas delivery system

Dissertação para obtenção do Grau de Mestre em
Engenharia Química e Bioquímica

Orientadora: Susana Palma, Post Doctoral Researcher,
FCT-NOVA
Co-orientadora: A. Cecília Roque, Associate Professor,
FCT-NOVA

Júri:

Presidente: Prof. Doutor Mário F. J. Eusébio
Arguente: Doutor Rui P. P. L. Ribeiro
Vogal: Doutora Susana I. C. J. Palma

FACULDADE DE
CIÊNCIAS E TECNOLOGIA
UNIVERSIDADE NOVA DE LISBOA

Setembro 2018

Henrique Miguel Aljustrel da Costa

Licenciatura em Engenharia Química e Bioquímica

Sensing humidity with multicomponent hybrid gel films and characterization of an optimized gas delivery system

Dissertação para obtenção do Grau de Mestre em
Engenharia Química e Bioquímica

FACULDADE DE
CIÊNCIAS E TECNOLOGIA
UNIVERSIDADE NOVA DE LISBOA

Sensing humidity with multicomponent hybrid gel films and characterization of an optimized gas delivery system

Acknowledgments

First and foremost, I would like to thank my co-advisor professor Ana Cecilia Roque for giving me the opportunity to enter her research group and for all the valuable help, support and optimistic disposition with which I was always met with. Much appreciation also goes to doctor Susana Palma, I feel very much blessed for having you as my advisor; all the great help, feedback and work developed, much like a team, helped turning everything into a much more positive experience. Claudia Alves, a fundamental member of this team, thank you for all the much-needed help on a big portion of my research and for the awesome team work.

Next, I would like to thank my sister, not only for helping me keep my sanity on the weekends but, of course, for all the years of unswerving support, given throughout each and every obstacle. I must also thank my mother, for always caring that I maintained my feet on the ground & supporting me in everything and to my father for all the useful tips and much needed material and, of course, for the support and interest shown.

Special thanks go to the one and only, Beatriz Santos, who has been a fundamental pillar throughout this important period, from beginning to end, and to whom I always resorted to in the moments of most mental struggle.

I am grateful as well for my pets, Balu for helping me grow in a way I did not expect and for becoming a very dear friend, Tobias who is an amazing little dog, always ready to show some love when needed, and of course, my cherished cat, Peri, who, though I am not the perfect owner, is the most perfect cat.

Finally, I must thank all the remaining friends, family, team members and professors/researchers who helped throughout. Also, Caçador and João, for the company & useful tools and help in handling them, and, of course, my swimming teacher, Bruno, and colleague & friend, Filipe, who indirectly helped and still do, physically and mentally, by believing in me and proving I am capable of the inconceivable act of swimming.

Abstract

An electronic-nose (e-nose) is a device that mimics the biological olfactory system[1,2], being used to sense gaseous samples and having applications in the medical and quality control fields.

The sensitivity of an e-nose and the interference of humidity on gas sensing are fundamental factors defining its performance. This work addresses those aspects on an e-nose that is under development at the Biomolecular Engineering Lab with the final goal of bacterial infection diagnosis.

First, a system for generating fixed relative humidity values was developed and an evaluation of humidity effect on the e-nose's sensitive materials (hybrid gel films) was performed. Then, the current concentrations of volatile organic compounds (VOCs) being sampled to an in-house built e-nose were estimated and a VOC delivery system to create a wide range of known VOC concentrations was designed.

Supersaturated inorganic salt solutions were used for generating fixed relative humidity values at room temperature. The response and morphological features of two sets of hybrid gel films differing in the ionic liquid (IL), 1-Ethyl-3-methylimidazolium dicyanamide or 1-Ethyl-3-methylimidazolium chloride, were evaluated. The response of three VOCs was further analysed under three relative humidity environments. The hybrid gel films display distinct responses towards humidity, dependent on the different ILs' properties. Distinct behaviours also occur when combining VOCs with humidity.

The evaporation rates of eight VOCs were measured during a VOC sampling procedure to the e-nose and the gas-phase composition of the sampling stream calculated. It was found that the VOC concentrations being currently sensed by hybrid gels in the in-house built e-nose are between $10 - 40$ *% (v/v)*. For a future dilution of the VOCs delivered to the e-nose, a controllable VOC delivery system was designed to generate VOC concentrations between $10^0 - 10^6$ ppm, for performing a future characterization of the e-nose sensitivity and limits of detection.

Keywords: volatile organic compounds; relative humidity; sensitivity; drift effect; electronic-nose; ionic liquid.

x

Resumo

Um nariz electrónico (e-nose) é um dispositivo que mimetiza o sistema olfactivo biológico[1,2], sendo usado para detectar amostras gasosas, com aplicações nas áreas médica e de controlo de qualidade. A sensibilidade de um e-nose e a interferência da humidade na detecção de gases são factores fundamentais que definem o seu desempenho. Este trabalho aborda esses aspectos num e-nose sob desenvolvimento no laboratório de engenharia biomolecular com o objectivo de diagnosticar infecções bacterianas.

Primeiro, foi desenvolvido um sistema para gerar valores fixos de humidade relativa e o efeito da humidade em materiais sensíveis (filmes de géis híbridos) integrados no e-nose foi avaliado. Posteriormente, as concentrações actuais de compostos orgânicos voláteis (VOCs) que são alimentadas ao e-nose foram estimadas e um sistema de alimentação foi desenhado para criar uma maior gama de concentrações de VOCs conhecidas.

Soluções supersaturadas de sais inorgânicos foram usadas para gerar valores fixos de humidade relativa à temperatura ambiente. A resposta e características morfológicas de dois conjuntos de géis híbridos, diferindo no líquido iónico (IL), dicianamida 1-Etil-3-metilimidazólio ou cloreto de 1-Etil-3-metillimidazólo, foram avaliadas. A resposta a três VOCs foi ainda analisada sob três humidades relativas. Os filmes de géis híbridos demonstram respostas distintas face à humidade, sendo dependente das diferentes propriedades dos ILs. Respostas diferentes também ocorrem quando se combinam VOCs com humidade.

A taxa de evaporação de oito VOCs foi medida durante um procedimento de alimentação de VOCs ao e-nose e a composição da fase gasosa da corrente de alimentação foi calculada. Descobriu-se que as concentrações de VOCs actualmente detectadas pelos géis híbridos no e-nose estão entre 10 – 40 % (v/v). Para uma futura diluição dos VOCs alimentados ao e-nose, um sistema de alimentação controlável foi desenhado para gerar concentrações entre $10^0 – 10^6$ ppm, para executar uma futura caracterização da sensibilidade e limites de detecção do e-nose.

Termos-chave: compostos orgânicos voláteis; humidade relativa; sensibilidade; efeito de desvio; nariz electrónico; líquido iónico.

Table of Contents

Index of Figures

Index of Tables

List of Abbreviations

[BMIM][Cl]: 1-Ethyl-3-methylimidazolium chloride

[BMIM][DCA]: 1-Ethyl-3-methylimidazolium dicyanamide

5CB: 4- Cyano- 4' – pentylbiphenyl

ANN: Artificial neural network

CNT: Carbon nanotubes

CNR: Carbon nanorods

e-nose: Electronic nose

FID: Flame ionization detector

GC-FID: Gas chromatography coupled with flame ionization detector

GC-MS: Gas chromatography coupled with mass spectrometry

IL: Ionic liquid

LDR: light dependent resistor

LOD: Limit of detection

MS: Mass spectrometry

MFC: Mass flow controller

MOS: Metal oxide semiconductors

MEMS: Microelectromechanical systems

N/A: Non-applicable

NPT: Normal pressure and temperature

PLS: Partial least-squares

PTFE: Polytetrafluoroethylene

POM: Polarized optical microscopy

PCA: Principal component analysis

PVA/MWCNT: Poly (vinyl acetate)/multi-wall carbon nanotubes

PVA/PLA: Poly (vinyl acetate)/poly (lactic) acid

vQRS: Quantum resistive vapour sensors

QCM: Quartz crystal microbalance

RH: Relative humidity

SPME: Solid phase micro-extraction

SAW: Surface acoustic-wave

VOCs: Volatile organic compounds

1. Introduction

1.1. Electronic Noses

The human olfactory system can recognize up to ten thousand distinct odours[2]. This occurs when odorant molecules, transported through the aqueous mucus layer in soluble odorant binding proteins are led to interact with olfactory receptor proteins in the epithelium of the nasal cavity[1,2], resulting in the generation of a nervous signal which, through further processing in the brain's olfactory cortex and subsequent storage of the information perceived in the subconscious memory, results in a learning process, permitting the recognition of simple and complex odours[3], i.e. a single odorant molecule or mixtures of them, respectively[1,2].

Electronic noses (e-noses), have been developed following the principles of odour differentiation of the biological olfactory system[2,4], and are defined by Gardner & Barlett (1994) as "*an instrument, which comprises an array of electronic chemical sensors with partial specificity and an appropriate pattern-recognition system, capable of recognising simple or complex odours*"[1].

Such definition is equally valid for devices which detect individual odorants or mixtures thereof, as long as they are constituted by more than one sensor and able to detect more than one odour[1,4].

The odorants i.e. analytes, are volatile organic compounds (VOCs) - organic chemical compounds with a high vapour pressure and, thus, a low boiling point at normal pressure and temperature conditions[5], thus easily evaporating[6].

As schematized in Figure 1.1, an e-nose is composed by an odorant delivery system that carries the gaseous sample (e.g., the headspace of a bacterial culture or of a chemical solution) into contact with an array of gas sensors, a chamber where these sensors are held -where a chemical response is triggered by sorption of the odorant molecules - a proper system which conditions and converts the sensors' responses into digital signals, a signal pre-processing and pattern recognition module, which allows for the odour identification[2,4,7].
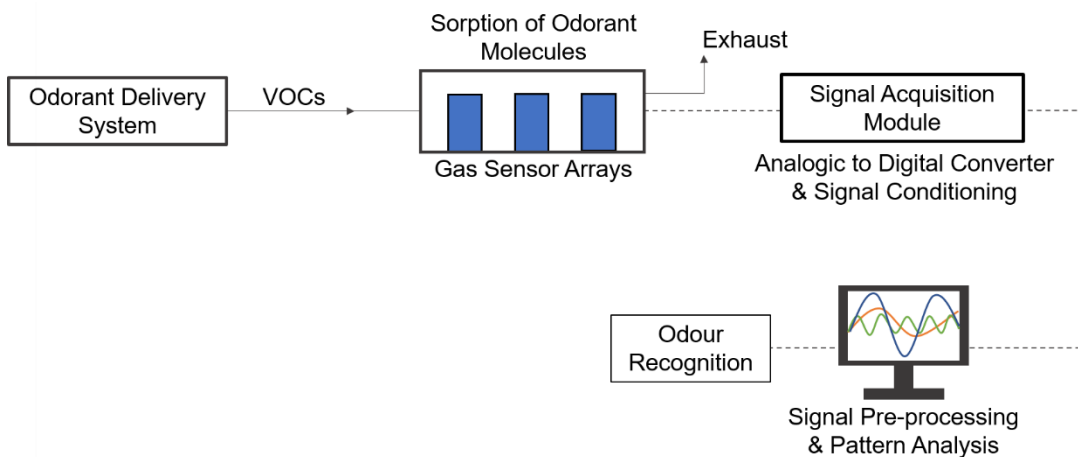
Figure 1.1- General arrangement of an e-nose measuring system[1,4,7].

1

The signals generated due to exposure to the gas analytes may be represented by several physical properties (e.g. conductance, absorbance), depending on the type of sensor and respective triggered response[2].

When a gas sensor is subject to a given reference gas its response is fixed on a steady value, representing the sensor's stable condition, i.e. baseline. As represented in Figure 1.2 for a sample flow system[2], the repetitive cycles of exposure to the sample analyte and recovery (purging of the sensors with the reference gas) creates a pattern response[8], which through pre-processing and analysis for patterns recognition, contributes for the odour identification.[2,9]
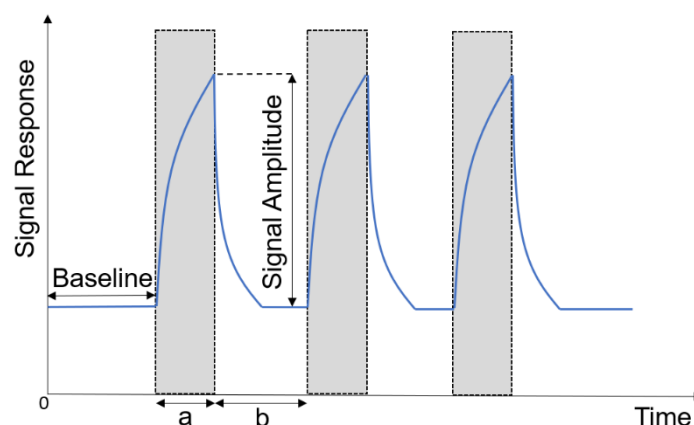
Figure 1.2 - Example of pattern response generated by a gas sensor after exposure to a volatile; (a) exposure to gaseous sample highlighted in grey; (b) recovery of the initial signal[8].

The signal pre-processing stage acts on the reduction of noise and unnecessary or detrimental data (e.g. drifts in the response) and, on the other hand, extracts the relevant information from the sensors' signals[9]. For these purposes, a few techniques are implemented, namely baseline manipulation, feature extraction (e.g. amplitude, derivatives) be it separately, or analysed as a whole (i.e. transient analysis) and normalization of the response, thus aiding in visualization[2,9].

The final stage for odour identification is the pattern recognition step[2]. This comprises the application of a series of algorithms, be it principal component analysis (PCA), partial-least squares (PLS), or the more advanced artificial neural networks (ANN), which are applied on the pre-processed signal, thus linking pattern response fingerprint to the target odour[2,9].

E-noses have great potential in many fields of application[2,7], such as in agriculture[10], food and beverage quality assurance[11,12], environmental control[13], military, for the detection of landmines[14], medical diagnostics and clinical monitoring[15,16].

The medical diagnostics area is particularly interesting as there is the need for the development of non-invasive and fast disease infection diagnosis tools[4,15]. With the current employed methodology, it takes about 24 to 48 hours to properly identify the bacterial strain responsible for a given condition[16], which delays the application of efficient treatment procedures[6] and contributes to the spread of antibiotic resistant bacterial strains.

It is known that different bacteria produce a set of distinct VOCs resulting from their metabolism[15], which can potentially be used as early disease biomarkers both *in vitro* and *in vivo* conditions with the e-nose systems[4], ideally at the sub-ppm concentration[17], through the identification of specific fingerprint pattern responses. Thus far, however, no developed technology has been launched in the market[6,7].

Classification of bacterial strains, through their VOC biomarkers, has been previously achieved. An array of electroconductive polymer chemoresistors allowed for the correct identification of twelve different bacteria[18]. Other sensor arrays – as metal-oxide semiconductors – proved similar potential for discriminating between different groups of bacteria[19,20], through headspace analysis.

1.2. Types of gas sensors in e-noses

The gas sensors that thus far have been developed for industry, or that are currently under research, include metal oxide semiconductors (MOS)[21,22], organic conducting polymers (CP)[23], quartz crystal microbalance (QCM)[24], surface acoustic wave (SAW)[25,26], among others.

MOS contain doped semi-conducting metal oxides, which sense VOCs through a change in the electrical resistance of the material upon exposure[4,7]. CP usually functions under resistance change as well, but the sensitive material is a modified conducting polymer[4,7]. As for QCM and SAW, both responses are generated by a mass change of the sensitive material (organic or inorganic film layers), translated as a frequency shift[4].

The MOS are the gas sensors most widely established and applicable for use in e-nose sensing arrays[4,7]. The CP however, are among the sensing materials most sensitive to VOCs, bringing a range of advantages relative to the MOS, namely on low-cost manufacture[7] and higher reproducibility[27].

MOS sensors consist of doped metal oxides (e.g. SnO_2, TiO_2 and ZnO)[2,21,28], in which the adsorption of the gas molecules triggers a change in conductance, prompted by reaction with oxygen present in the sensor's sensing layer, resulting in the generated signal[2,29]; depending on whether the sensor is an *n-* or *p-type*, the conductance will either increase or decrease upon contact of reactive species[2]. The key disadvantage of these kind of sensors is their high operating temperature requirements, i.e. from about 200 to 500 ºC[2,4,7], which demands a rather high power consumption, however, this aspect renders them rather insensitive to changes in ambient humidity and temperature[2,4,7].

CP sensors form continuous chemical bonding, resulting in one unpaired electron, i.e. a π-electron, per carbon atom; overlapping of the orbitals of such electrons results in electron delocalization, which allows for charge mobility[7], essential feature for the polymer's conducting properties and interactions with surrounding molecules. These sensors must operate at room temperature, while maintaining a high sensitivity. Nevertheless, their response signal is highly susceptible to changes in environmental conditions, i.e. temperature and humidity[2,7,30].

1.3. Factors that affect e-nose sensors' performance

The performance of an e-nose is directly related to that of its most important component, the gas sensors[4]. Several criteria contribute for achieving an optimal operation, namely a high sensitivity, with a detection capability at least similar, or below that of the human nose[4,9,27], semi-selectivity, conferring a good reversibility of the sensing mechanism[9], and long-term stability[4,7,9]. When the sensor arrays' stability is jeopardized by factors such as aging[2] or poisoning[9], due to exposure to the sensed chemical compounds, what is termed as a drift in the response might occur[2].

1.3.1. Drift effect on gas sensors

Different types of sensors may present distinct disadvantages or functional limitations, which may cause an unintentional variation in the sensor's response to the gas analytes, leading to measurement uncertainty.

Sensors' response variation can be due to several factors, namely, fluctuations in operating temperature[31,32], ambient relative humidity[33], possible reactions within the gas mixture[2], aging and poisoning[9], among others, being some of these factors more or less relevant, depending on the type of sensor.

These said variations may be interpreted as drift effects, i.e. a change in the sensor's response when exposed to the same analyte, due to the aforementioned disturbances[2,9]. Therefore, to properly characterize this behaviour, it is important to recognize the responsible variables[2,9].

Depending on the impact observed in the sensor's response, the drift can be categorized in two distinct types[2,9] (Figure 1.3). When a change in baseline occurs – an hysteresis effect[30] – the drift is termed additive[2,9] and the response is shifted by the same amount as the baseline variation, be it an increase or decrease[2]. If, instead, a change in sensitivity is verified – the amplitude of the response for different VOCs varying by distinct proportions – then the drift is multiplicative[2,9], as the response is changed by a given factor[2].
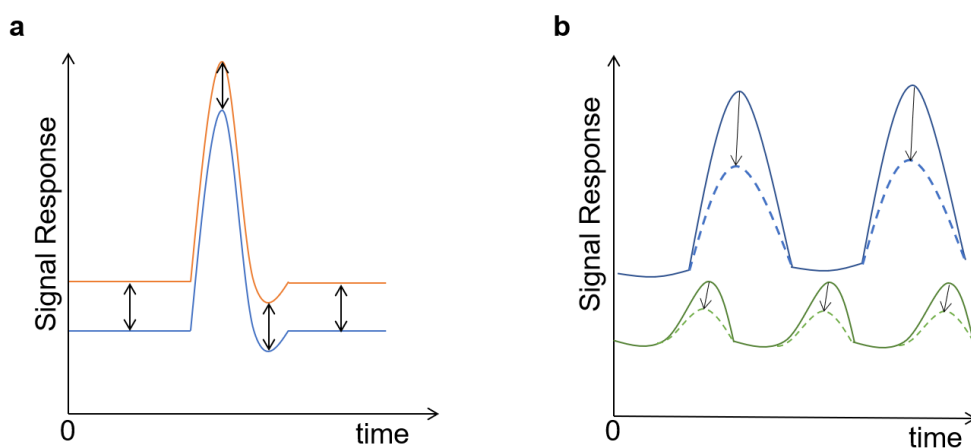
Figure 1.3 – Schematic representation of shifts on a sensor's response. a: Additive drift; b: Multiplicative drift.

For either circumstances, the amount of drift may be measured using an adequate reference gas, be it an analyte of known concentrations or an inert gas, like humid or dry air or nitrogen, depending on the source that originates it and on the final goal[2,9].

It is important to implement proper procedures to control and manipulate the external conditions causing drift, in order to characterize its impact on the sensors' responses[2,9].

Several studies have already been conducted to address these interferents. In the work of Ghanbarian et al.[34], the resistance of a nanocomposite based resistive gas sensor progressively grew with increasing relative humidity; inversely, in Hossein et al.[31], an opposite behaviour was observed in their chemoresistive gas sensor, with resistance decreasing for higher relative humidity.

Other groups evaluate as well how the response to VOCs varies with changing relative humidity conditions, as in the work of Chiang et al.[26], where the frequency shift of a SAW gas sensor altered under different proportions with humidity, for several ammonia and methane gas-mixture compositions tested. Mohammadreza et al.[32] equally analysed how the change in resistance of a chemoresistive gas sensor to methanol varied for a range of humidity conditions, depending on the exposed concentration.

1.3.2.   Sensitivity and limit of detection

A sensor's limit of detection (LOD) is defined as the output signal equal to the blank (baseline signal of the reference gas) plus three standard deviations, according to the equation

$$LOD = y_{blank} + 3S_{blank}$$ [35,36].   (eq. 1.1)

Several works in the context of quantitative analysis of volatiles and characterization of the respective LOD in e-noses have been conducted for distinct types of sensors[37–40]. Tables 1.1 – 1.2 summarize the most relevant reports regarding LOD and operating conditions of CP and MOS, respectively.

The key differing characteristic between the two categories of sensing materials resides in their operating temperature, being the MOS much more energetically demanding than the CP for the same LOD[4,7], when directly comparing the most relevant works (i.e. with LODs at the sub-ppm range)[40–43].

Generally, both sensor types can detect volatiles in the 0.01 to 0.5 ppm concentration range[40–43]. Previous works showed a LOD of 0.1 ppm for acetone, however the high sensitivity towards this VOC conferred a lower affinity for other VOCs[43]. An equal sensitivity towards a wider selection of VOCs recognized as lung cancer biomarkers as been shown, with LODs in the order of 0.4 ppm and the capability to discriminate between the several VOCs through PCA, evincing a potential application in the medical field[40].

Regarding the MOS sensor types, the same detail as mentioned above is found in part of the reviewed works: of sensitivity towards a strict range of VOCs. Herberger, S. et al. shown a LOD at the sub-ppm threshold for toluene and ethanol, yet for the remainder tested gases (carbon monoxide and ethyl acetate), this was limited to 1 to 2 ppm[44]. Another work analysed four distinct VOCs, however limited to

a tested concentration of 10 ppm[39].

Lower LODs are described in other works, showing the capability to detect benzene at 0.01 ppm[42]. This, however, addressed the detection of a single representative VOC, being focused on indoor air quality control.

Table 1.1- LOD analysis for Polymer-based gas sensors.

Sensor Type	Analyte	LOD (ppm)	Signal Type	Sensor Temperature	VOC Temperature	Reference
Polymer-Dispersed Liquid Crystal	Acetone	100[a]	Electrical Resistance	Ambient Temperature	Ambient Temperature	45
Carbon Black-Polymer Composites	Acetone	3.7	Electrical Resistance	Ambient Temperature	[-30,30] ºC	46
Polymer Coated Quartz Crystal	Water	88.5	Frequency Shift	50 ºC	Ambient Temperature	24
	Toluene	20.2				
	P-Xylene	3.9				
	1-Octanol	18.4				
	Ethanol	39.1				
	Acetone	77.6				
	Acetate acid	20				
Polymeric Chemiresistor	Trichloroethylene	1000[a]	Electrical Resistance	Ambient Temperature	Ambient Temperature	30
Metal-Polymer Composite Sensor	Hexane	280	Electrical Resistance	Ambient Temperature	[-55,100] ºC	47
	Tetrahydrofuran	200				
Polymer Coated-CNT	Ethanol	N/A	Electrical Resistance	[20,70] ºC	Ambient Temperature	48
Polymer Functionalized-CNT	Chloromethanes	4[a]	Electrical Resistance	Ambient Temperature	Ambient Temperature	49
IL-Conductive Polymer Composite	Dichloromethane	5000[a]	Frequency Shift	Ambient Temperature	Ambient Temperature	23
	Ethanol					
	Benzene					
IL-Based Polymer Electrolyte	Nytrogen Dioxide	0.006	Current Change	60 ºC	Ambient Temperature	50
IL-Patterned Porous Silicon	Ethanol	1.3	Optical Response	25 ºC	Ambient Temperature	51
PVA/MWCNT	Ethanol	9.7	Electrical Resistance	Ambient Temperature	Ambient Temperature	52
Polymer-Coated Microring Resonator	Acetone	0.1	Refractive Index Change	Ambient Temperature	Ambient Temperature	43
	Toluene	20[a]				
PVA/PLA Functionalized QNR-vQRS	Ethanol	0.4	Electrical Resistance	Ambient Temperature	Ambient Temperature	40
	Methanol	0.4				
	Acetone	0.4				
	Isopropanol	0.4				
	Toluene	0.4				
	Benzene	0.4				

| | Diethyl Ether | 0.4 | | | | |

a – Minimum tested concentration; b – Not included all VOCs tested due to the low sensitivity evinced.

Table 1.2 - LOD analysis for Metal Oxide based gas sensors.

Sensor Type	Analyte	LOD (ppm)	Signal Type	Sensor Temperature	VOC Temperature	Reference
CNT-SnO2	Methanol	100 [a]	Electrical Resistance	[250,300] ºC	Ambient Temperature	53
	Ethanol	100 [a]				
Metal Oxide decorated-CNT	Ethanol	10 [a]	Voltage	300 ºC	Ambient Temperature	22
TiO2 decorated-CNT	Acetone	N/A	Electrical Resistance	Ambient Temperature	Ambient Temperature	21
	Ammonia					
Pd-Doped MOS	Toluene	0.5	Electrical Resistance	[250,350] ºC	Ambient Temperature	44
	Ethyl Acetate	2				
	Ethanol	0.1 [b]				
Mesoporous Al2O3 MO-Loaded	Ethanol	10 [a]	Voltage Change	[150,450] ºC	Ambient Temperature	39
	Ethyl Acetate	10 [a]				
	Acetone	10 [a]				
	Toluene	10 [a]				
MOS-MEMS Gas Sensor	Benzene	0.01	Conductance	[200,450] ºC	Ambient Temperature	42
p-MOS Nanowire Array	Hexane	1 [a]	Electrical Resistance	[200,350] ºC	Ambient Temperature	17
In(III)-SnO2/g-CN	Toluene	1	Electrical Resistance	[90,200] ºC	Ambient Temperature	54
ZnO Thin Film	Acetone	50	Electrical Resistance	Ambient Temperature	Ambient Temperature	28
	Ethanol	50				
CoO/SnO2	Ethanol	10	Electrical Resistance	250 ºC	Ambient Temperature	55
	Acetone	100 [a]				

a – Minimum LOD tested; b – Not included other tested VOCs due to the low sensitivity it evinced.

1.4. Hybrid gas-sensing gels as new sensors for e—noses

A new class of gas sensors based on multicomponent hybrid gel films are currently under development at the Biomolecular Engineering Lab through the combination of biopolymers and liquid crystal (LC) droplets, self-assembled in the presence of ionic liquid (IL) and a trace amount of water[8]. As the ionic liquid is amphipathic, IL droplets form, in which the LC, being hydrophobic, remains encapsulated in a radial configuration[8], whose assembly is aided by the structural support of the hydrophobic tail of the IL (Figure 1.4).
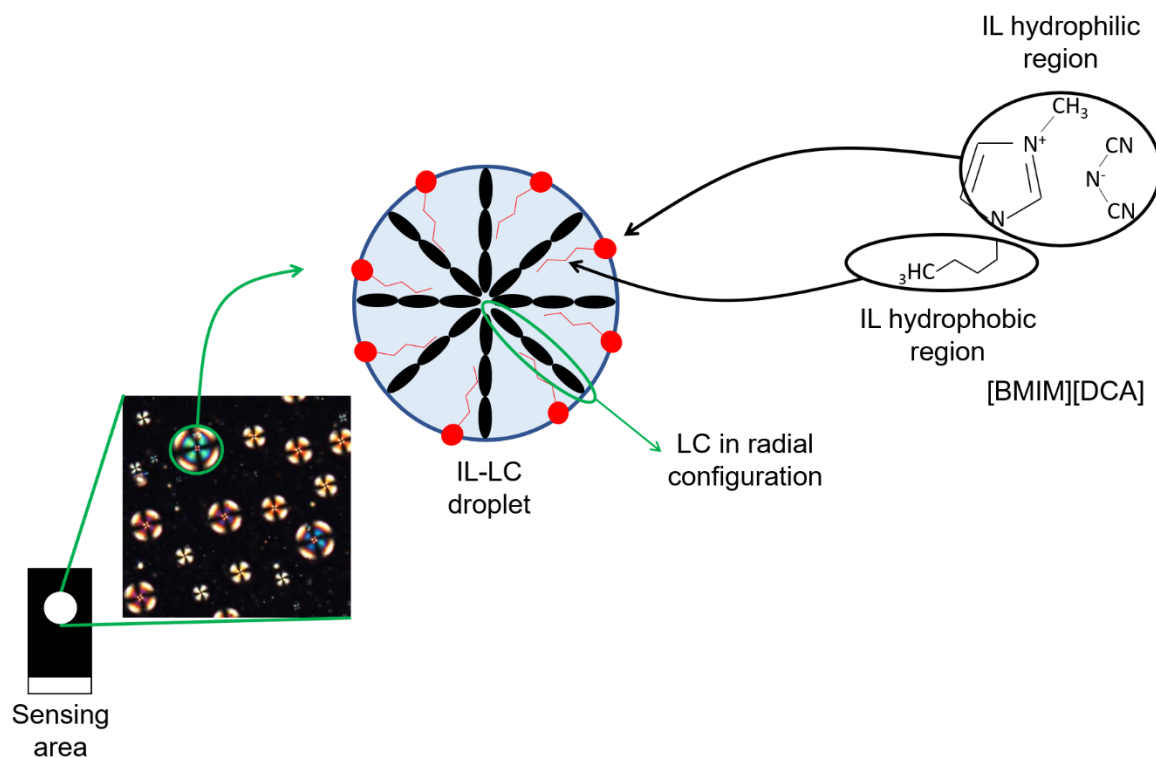
Figure 1.4 - Two-Dimensional model of IL-LC droplets present in the hybrid gel films' sensing area seen through polarized optical microscopy (POM). The hydrophobic region of the IL aids in the formation of the LC radial configuration, providing structural support[8].

Due to the electrical properties of the IL and the optical properties of the LC, the sensors can provide a combined optical and electrical response to VOCs, in the form of conductance and admittance, respectively[8].

By varying the composition of the hybrid gels, these can be combined for assembling an array on an e-nose device designed in-house. The sensing chamber houses a total of six hybrid gel films, which are placed between two crossed-polarizers. Light emitted by the LEDs passes through the films and reaches the light-dependent resistor (LDR), installed after the second polarizer (Figure 1.5). The resistance of the LDR is inversely proportional to the conductance and thus, to the light that reaches it. This resistance is further converted into voltage by a signal transduction system, thus giving the optical-response[56].

Due to the hybrid gels' inherent combinatorial nature, their affinity towards specific compounds may be tuned by individually changing the LC, IL or polymer matrix separately[8], achieving a set of distinct properties.
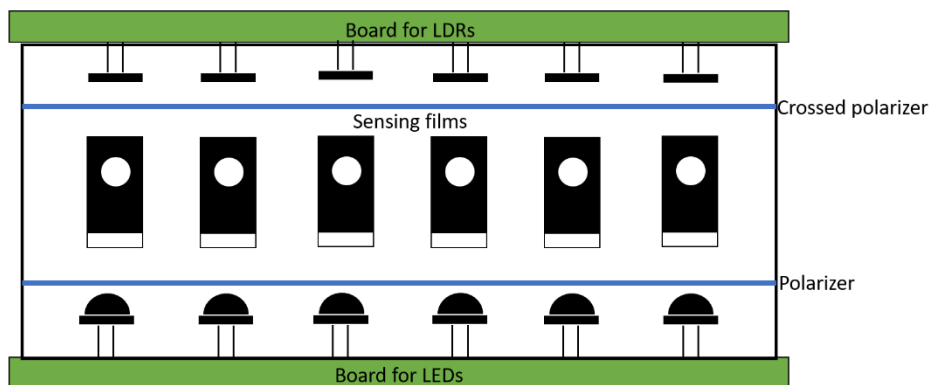
Figure 1.5- Sensing chamber housing the array of hybrid gel films[56].

As polarized light goes through the LC, its radial configuration causes a rotation of 90º of the plane of polarization, thus making it pass through the crossed polarizer (Figure 1.6a). In turn, the LDR exhibits a minimal resistance, resulting in a minimal signal voltage (Figure 1.6c). After exposure to VOCs, the radial configuration is disrupted, preventing the polarization of light by the LC, thus no light reaches the LDR (Figure 1.6b), which originates a maximum resistance and a maximum signal voltage (Figure 1.6c)[8,56]. The recovery period (i.e. purging of the hybrid gel films with ambient air), re-establishes the initial LC configuration. The repetitive exposure to VOCs and recovery generates a pattern-response (Figure 1.6c), unique for each VOC.
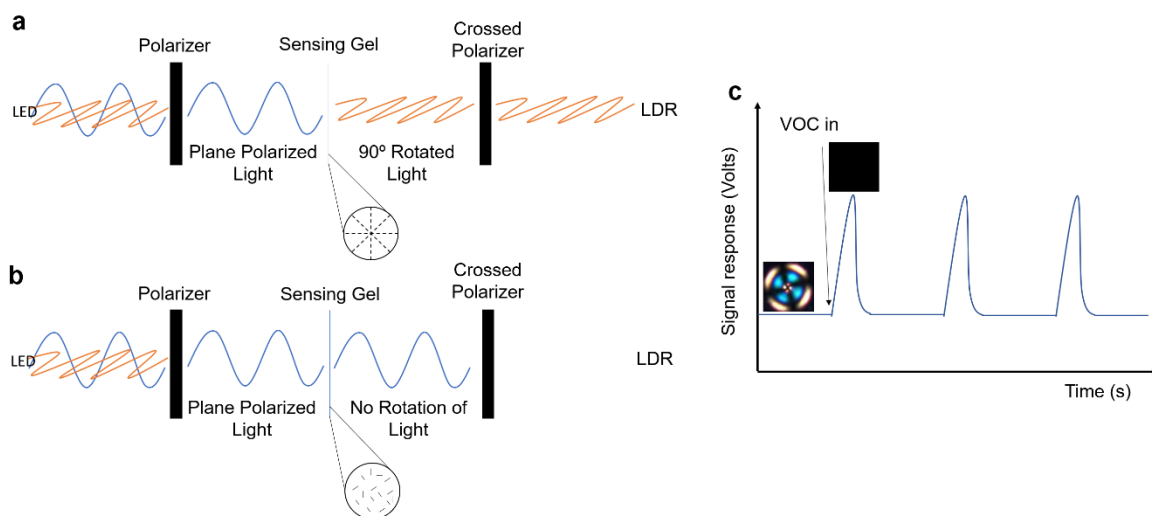
Figure 1.6- Mechanism of the sensing chamber for generating the optical-response; (a) polarized light reaches the LDR when no VOCs are interacting with the hybrid gel films; (b) no light reaches the LDR, as the hybrid gel films' interaction with VOCs prevents the light rotation; (c) optical response generated by the successive interchange between radial and isotropic configuration of the LC in the hybrid gel film[8,56].

Considering that the ILs are linked to the biopolymer matrix through non-covalent bonds, an increase in admittance of the gel is generated due to VOC exposure because VOCs intensify the ion mobility of the IL in the gelatine[8]. The admittance pattern response corresponds to the electric signal of the gel.

The optical and electrical pattern responses are further analysed through Principal Component Analysis (PCA), to differentiate gas samples.

The hybrid gels thus designed operate at room temperature and green solvents and reagents are used for its manufacture.

2. Aim of the work

In the field of detecting gaseous samples from biological media – particularly for early infectious diseases diagnosis – through artificial olfaction, two major challenges emerge – the presence of humidity[2,7] and the low concentrations of the gas analytes[7,57] in the gas mixture.

The hybrid gel thin film gas sensors that integrate the in-house built e-nose system developed in the Biomolecular Engineering Lab are composed by a polymeric material and ionic liquids, which due to being hygroscopic[58] and operating at room temperature[2,7,8], makes the sensors sensitive to the humidity present in the target VOC samples. This means that, for different environmental contexts, the same VOC may induce distinct responses of the hybrid gel thin films[31], possibly both in signal intensity and baseline. Thence, there exists the need to properly characterize this impact, so that the effect of humidity may be corrected or compensated for, thus obtaining the individual response of the VOCs (Left column of Fig. 2.1).

To accomplish this, a literature review was first performed to assess the different approaches towards compensating for the effect of humidity on the e-nose. A method for generating controlled levels of relative humidity through supersaturated binary salt solutions was developed and the respective response of the proprietary hybrid gel thin films characterized through the e-nose and polarized optical microscopy (POM). Two distinct approaches were studied for neutralizing its effect, using molecular sieves for drying the sampled VOCs or equilibrating the hybrid gel thin films towards a reference humidity, prior to VOC sampling.

Further, given the context in which the e-nose under development is to be applied, i.e. the rapid microbial detection for early disease diagnosis, it is especially required that it displays a strong sensitivity to the several VOCs, in the concentration's range of ppm to sub-ppm[17]; at present however, no thorough quantitative and sensitive analysis on the sensing gel's limit of detection (LOD) has been conducted, being only known, thus far, that it detects VOC concentrations under saturated conditions, a gap in knowledge meant to be mitigated, as planned in the right column of Figure 2.1.

For this second part of the work, a literature review was also performed for studying the techniques used for VOC quantification and sensitivity analysis. The current concentrations of eight VOCs being sampled to the e-nose were estimated and an apparatus for generating different dilutions was proposed, for which a study on the mass flow controllers constituting this equipment was performed.

The future aim of this work is to combine the controlled relative humidity and VOC quantification systems in one single apparatus, for performing a cross study on both parameters. It is also desired to optimize the system of humidity removal, thus applying it on assays for sensing VOCs from bacterial culture media, in which humidity is a known interferent.
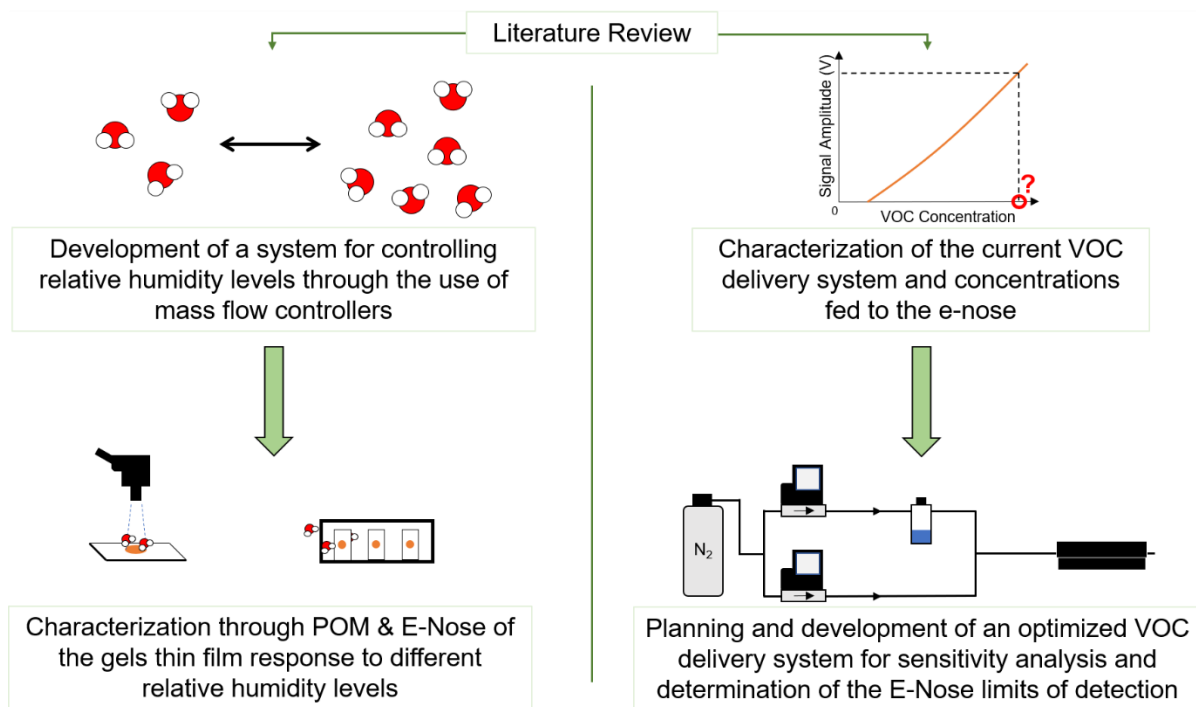
Figure 2.1- Schematic layout of the dissertation work plan.

3. Sensing humidity with hybrid gel thin films

3.1.   Introduction

Most gas sensors are affected by the relative humidity of the environment where they operate, which introduces errors in the measurements if no control or correction is made[2]. The interference of humidity on gas sensors can cause drifts in the response to VOCs or other gas analytes. These drifts can be additive – delocalizing the response without affecting the amplitude[59,60] – or multiplicative – changing the response amplitude[26,34,36]. Therefore, to develop a reliable gas sensor, it is important to characterise its response to relative humidity.

Several techniques can be employed to attain a controlled atmosphere with known and constant relative humidity, to which the sensing system should be exposed for characterisation purposes (Table 3.1). Among the several approaches, some show more potential than others, regarding simplicity and effectiveness.

Table 3.11- Methods for generating controlled humidity atmospheres.

Method of Relative Humidity Control	Simplicity	Effectiveness	Reference
Temperature change of liquid water containers	+	-	33
Evaporation of pre-determined volumes of distilled water	+	-	31
Supersaturated binary salt solutions	+	+	61–65
Mixture of dry and humid gas regulated through flowrate ratio with mass flow controllers or valves	-	+	32,36,59,66
Computer controlled gas dosing system	-	+	67
Humidity Generator	-	+	60

The use of supersaturated binary salt solutions in closed containers is a simple, economical and effective method, if the solutions are maintained under a fixed temperature. The distinctive feature of supersaturated salt solutions is the ability to release or adsorb large amounts of water while maintaining a constant salt concentration and, thus, equilibria conditions.[65] Since each salt solution provides a fixed equilibrium with a fixed water partial vapour pressure, a fixed relative humidity level is achieved for each of these salts[62,65]. Paknahad, M. et al. utilized these solutions to generate desired levels of humidity in a sealed atmosphere where the gas sensor is located, and where the analytes are to be sampled, thus providing controlled conditions to properly evaluate the impact of humidity on the sensor's response and recognition of the target analytes[63]. Xiao, X. et al. followed a similar approach, but with direct contact of the sensor with the headspace of the solutions[61].

Other methodologies result in either a less effective control or an increased complexity of the system. Wongchoosuk, C. et al., for instance, resorted to water containers at different temperatures to generate fixed humidity levels. This however, proved a limited control, as exposure to ambient air easily altered

the relative humidity in those containers[33], since no other factor other than temperature was used to compensate for the added water vapour.

Once the effect of humidity on the gas sensors is known and controlled, the drift needs to be mitigated or compensated for, a process which, depending on the established assumptions, may be based on a univariate or multivariate approach. The univariate approach considers that each individual sensor in the e-nose sensing array acts independently of one another, thus one drift correction method is applied separately for each sensor. If, otherwise, the sensors act as a group, one drift correction method is applied for the entire array data (multivariate approach)[2,9].

The methods employed for correcting the drift are several. While some involve eliminating the source of the drift by manipulating the conditions in which the analyte is sampled, others consist in developing mathematical models that account for that drift and correct it by incorporation into the database of the e-nose system, be it through linear or nonlinear functions, artificial neural networks (ANN), among others[2,4,9].

In the context of drift correction due to humidity fluctuations, several works have been developed, as summarized in Table 3.2.

Table 3.12- Drift correction approaches for compensating the effect of humidity.

Adopted approach	Nature of drift	Drift correction approach	Reference
Univariate	Multiplicative	Non-Linear Regression	33
		Multiple Linear Regression	36
		Artificial Neural Network	31,32,68
		Humidity Removal	63
		Humidity Reduction	34
		Partial Least Squares	30
	Additive/Multiplicative	Optimal Operation Conditions	60
Multivariate	Multiplicative	PCA + ANN	59
	Additive/Multiplicative	Optimal Operation Conditions	26
-	-	Humidity Reduction	69
		Humidity Removal	70,71

Wei, P. et al., developing electrochemical gas sensors for air quality control, tested four distinct sensors and developed three alternative mathematical models to compensate for the effect of humidity. For prior characterization of the sensors' responses in the presence of humidity, different gas analytes concentrations and different levels of generated humidity were combined. Then, for each sensor, the model that proved the best fitting was implemented[36]. Wongchoosuk, C. et al., working on the detection of armpit odour, also employed an univariate correction, through the characterization of the percentage change in resistance of several sensors for fixed levels of relative humidity and further fitting through non-linear functions for insertion into the data pre-processing module[33].

Other works, as the one led by Chang, J. E. et al. for the detection of lung cancer through the sampling of exhaled breath, opted by removing the humidity through the use of an oxide polymer-based porous membrane, which adsorbs most of the VOCs and lets through the majority of water vapour, further desorbing the volatiles by high temperature increase, and using nitrogen as a carrier gas, thus mitigating the need to compensate for humidity interference[71].

When the mathematical characterization of the drift through becomes impractical, more refined correcting techniques can be implemented, such as artificial neural networks. For example, Nenova, Z. et al.[68], implemented a system with learning and generalization capabilities of the acquired knowledge for application in uncharacterized situations[72].

In this work, supersaturated inorganic salt solutions were implemented in a bubbling system to generate fixed values of relative humidity in a carrier gas. With this arrangement, the effect of humidity on the optical response and morphology of hybrid gel films were evaluated. Two hybrid gel formulations differing only in the IL – either [BMIM][DCA] or [BMIM][Cl] – were studied.

Two approaches for compensating for the drift effect caused by humidity were investigated. Namely, the hybrid gel films' optical response to humidified nitrogen was fitted to linear and non-linear functions, and, in an alternative approach, molecular sieves were implemented, for attempting to remove the humidity from the carrier stream.

Finally, a combined study of the hybrid gel films' optical response to three different VOCs, sampled under three levels of relative humidity was further performed, assessing the drift effect on the optical responses to VOCs of different polarity.

3.2. Materials & Methods

3.2.1. Chemicals

The biopolymer gelatin (from bovine skin, gel strength ~225 Bloom, Type B) was purchased from Sigma-Aldrich (Portugal). The liquid crystal 4-cyano-4'-pentylbiphenyl (5CB, >98.0%) was purchased from TCI Europe (Belgium). The ionic liquids 1-butyl-3-methylimidazolium dicyanamide ([BMIM][DCA], >98.0%) and 1-butyl-3-methylimidazolium chloride ([BMIM][Cl], >98.0%) were purchased from IoLiTec (Germany). The organic solvent n-hexane (>95.0%) was purchased from Fisher Chemical (Portugal), acetone (>97.0%) was purchased from Sigma-Aldrich (Portugal), ethanol (96.0%) was purchased from Panreac AppliChem (Portugal). All solvents were used as purchased. Molecular sieves ($Na_{12}[(AlO_2)_{12}(SiO_2)_{12}] \cdot xH_2O$, 4Å, beads 8-12 mesh) were purchased from Sigma-Aldrich (Portugal). The anhydrous binary salts magnesium chloride (≥98.0%), potassium carbonate (99.9%) and sodium bromide (≥99.0%) were purchased from Sigma-Aldrich (Portugal), sodium chloride (>99.5%) was purchased from VWR Chemicals (Portugal).

3.2.2. Equipment

An in-house developed signal transducer device (e-nose) equipped with a 6-sensor sensing array[56] was used for reading the optical response of hybrid gel thin films to the supplied gas samples and to register the relative humidity at the e-nose outlet.

Tailor-made glass vials with an approximate volume of 27 cm^3, inlet and outlet channels with an external diameter of 6.45 mm (Fig. 3.1) and a Teflon lid were employed as bubbler flasks and as sample chamber. Silicon tubes of 4 mm internal diameter were used to interconnect elements of the experimental apparatus. A mass flow controller (MC-5SLPM-D/5M, 5IN, Alicat Scientific Inc.) was employed to generate known flows of nitrogen gas (UN 1066, Air Liquide, Portugal), which was used as carrier gas for the e-nose. Temperature and humidity sensors (HTU21D-F, Adafruit, New York, USA) were used for measuring generated relative humidity conditions. An Arduino UNO was used for reading of the temperature and humidity sensor at the e-nose inlet.

A thermal plate (VMS-C7, VWR Advanced) was used to produce the hybrid gels. An automatic applicator (TQC) was used to spread the hybrid gels as thin films.

Figure 3.11- Tailor-made glass vial used as sample chamber and bubbler used in the e-nose experiments.

3.2.3. Software

Tailor-made python script (python 3.6, alicat library 0.2.2) developed in the Biomolecular Eng. Lab (by Cláudia Alves) was custom-made to program the mass flow controller operation and synchronize it with the e-nose transducing system and the readings of the temperature and humidity sensors. A tailor-made python script (python 3.6) developed in the Biomolecular Eng. Lab (by Ana Pádua) was custom-made to extract the features from the e-nose optical signals.

3.2.4. Gas-sensing hybrid gel thin films

3.2.4.1. Preparation of hybrid gel thin films

Hybrid gels were produced as described elsewhere[8], through gelation of viscous solutions containing the four components of the hybrid gel – 150 µL of ionic liquid ([BMIM][DCA or [BMIM][Cl]), 10 of µL liquid crystal (5CB), 50 mg of biopolymer (gelatin from bovine skin), and 50 µL of milliQ water [8]. 10 µL of gel were deposited onto an untreated glass slide and spread using an automatic applicator with a quadrupole spacer (30 µm spacer) sliding at 50 mm/s. A negative control gel thin film was also prepared following a similar procedure but replacing ionic liquid with milliQ water. Three replicates of hybrid gels thin films made with [BMIM][DCA] (type D) and three made with [BMIM][Cl] (type C) were used in each e-nose experiment. When the negative control gels thin films (type CT) were used, two replicates of each gel type were inserted on the e-nose.

3.2.4.2. Characterization of hybrid gel thin films morphology by Polarizing Optical Microscopy (POM)

A polarized optical microscope (Olympus CX41), equipped with an Olympus SC30 camera was used. Two replicates of each hybrid gel type (D and C), or one of each when the negative control gel was used, were observed in transmission mode with crossed polarizers (at 90º), immediately before and one hour after the experiments. Zeiss ZENPro software, associated to the microscope, was used to produce panoramic images of the gel thin film sensing area before and after gas exposure in the e-nose. For that, the "Tiles" tool was employed: each panoramic image comprised of a total of 63 pictures of the distinct image fields that comprise the total sensing area of the hybrid gel, automatically taken and aligned. Prior to performing the tiles, key regions of the gel were individually focused. The superposition of the pictures was further corrected using the "Stitching" tool.

3.2.5. Hybrid gel thin films' responses to humidity

3.2.5.1. Preparation of supersaturated binary salt solutions

The mass of binary salt was weighted according to its solubility in water (Table 3.3) and dissolved in 10 mL of distilled water in a glass vial. For magnesium chloride and potassium carbonate, small amounts of distilled water and salt were incrementally added on the glass vial, due to the strong exothermic reaction upon mixture. An excess of 2 - 3 g of salt were further added for supersaturating the solutions. 10 mL of distilled water was used to generate the maximum relative humidity (Table 3.3). Afterwards, the vial was closed with the lid and inlet and outlet channels sealed with clamps, connected to silicon tubes and left to rest at room temperature for allowing the salt solutions to equilibrate. All procedures were performed in the hotte.

Table 3.13- List of binary inorganic salts corresponding generated relative humidity at ~20 ºC, when prepared as supersaturated solutions. For the maximum relative humidity, distilled water was used.

Salt	Theoretical Relative Humidity (%)	Solubility in water (g/10 mL)	Generated relative humidity (%) at e-nose outlet
Magnesium Chloride	33.07	5.4	25.00
Potassium Carbonate	43.16	11.2	36.00
Sodium Bromide	59.14	9.4	50.00
Sodium Chloride	75.47	3.6	65.00
Distilled Water	100.00	-	80.00

3.2.5.2. Controlled relative humidity delivery system

To generate controlled levels of relative humidity (RH) to be sampled to the e-nose, an experimental apparatus was prepared (Fig. 3.3a-b). One mass flow controller (MFC) was fed with nitrogen as a carrier gas (at 1.500 slpm). Three similar glass vials with a supersaturated salt solution at room temperature were installed in series. Distinct RH levels were generated in the carrier gas using a bubbling configuration with the distinct supersaturated salt solutions (Table 3.3). The nitrogen was bubbled through the first two salt solutions for saturating with the generated humidity, further passing by the third vial's headspace in which a temperature and humidity sensor was installed (Fig. 3.2) to measure the RH at the e-nose inlet. The RH at which the hybrid gel thin films will be exposed was measured by the temperature and humidity sensor at the e-nose outlet, inside an empty vial. The empty vial at the e-nose outlet was previously dried in the oven for removal of excess humidity, ensuring a precise reading.

Figure 3.12- Temperature & humidity sensor adapted to the sample chamber's lid.

3.2.5.3. Signal acquisition from hybrid gel thin films in distinct relative humidity conditions

Distinct sets of hybrid gel films (three type D, three type C) were placed on the e-nose and exposed to five exposure/recovery periods, under different RH levels (Table 3.3). The MFC was programmed to alternate between periods of:

- 120 seconds (at 1.500 slpm) – Exposure

- 20 seconds (at 0.000 slpm) – Pause
- 120 seconds (at 1.500 slpm) – Recovery

During the exposure period (120 s), the e-nose was exposed to the humidified nitrogen. During the recovery period (120 s), pure nitrogen purged the e-nose to ensure 0 % relative humidity. During the pause period (20 s), a pair of clamps were manually alternately opened and closed (Fig. 3.3c), permitting the exchange between exposure and recovery periods. Independent experiments were made for each generated humidity.
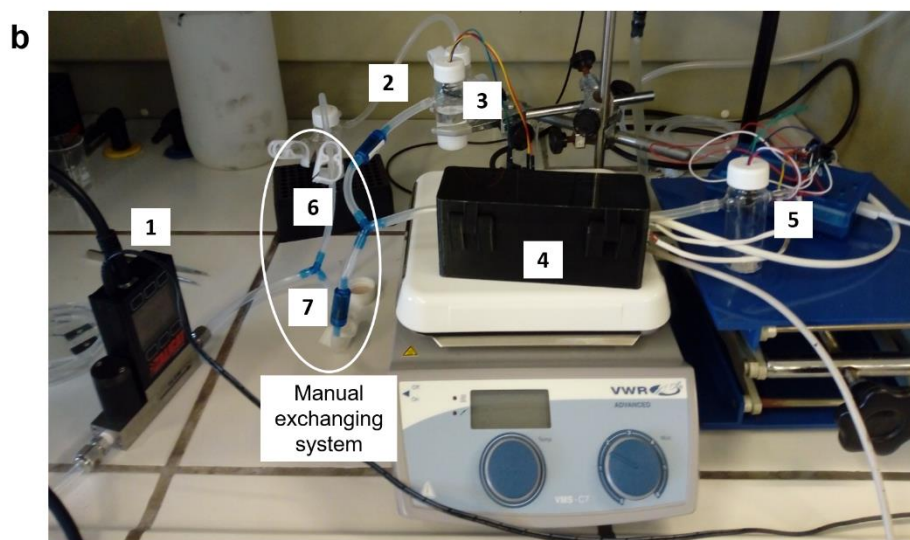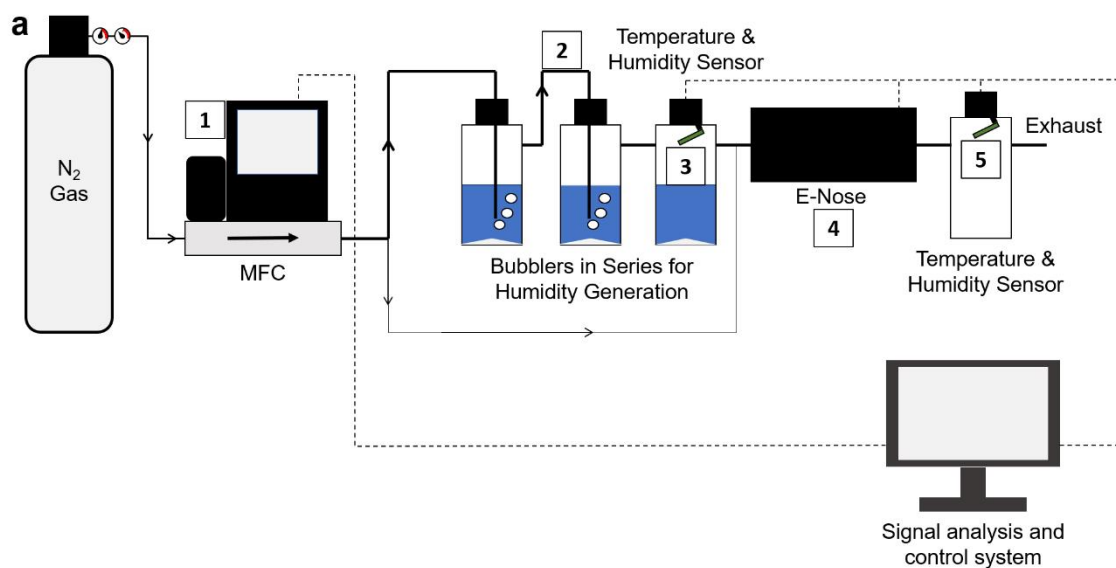
Figure 3.13- Experimental setup of the RH delivery system; (a) basic schematic, with exposure course is highlighted in bold; (b) and picture of the system; (c) manual system for alternating between exposure and recovery periods; (1) mass flow controller; (2) bubblers in series of supersaturated salt solutions; (3) first temperature & humidity sensor; (4) e-nose housing the array of hybrid gel thin films; (5) second temperature & humidity sensor; (6) clamp in exposure course; (7) clamp in recovery course.

3.2.5.4. Signal pre-processing and features extraction

The e-nose signal transduction system provided the voltage change (between 0 and 3 V), translating the optical signal of the hybrid gels. From the signals generated upon exposure and recovery from humidity, features of relative amplitude (eq. 3.1), absolute maxima, derivatives and onset (delay in the response) were extracted. Average values and standard deviation of the signals and features were calculated and considered for further analysis. The generated signals were smoothed by a factor of 50 prior to feature extraction. Python software was used for generating the signals and extracting the features.

$$Relative\ Amplitude = \frac{\left(V_{Exposure} - V_{Recovery}\right)(Volts)}{V_{Recovery}\ (Volts)}$$
(eq. 3.1)

where *V* corresponds to the optical signal voltage at the stable-state response in either the exposure or recovery periods. The optical signal obtained in recovery is deemed as the baseline for all circumstances.

3.2.6. Using molecular sieves for humidity removal from a carrier gas

To remove the humidity from a sampling gas stream, an experimental apparatus was assembled (Fig. 3.4), maintaining the main elements of the system previously used (Fig. 3.3).

Three glass vials with 10 mL of distilled water at room temperature were installed in series. The carrier gas (Nitrogen, at 1.500 slpm) was bubbled through the first two vials for saturation and sampled to the headspace of the third vial, to generate a relative humidity of ~80 %. A fixed-bed of molecular sieves was installed at the outlet of the third vial, to retain the humidity present in the carrier gas through size exclusion. A glass vial with a temperature & humidity sensor adapted, was connected to the outlet of the molecular sieves' bed, to measure the RH of the carrier gas after passing through the molecular sieves.

The molecular sieves were stored in the oven at ~80 ºC for several days, on a glass petri-dish, prior to be used and then placed inside a silicon tube (7 mm internal diameter; 14.5 cm length), previously purged with pure nitrogen gas for removal of humidity.
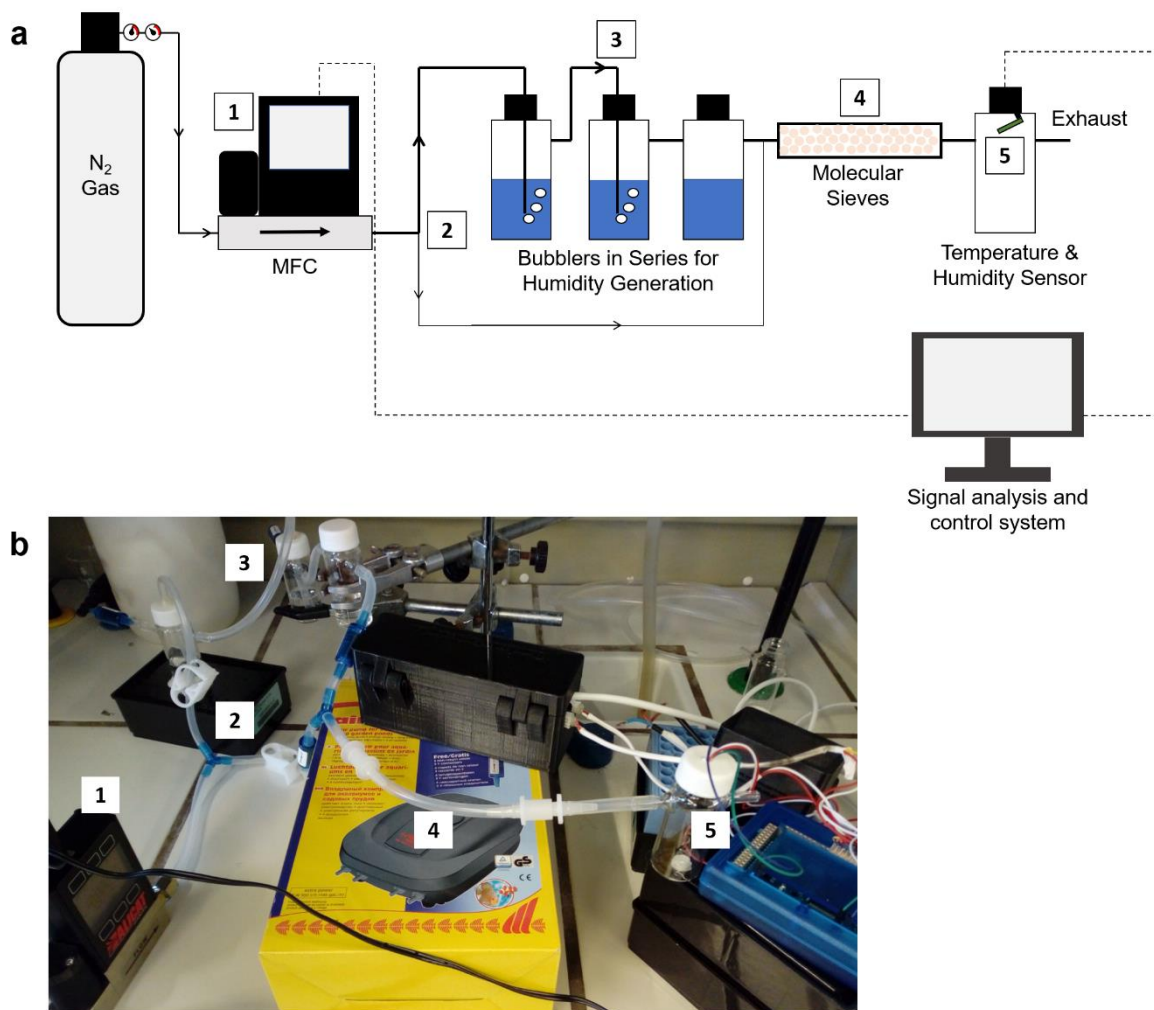
Figure 3.14- Experimental setup for humidity removal with molecular sieves; (a) basic schematic, with exposure course highlighted in bold; (b) and picture of the system; (1) mass flow controller; (2) clamps for manually alternating between exposure and recovery periods; (3) bubblers of distilled water in series; (4) tube for molecular sieves; (5) temperature and humidity sensor.

The MFC was programmed to alternate between periods of:

- 60 seconds (at 1.500 slpm) – Exposure
- 15 seconds (at 0.000 slpm) – Pause
- 60 seconds (at 1.500 slpm) – Recovery

During the exposure period, nitrogen was humidified and passed through the molecular sieves. During the recovery period, dry nitrogen passed through the molecular sieves. Both periods were manually alternated by switching the open clamp in the circuit during the 15 seconds pause period of the mass flow controller (Fig. 3.4b, no.2).

The above procedure was first performed without the addition of the molecular sieves, as represented in Fig. 3.4b, without control over the humidity of the saturated carrier gas. Afterwards, the molecular

sieves were inserted, and a similar procedure was performed. The humidity sensor at the outlet of the molecular sieves' fixed-bed measured the resulting RH.

3.2.7. Sensing VOCs under different relative humidity environments

To sense VOCs in the e-nose under different relative humidity environments, an experimental apparatus was prepared (Fig. 3.5), maintaining the main elements of the system previously used (Fig. 3.3). The mass flow controller was set to 1.500 slpm. A system with three vials in series of supersaturated solutions in a bubbler configuration was prepared to humidify the carrier gas (Nitrogen).

Distinct sets of hybrid gel films (three type D, three type C) were placed on the e-nose and exposed to 29 exposure/recovery periods of different VOCs under three RH levels each. The MFC was programmed to alternate between periods of:

- 5 seconds (at 1.500 slpm) – Exposure
- 5 seconds (at 0.000 slpm) – Pause
- 5 seconds (at 1.500 slpm) – Recovery

In the exposure period, the humid carrier gas was sampled to the headspace of a VOC solvent, thermostatized at 37 ºC, and fed to the e-nose. In the recovery period, humidified nitrogen purged the e-nose. Both periods were manually alternated by switching the open clamp in the circuit during the 5 seconds pause period of the mass flow controller (Fig. 3.5b, no.3).

The RH at the outlet of the e-nose was of 0, 65 and 80 %, using nitrogen, sodium chloride supersaturated salt solution and distilled water, respectively. Separate experiments were made for each humidity level. The tested VOCs were hexane (~20 % (v/v)), acetone (~15 % (v/v)) and ethanol (~13 % (v/v)), in that order, according to increasing polarity relative to water. The effect of each humidity level was tested for each VOC, giving a total of 9 experiments.

Prior to each experiment, the hybrid gels baseline signal was stabilized to the generated humidity by purging it with humidified nitrogen for 15 minutes. As the RH remained constant throughout the experiment, the only change in the e-nose signal occurred due to VOCs exposure and recovery.
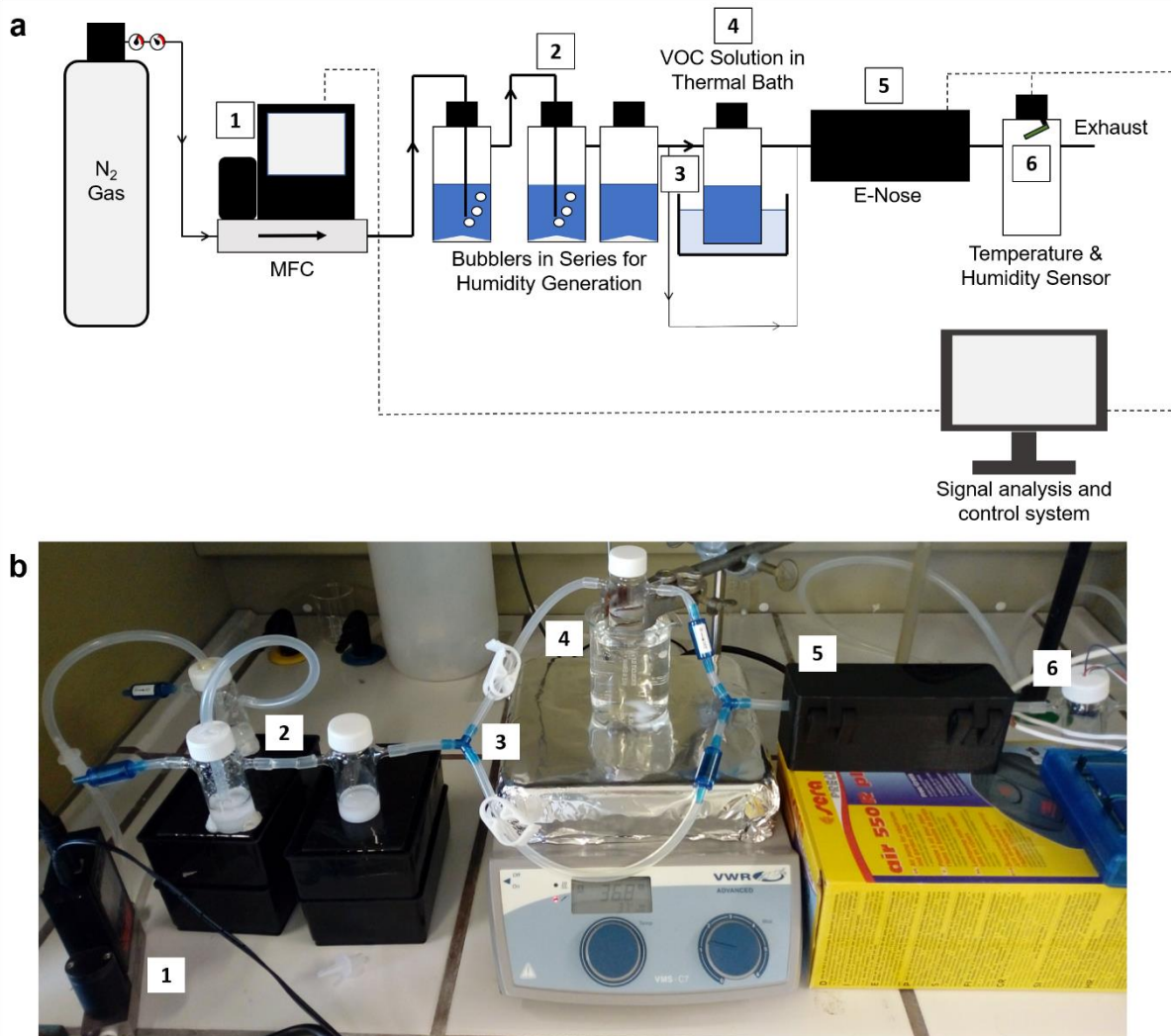
Figure 3.15- Experimental setup for sensing VOCs under different RH; (a) basic schematic, with exposure course highlighted in bold; (b) and picture of the system; (1) mass flow controller; (2) bubblers in series of supersaturated salt solutions; (3) clamps for manually switching between exposure & recovery periods; (4) VOC solution in thermostatized bath at 37 °C; (5) e-nose housing the array of hybrid thin films; (6) temperature & humidity sensor.

3.3. Results & Discussion

3.3.1. Development of a controlled relative humidity atmosphere inside the e-nose

Supersaturated binary salt solutions constitute simple chemical systems which provide a fixed relative humidity[62]. Due to the excess salt, the concentration of the solution remains constant when exposed to humidity sources or sinks[61,62], being temperature the only variable altering its equilibrium. Thus, when such a solution in kept in a closed chamber, under controlled temperature, a constant relative humidity is generated, specific of that salt and independent of the exterior conditions.

To expose hybrid gel sensing films to controlled values of relative humidity, the humidity generated in the chamber needs to be sampled into the e-nose, thus exposing the controlled humidity in the chamber to a carrier gas (nitrogen). The way the nitrogen is sampled to the salt solutions must be considered, as it can potentially dry the generated humidity[71]. Therefore, two sampling approaches were tested with sodium chloride supersaturated salt solutions: headspace sampling and bubbling (Fig. 3.6).

Using headspace sampling (Fig. 3.6a), constant values of relative humidity are registered in the initial recovery period, before nitrogen exposure. At the start of each exposure, an immediate decrease of ~30 % of the relative humidity at the headspace of the salt solution occurs. At the e-nose outlet, a slight increase of ~5 to 10 % is observed, quickly followed by a slower decrease, with a profile like that of the relative humidity on the salt solution. During the recovery period, there is a partial re-establishment of the salt solution's equilibrium conditions, while the e-nose outlet maintains the final humidity level of the exposure period. The nitrogen purges most of the equilibrated humidity in the three vials upon exposure, causing a significant reduction in the RH. When it reaches the e-nose outlet, a slight peak in the humidity occurs, however re-establishing to the initial value by the end of exposure. Herewith, the humidity level equilibrates at ~30 %.

When the bubbling method is used (Fig. 3.6b), regardless of exposure or recovery from carrier gas, a fixed relative humidity is maintained in the salt solution. The relative humidity at the e-nose increases continually, stabilizing in ~60 %, a value much closer to the RH in the salt solutions. When nitrogen is bubbled through two of the three salt solutions, its saturation with the equilibrated relative humidity is promoted[2,73], thus attaining a similar water vapour content as initially established in the solutions' headspace. This indicates that the humidity equilibrated in the vial is not perturbed when nitrogen is bubbled through the solution (Fig. 3.6b). The relative humidity in the e-nose is ~15 % lower than the generated by the supersaturated solution (Fig. 3.6b) due to condensation in the equipment tubing. Nonetheless, a stable relative humidity value is achieved by the end of the exposure period, as required to study the impact of humidity on the hybrid gel thin films response.

In the bubbling approach (Fig. 3.6b), the exposure and recovery periods were lengthened relative to the headspace sampling approach (Fig. 3.6a), achieving the optimum duration for stabilizing the RH at the e-nose outlet during exposure and for fully drying it during recovery.
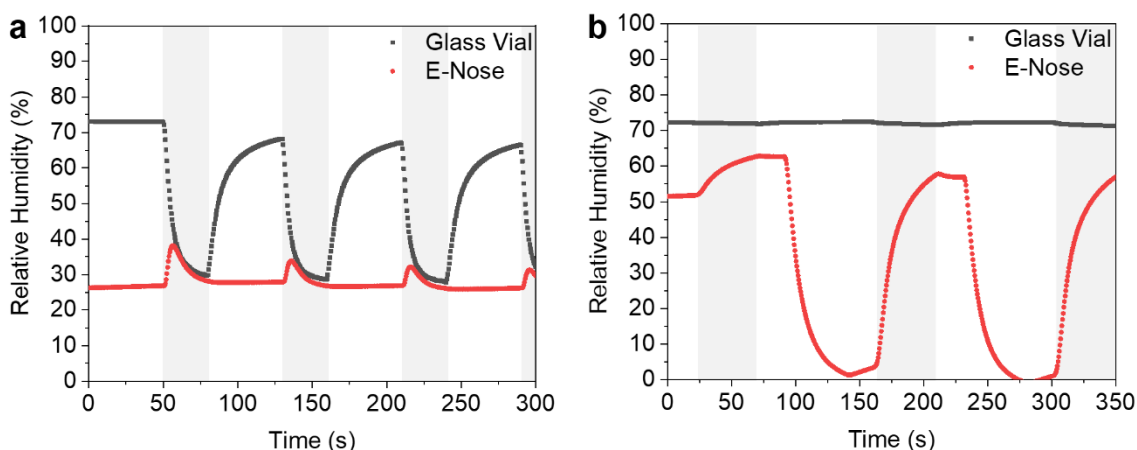
Figure 3.16- Relative humidity profile in the salt solution's headspace (grey) and e-nose outlet (red), during exposure and recovery from nitrogen. (**a**) exposure through headspace sampling of the salt solutions; in the recovery period, the system could re-equilibrate; (**b**) exposure through bubbling of the salt solutions; in the recovery period, the e-nose was purged with pure nitrogen. Exposure periods highlighted in light grey. Recovery periods highlighted in white.

The effect of relative humidity on the properties of gas sensors has been analysed before[26,33,34,63], in some circumstances however, dependent upon the ambient humidity[26,34], so that the evaluated range was limited to the days of the experiments, mostly when strict values were desired[34]. Inorganic salt solutions have been previously used in closed glass vessels[61], where the sensor is placed for direct contact (static sampling), in which case the exact desired humidity is obtained. When a control of the relative humidity with dynamic sampling is performed, the obtained values may differ from those generated[33], or be limited to a maximum value due to the flowrate ratio between VOC and humid carrier gas[59].

Depending on the chosen salt, several relative humidity equilibria can be generated, from near 0 to 100 %[62], independently of the external ambient conditions. With the current bubbling experimental setup, relative humidity levels of 25, 36, 50, 65 and 80 % were obtained in the e-nose. The effect of humidity in the hybrid gel thin films was then evaluated by sampling nitrogen humidified by bubbling into the e-nose.

3.3.2. Hybrid gel thin films' response to humidity & structural characterization

Evaluating the signal's response in the e-nose upon successive cycles of exposure to humidified nitrogen and recovery with dry nitrogen, hybrid gels containing [BMIM][DCA] (Fig. 3.7a-e), display an optical response directly proportional to the relative humidity, with a strong linear relationship (R^2 = 0.98) (Fig. 3.8a). For the lower relative humidity (Fig. 3.7a), a minimum signal amplitude is displayed, accompanied by an extended delay in the response – more than half the duration of the exposure cycle – and a lack of stabilization. As the relative humidity increases (Fig. 3.7b-e), the observed delay is mitigated, and a stable-state response quickly achieved. A similar cyclic waveform is observed for all relative humidity levels, with good repeatability throughout, a signal decrease upon exposure and increase upon recovery, always stabilizing in the maximum scale limit during recovery (Fig. 3.7a-e).

The maximum slopes of the optical signal at the start of each period – negative for exposure and positive for recovery – show that the signal's change rate increases in an exponential fashion as RH grows (Fig. 3.8b), more noticeable for the negative variation (R^2 = 0.996). This suggests that the interference of RH in the optical signal is quite relevant. Namely in the context of sampling highly humid VOC gas mixtures, as in breath analysis[57,71], the effect of humidity may potentially interfere with the optical response coming from the VOCs.

The repeatable waveform of the D type hybrid gel films optical response (Fig. 3.7a-e) is an indication that, upon successive cycles of exposure and recovery from humidity, the gel's matrix structure is essentially conserved, as suggested by the similarities between POM images of the gel's sensitive area before and after 5 cycles of exposure/recovery from 80 % RH, ending in exposure (Fig. 3.9e-f). Further, given the near inexistent standard deviation of the optical signal at the stable-state response during recovery (Fig. 3.7a-e), all gels present the same maximum signal (2.7 V) – which corresponds to a null optically active area, i.e. the gel's sensitive area is opaque black. Due to the amphipathic nature of the IL droplets, the near absence of water may prompt its disassembly, along with the radial configuration of LC – which is responsible by the bright optical response – transitioning to an isotropic state. This agrees, not only with the increase of the signal during recovery, but also with the gel's morphology after a recovery period (Fig. 3.9d), with only the smaller droplets in blue maintaining a radial configuration of the LC. A higher amount of water promotes a higher optically active area, as deduced from the progressively lower signal minima upon exposure with growing humidity and in accordance with the brighter gel´s sensitive area (Figure 3.9f).

Following this, the minimum relative humidity for which a response from VOCs can be detected should be 25 %, as below, the optical signal is saturated due to the darkness of the film in those conditions. The solution for compensating the sensitivity of type D gels to humidity may therefore, not lie in its removal from the system.
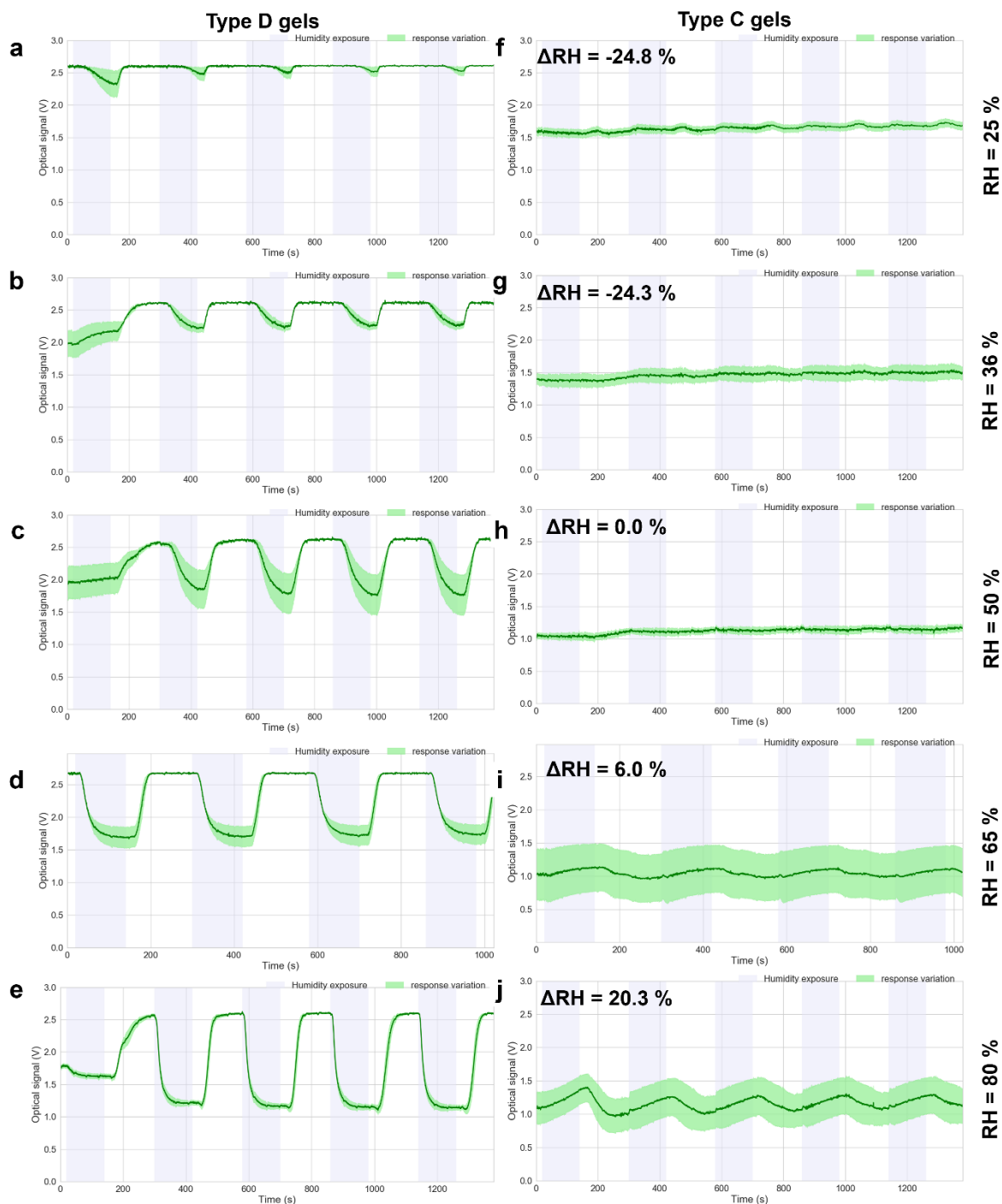
Figure 3.17- Optical signal response of the hybrid gel films containing [BMIM][DCA] IL (a-e) and [BMIM][Cl] IL (f-j), including the mean value (dark green) and the standard deviation (light green). At the rightmost is indicated the average relative humidity (%) sampled to the e-nose during exposure periods (highlighted in light blue). At the upper left corner of the C-type signals (f-j), is indicated the relative humidity gradient (Ambient – Generated). During recovery, the e-nose was purged with pure nitrogen. All obtained by averaging the signal of 2-3 replicates of each gel type. Relative humidity profiles available in Appendix I – Fig. A1.

The variation of [BMIM][Cl] hybrid gels response with humidity (Fig. 3.7f-j), is not linear. As the humidity decreases from its maximum value (Fig. 3.7j), a reduction in the response amplitude occurs, being virtually undetected at 50 % relative humidity (Fig. 3.15h). Further decreasing in humidity, a slight response is again discerned (Fig. 3.7f-g), however its amplitude is very low. A repeatable waveform is visible for the higher humidity (Fig. 3.7i-j), with signal increase upon exposure and decrease with recovery. For the lower range (Fig. 3.7f-h), such behaviour is not as discernible. Compared to the case of [BMIM][DCA], the response kinetics are much slower, with no effective stable-state response being reached and the signal never saturating in a maximum or minimum baseline (Fig. 3.7f-j).

Given the above features, it becomes impractical to consider a reference baseline of 0 % relative humidity. The results were evaluated as a function of the gradient (ΔRH) between the environmental relative humidity at the day of experiment and the sampled relative humidity (equation 3.2), assuming the hybrid gels are initially in equilibrium with the ambient conditions.

$$\Delta_{Relative\ Humidity}(\%) = Generated_{RH}(\%) - Ambient_{RH}(\%) \qquad (eq.\ 3.2\ )$$

where *RH* denotes relative humidity.

According to the above principle, the near absence of response at 50 % relative humidity (Fig. 3.7h) is justified by the null ΔRH. As ΔRH increases, the signal oscillation significantly increases (Fig. 3.7i-j), with the response amplitude having similar magnitude for both exposure and recovery periods suggesting that the recovery signal is dependent on the exposure. Regarding the negative ΔRH, during the first exposure, the optical signal remains undisturbed (Fig. 3.7f-g), as likely no further sorption of water is promoted. Following the first recovery, where at least some humidity is removed from the gel, a slight growth of the optical signal occurs in successive exposures.

A quadratic polynomial fit (R^2 = 0.99) of the optical signal's relative amplitude as a function of ΔRH is obtained (Fig. 3.8c) and the relative amplitudes are positive. Despite the suitable polynomial fit, the lack of signal stabilization and absence of similarity of baselines during recovery introduces uncertainty in the calculation of signal amplitudes, especially for the null and negative humidity gradients. Nonetheless, an insight on how the signal is affected by different ΔRH was obtained. Namely, the slow and low response of type C gels to humidity, having a change rate – positive for exposure and negative for recovery – one order of magnitude lower comparing to the type D hybrid gels (Fig. 3.8d), indicates that these gels are much less sensitive to abrupt humidity changes, potentially rendering them more adequate, for example, in breath analysis context, given relatively short exposure periods are conducted.

Compared to type D, the C type hybrid gels display a higher number of droplets, of smaller diameter and distributed in aggregates (Fig. 3.10a). Post experiment (Fig. 3.10b), a rearrangement of the droplets distribution in the gel occurs, yet, the initial total black (empty) area of the hybrid gel film is not filled completely, supporting the reduced effect humidity has on these gels. After repetitive cycles of exposure and recovery, the morphology of the gel is more conserved, preserving the overall number and diameter of the initial droplets (Fig. 3.10a).
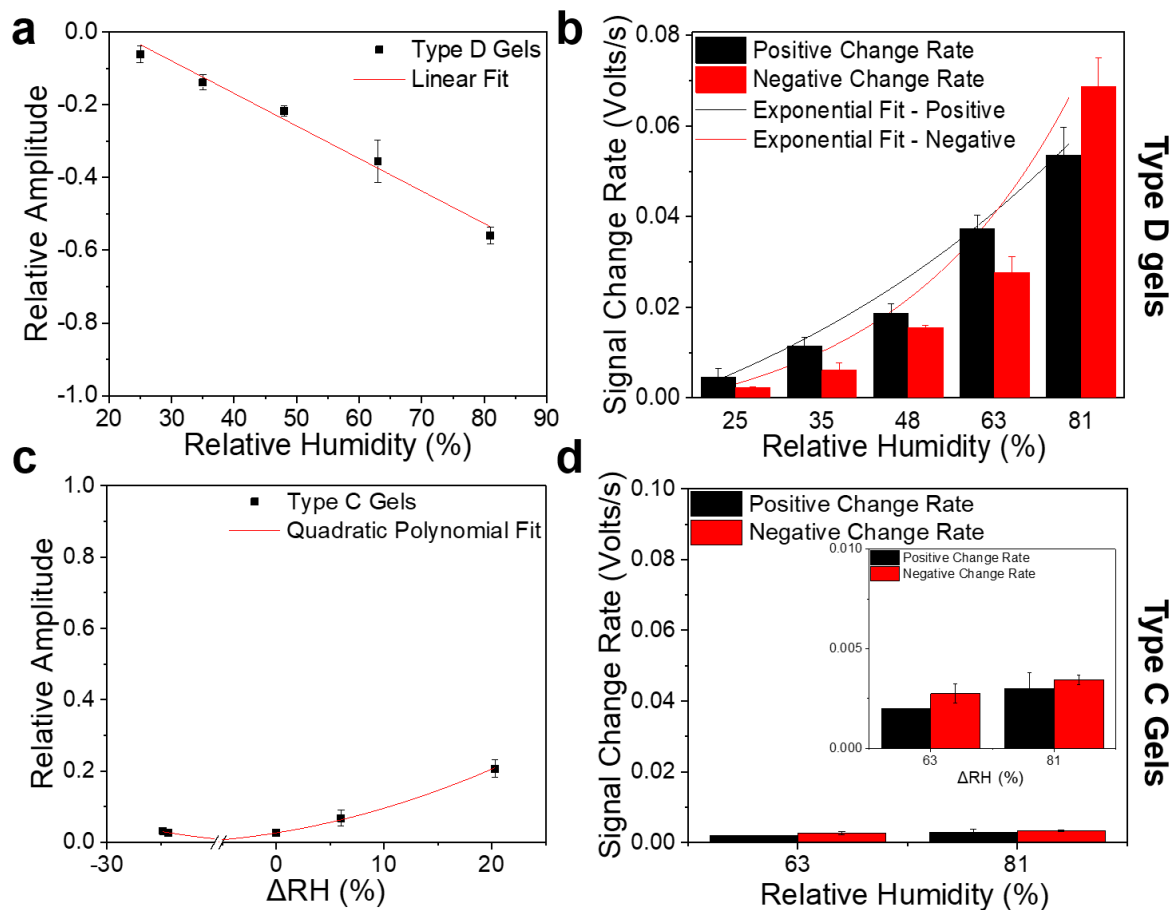
Figure 3.18- Analysis of features extracted from type D (upper panels) and type C (lower panels) hybrid gel films optical signals; (a) type D gels signal relative amplitude as a function of relative humidity, $r^2 = 0.98029$; (c) type C gels signal relative amplitude as a function of ΔRH, $r^2 = 0.99012$ (b) type D gels maximum slopes at the beginning of exposure (negative, $r^2 = 0.99639$) and recovery (positive, $r^2 = 0.97016$) periods as a function of relative humidity; (d) type C gels maximum slopes at the beginning of exposure (negative) and recovery (positive) periods as a function of ΔRH, with inset highlighted.
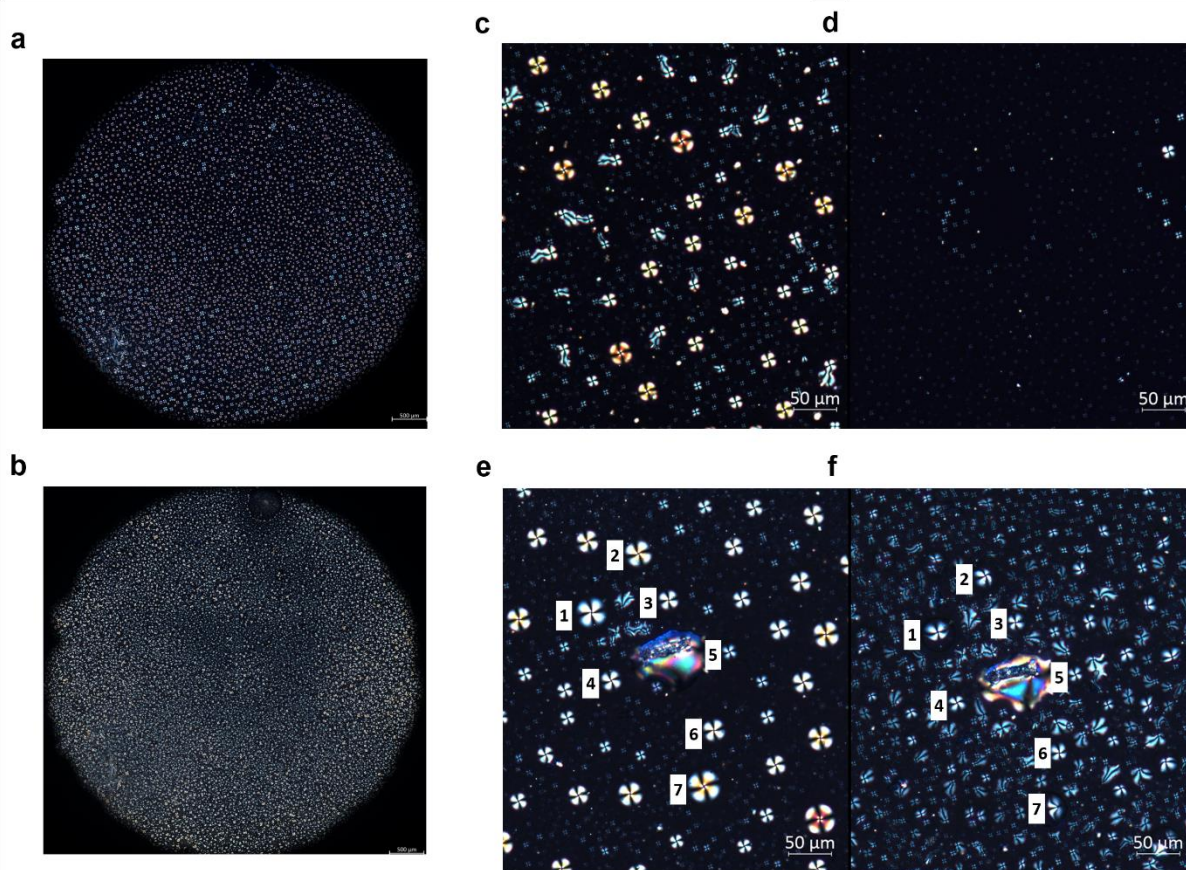
Figure 3.19- POM images of hybrid gel films, made with the IL [BMIM][DCA]; (a) total area of a film before an experiment; (b) total area of a film one hour after an experiment ending in a recovery period; (c, e) detail of an area of a film before an experiment; (d) detail of the same area immediately after an experiment ending in a recovery period; (f) and after ending in exposure period of 80 % RH. The numbers (1-7) indicate IL-LC droplets that maintained the same position before (e) and after experiment (f). Remaining POM images available in Appendix II – Fig. A2-A6.
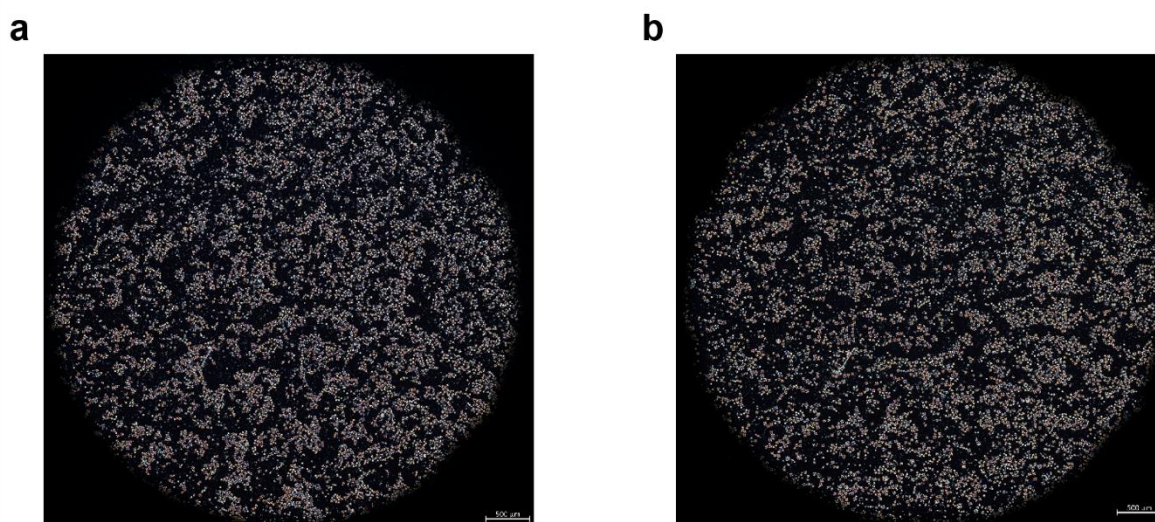
Figure 3.110- POM images of the same hybrid gel films, made with the IL [BMIM][Cl], before (a) and after (b) an experiment, ending in a recovery period. Remaining POM images available in Appendix II – Fig. A2-A6.

Assuming, from the slow response to humidity changes (Fig. 3.8d), that the C type hybrid gel films are diffusion limited; and from the weak response in recovery for null and negative ΔRH, that the gels can retain the water initially equilibrated (Fig. 3.7f-h), their behaviour could be described as follows: upon exposure to humidity, a given amount of water is adsorbed at the film's surface, creating a gradient with the film's bulk water content. During recovery, the water that has been absorbed into the film is retained, being the remainder at the surface purged. By successive cycles, the thin film tends towards a new equilibrium, causing the mean optical signal to slowly drift towards higher values, as more water is retained in the gel's bulk.

Studying the properties of the ILs contained in the hybrid gel films (Table 3.4), some insight on their behaviour towards humidity may be drawn.

The different magnitude between both ILs' viscosities, paralleled with the rate of water vapour diffusion (equation 3.3) – above the average for [BMIM][DCA], as opposed to [BMIM][Cl][74] – are an indication of the more diffusion limited mass-transfer regime of the [BMIM][Cl] IL[58,75–78], supporting the slow responsiveness of the type C hybrid gels towards humidity, compared to the type D ones. Further, [BMIM][Cl] high basicity and hygroscopicity makes it difficult to equilibrate with surrounding water[76,77,79], compared to the other IL – translating into the lack of optical response stabilization for the type C gels. Those same features render an IL difficult to dry, requiring vacuum and high temperature procedures[75,78,80] – supporting the hypothesis of the type C gels retaining water.

$$D_{12} = 2.66 \times 10^{-3} \frac{1}{\mu_2^{0.66\pm0.03} V_1^{1.04\pm0.08}}$$ (eq. 3.3) [74]

where indexes *1-2* denote the gas and IL, respectively, *μ* the viscosity (mPa.s) and *V* the molar volume (cm^3.mol^{-1}). D_{12} is the diffusivity of compounds *1* in *2* (cm^2.s^{-1}).

Table 3.14- Comparison of key properties of the ILs used to produce hybrid gel thin films.

	[BMIM][DCA]	[BMIM][Cl]
BASICITY	No Data	High[75,79,81]
VISCOSITY	24.4 to 28.8 cP[82,83]	10^4 to 10^6 cP[84,85]
TIME TO EQUILIBRATE	Short	Long[76,77,79]
WATER DIFFUSION[74]	10^{-5} cm^2.s^{-1}	10^{-7} to 10^{-9} cm^2.s^{-1}

The physical-chemical properties of the combined IL and gelatine may be different from the individual compounds[86], yet, for a mixture of [BMIM][Cl]-gelatine-water, the gel's viscosity approaches that of the IL, for higher concentrations of IL[87]. The way the hybrid gel films are produced – with a rather high IL content (~67 % (w/v))[8] – suggests that the gel's viscosity approaches that of the IL. Despite no similar data being available for a mixture with [BMIM][DCA], the gel's fast response to humidity and changes in the gel's matrix structure in the same period (Fig. 3.12, a-b), suggests an ease of water diffusion and no retention when purged with a dry nitrogen gas stream.

An additional test with a negative control hybrid gel film – without IL – was performed (Fig. 3.11), to infer on the IL's influence on the hybrid gel's properties and behaviour towards humidity. The control gel (Fig. 3.11a) displays features of both C and D type hybrid gel films: of low response fluctuation as the type C gels (Fig. 3.11b) and cyclic waveform with fast response stabilization as the type D gels (Fig. 3.11c).

Due to its ability to retain water, the addition of [BMIM][Cl] may justify the loss of the hybrid gel film's repeatable waveform (Fig. 3.11b), linked to an irreversible condition over time. Further, the difficulty to reach a stable-state response could be due to the IL's long time to equilibrate with surrounding water[76,77,79].

The faster response to humidity changes upon addition of [BMIM][DCA] (Fig. 3.11c; Fig. A8 – Appendix III) could result from a viscosity reduction, due to the high IL content[8]. The reversibility of the response could be linked to the ease with which [BMIM][DCA] loses water. Further, the opposite response and the transition of the optical signal to total darkness upon recovery may be, coupled with the accentuated loss of water, linked to the interaction of IL-LC. After disassemble of the IL droplet and transition of the LC from radial to isotropic configuration[8], the LC cannot transmit light, as opposed to when no IL is added and the LC remains in bipolar configuration.
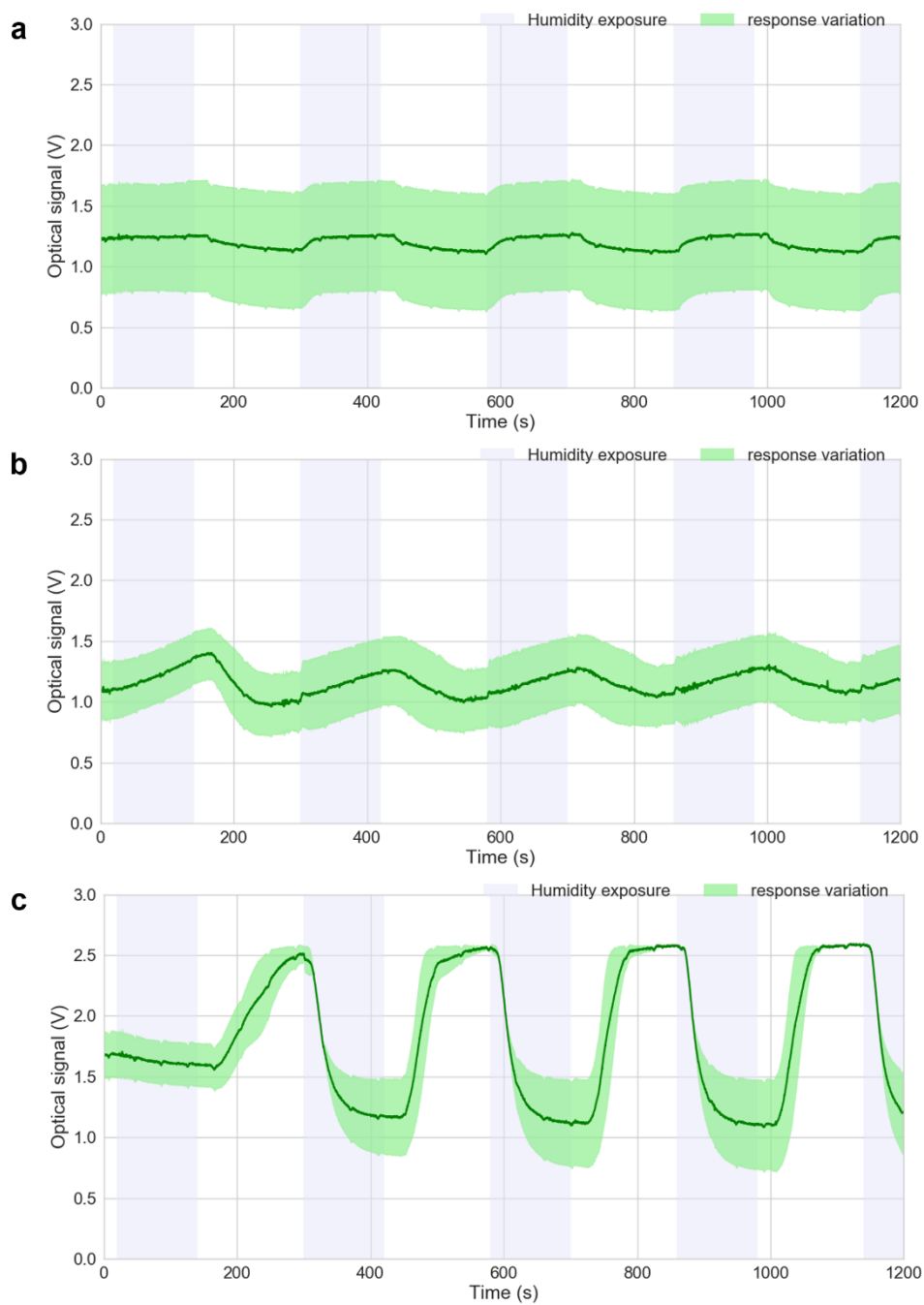
Figure 3.111- Optical signal response of the negative control hybrid gel films (a), films containing the IL [BMIM][Cl] (b) and [BMIM][DCA] IL (c). Highlighted the mean value (dark green) and the standard deviation (light green). The approximate exposed relative humidity was 80 % and the gradient ~20 %. All signals were obtained by averaging 2 replicates of each gel type. All corresponding POM images are available in Appendix I – Fig. A7.

3.3.3. Molecular sieves for humidity removal from a humidified carrier gas

Using molecular sieves of 4Å size, the aim is to retain the water molecules present in the carrier gas through size exclusion phenomena – molecules smaller than 4Å in size (water size=2.8Å) are retained inside the sieves – so that the e-nose is fed with dry gas to avoid interference of water vapor in the gels.

Fig. 3.12 shows the drying effect of molecular sieves on humidified nitrogen. At the beginning of the assay, the relative humidity at the outlet of the system (Fig. 3.4) is fixed at room conditions. After 1-minute recovery with pure nitrogen gas, it reduces to 0 %. When nitrogen with ~85 % relative humidity is sampled, in the absence of molecular sieves, there is an immediate increase of the RH at the outlet, reaching 70 % in about 15 seconds and the maximum of 85 % by the end of the humidity exposure period. After addition of the molecular sieves' fixed-bed, no increase in humidity is registered at the outlet for ~30 seconds. Afterwards, only a slow increase ensues, reaching a maximum of ~7.0 % relative humidity in the duration of the experiment.
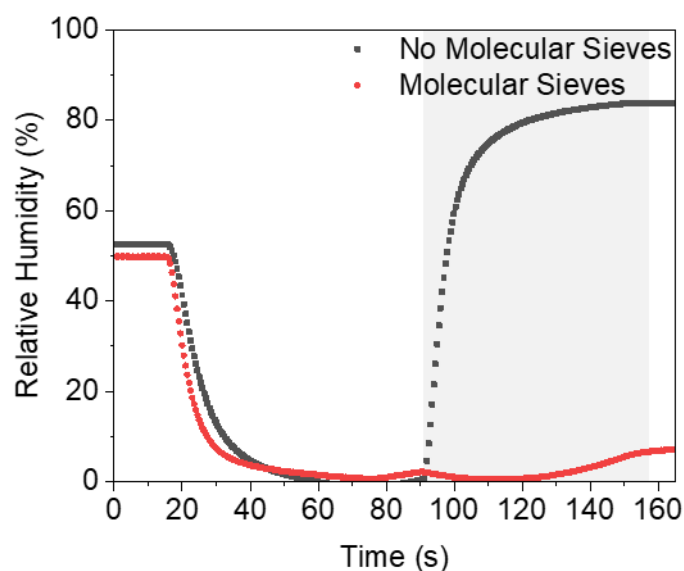
Figure 3.112- Effectiveness of humidity removal. Relative humidity in a glass vial exposed to 85% humidified nitrogen (grey) and to 85% humidified nitrogen that passed through a fixed-bed of molecular sieves (red). Exposure period highlighted in light grey.

Using saturated nitrogen as a carrier gas, the molecular sieves show an efficient removal of humidity, completely drying the sampled nitrogen. Under this context, about six exposure cycles of 5 seconds – as is the usual standard duration on the current VOC experiments on the e-nose – could be performed without interference from humidity. Afterwards, the molecular sieves start to saturate. Thus, either these should be replaced by a new batch or put to dry at high temperatures.

In an experiment in which nitrogen saturates with a lower percentage of relative humidity, a longer period of humidity removal without saturation of the molecular sieves should be expected. Activation of the molecular sieves at higher temperatures (~300 ºC) could as well provide a longer period of humidity removal.

Attempts to remove the humidity from a VOC gas-mixture, sampled to an array of gas sensors, has been already addressed[57,63,69–71]. The use of pre-concentrator membranes is a common technique, however requiring high temperature treatments to desorb the VOCs and multiple stages[2,57,71]. Inorganic salt solutions can be adapted in absorbent membranes, allowing for a continuous operation with no saturation, but not providing a complete removal of humidity[63,69].

Despite the effective capture of water, molecular sieves of 4Å pore size can similarly retain some small molecule VOCs, like ethanol, among others, this way saturating faster and impairing the results read on the e-nose, as some VOCs may be lost. For a more selective removal of water (2.8Å), molecular sieves of 3Å pore size would be more adequate. Additionally, the use of the 4-8 mesh alternative is more suitable for gas phase applications than the 8-12 mesh variety currently tested.

3.3.4. Sensing VOCs under different relative humidity environments

After assessing what is the isolated effect of humidity on the hybrid gel films, a preliminary study with VOCs sampled under different relative humidity environments was performed. Three VOCs were evaluated – ethanol, acetone and hexane – which have distinct chemical structures and polarity, and are expected to interact differently with the humidity in the carrier gas stream and with the components that constitute the hybrid gel films[8].

The humidity profiles measured at the outlet of the e-nose are presented in figure 3.13.
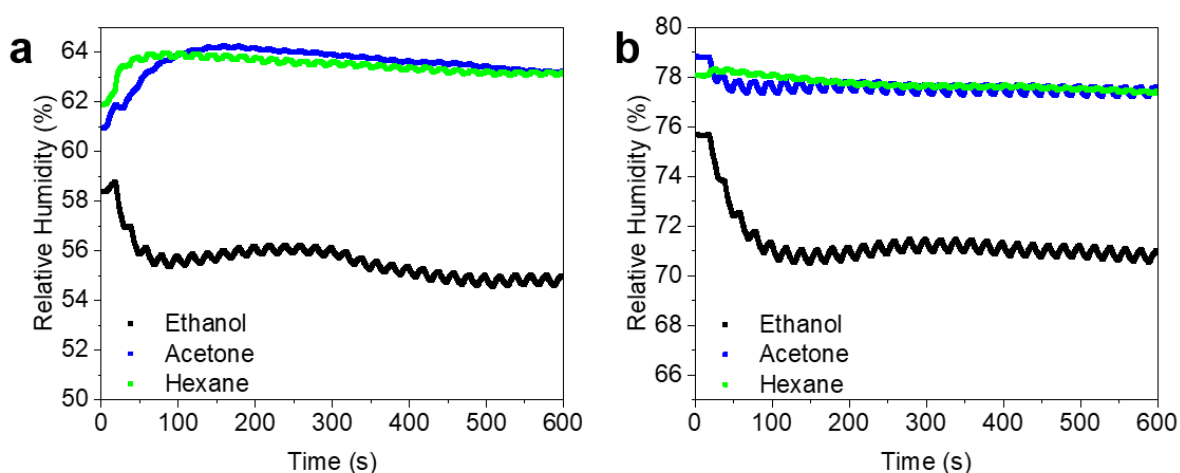
Figure 3.113- Relative humidity profile for each tested VOC, throughout the total duration of the experiments. (a) Assay with sodium chloride; (b) Assay with distilled water.

Interestingly, the degree of the VOC polarity seems to affect the uniformity of the relative humidity profile. For the RH in the 65 % range (Fig. 3.13a), the less polar VOCs hexane and acetone do not seem to significantly affect the relative humidity profile, while in the maximum generated humidity (Fig. 3.13b), the polarity of acetone already causes a fluctuation of the relative humidity profile, without

changing its mean value. Namely with ethanol, a visible reduction and higher fluctuation occurs (Fig. 3.13a-b) – probably due to its stronger interactions with the water vapour[26].

The response to VOCs of the type D hybrid gel films is presented in Figure 3.14. At 0 % relative humidity, the optical signal is kept constant in total darkness (Fig. 3.14a, d, g), being no response detected for either VOC (Fig. 3.16a).

For hexane and acetone, the response always saturates (Fig. 3.14e-f, h-i) and is accompanied by a decrease in baseline (signal minima) and increase of relative amplitude (Fig. 3.16a) as humidity grows. The fluctuation of the humidity for acetone (Fig. 3.13b) translates into a fluctuation of the optical response baseline (Fig. 3.14f).

The profile of the optical response to ethanol (Fig. 3.14b-c) is modulated by the inverse of the relative humidity profile (Fig. 3.13a-b), as it increases when humidity decreases and vice-versa. The relative amplitude intensifies with the increase of the mean relative humidity (Fig. 3.16a), without saturation and with reduction in the baseline (Fig. 3.14b-c).

As observed previously, when exposed to low relative humidity, D type hybrid gel films become inoperable, as the optical signal becomes saturated in the maximum due to the total darkness of the films, caused by the switching of the LC radial configuration to isotropic. This justifies the obtained results with the three VOCs. Furthermore, due to its ease of exchanging water with the environment, it was seen that these hybrid gel films were more responsive to humidity variations – the fluctuation of relative humidity increases in accordance with the VOC polarity – translated as a baseline drift of the optical signal (Fig. 3.14b-c, f), being that the response's amplitude remains approximately constant (Fig. 3.17).

The optimum operational conditions for this gel type appear to be found at the maximum RH, providing a higher optically active area – translated by a reduced baseline – and a stronger response to VOCs.
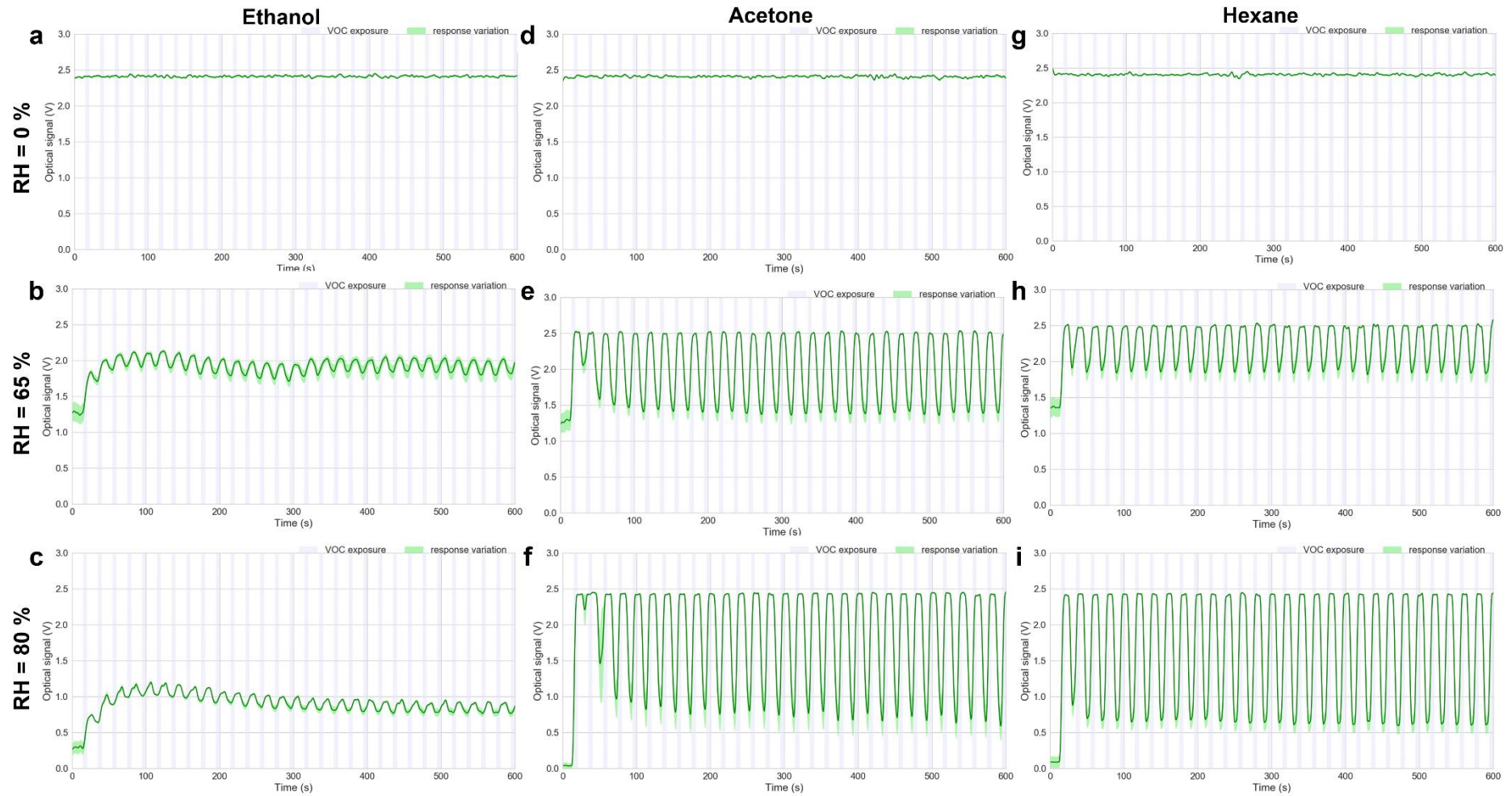
Figure 3.114- VOCs'-induced optical response of hybrid gels containing the IL [BMIM][DCA] (Type D) for three different generated humidity environments: (0 %) pure nitrogen; (65 %) bubblers on sodium chloride supersaturated solutions; (80 %) bubblers on distilled water. Presented the response of ethanol (a-c), acetone (d-f), and hexane (g-i). It is displayed the average response (dark green) and standard deviation (light green). Exposure period highlighted in light blue. All plots were obtained by averaging the signal of 2-3 replicates of each gel type. Signal stabilization in generated RH available in Appendix IV – Fig. A9a, c, e.

Regarding the optical response of the type C hybrid gel films to the less polar VOC hexane (Fig. 3.15g-i), the optical response saturates for all cases, thus the increase in relative amplitude for the higher humidity (Fig. 3.16b) is due to the lower baseline of the gel thin film.

A similar behaviour is observed on the optical response towards acetone (Fig. 3.15e-f). Yet, when sampled with pure nitrogen (Fig. 3.15d), saturation no longer occurs and the response waveform changes. This particularity makes it clear that for acetone a multiplicative drift of the response – of a growth of the relative amplitude – occurs at least from 0 to 65 % RH. The same conclusions cannot be safely drawn for hexane.

The increase in relative humidity for ethanol (Fig. 3.15a-c) results in an intensification of the relative amplitude (Fig. 3.16b), which is less ambiguous than for the other VOCs because with ethanol, the response does not saturate. For the assay with the highest humidity (Fig. 3.15c), fluctuations in the baseline are registered throughout, accompanied by a reduction of the relative amplitude – in parallel with the reduction of the RH profile, showing a visible correlation (Fig.17b).

Despite the response to VOCs increasing with humidity, the optimal operational conditions for the type C gels seems to be at 0 % RH, as a response to VOCs occurs without the interference of humidity – be it as a multiplicative or baseline drift.

.
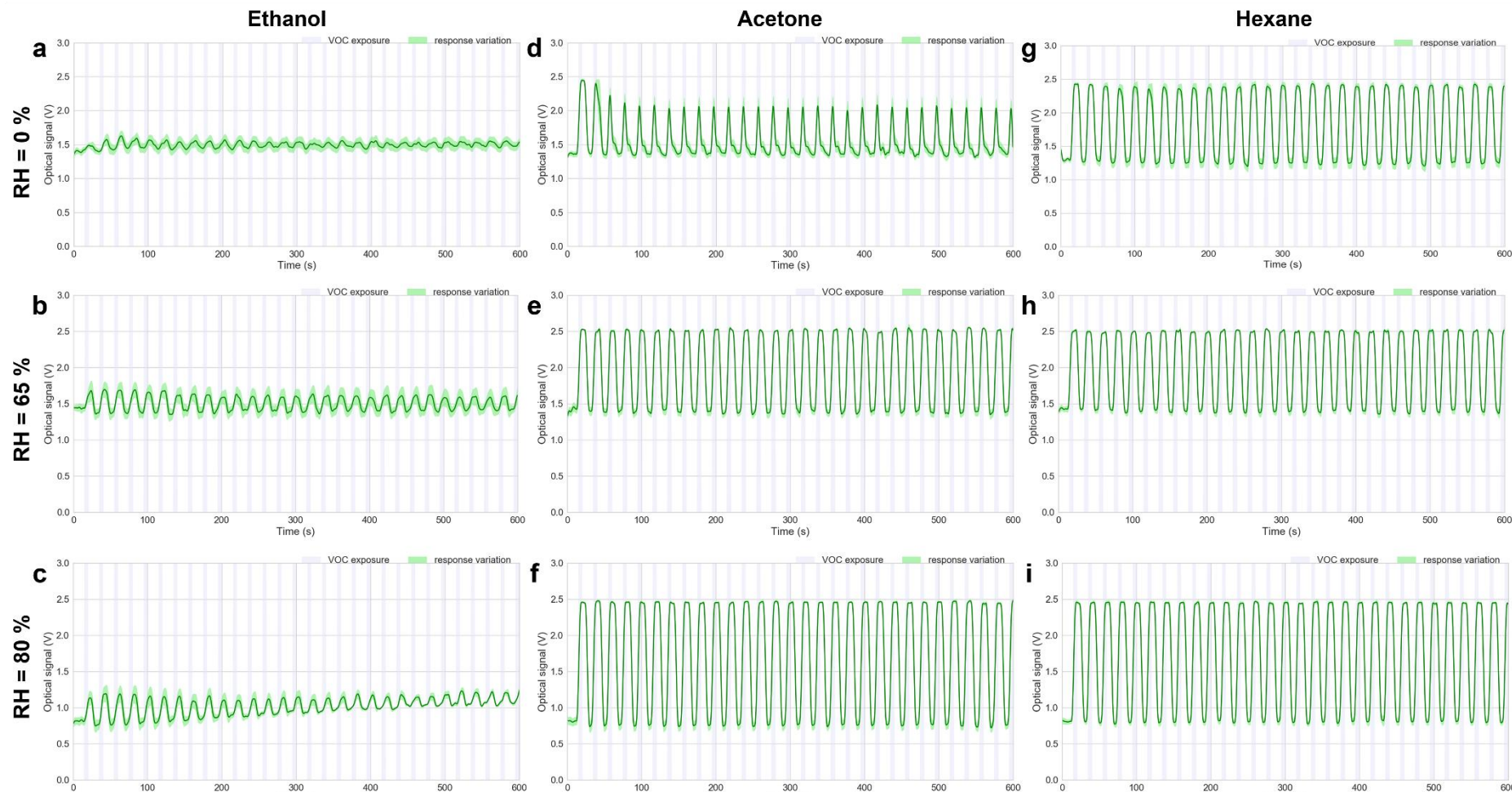
Figure 3.115- VOCs'-induced optical response of hybrid gels containing the IL [BMIM][Cl] (Type C) for three different generated humidity environments: (0 %) pure nitrogen; (65 %) bubblers on sodium chloride supersaturated solutions; (80 %) bubblers on distilled water. The responses of ethanol (a-c), acetone (d-f) and hexane (g-i) are shown. The average response is in dark green and standard deviation is represented in light green. The exposure period highlighted in light blue. All plots were obtained by averaging the signal of 2-3 replicates of each gel type. Signal stabilization in generated RH available in Appendix IV – Fig. A9b, d, f.

For either hybrid gel film type, the influence of relative humidity on the less polar VOCs – hexane and acetone – is less apparent. The optical response most often saturates with VOC exposure, limiting the comparison between different relative humidity conditions. Further tests should be performed with lower VOCs concentrations in the sampling stream, avoiding the optical response's saturation, to better analyse the variations in relative amplitude

Depending on the nature of the VOC, different interactions may take place within the hybrid gel films. If the VOC is more hydrophobic – as hexane and acetone – it will mainly interact with the LC within the IL droplet, disrupting its radial configuration and nullifying its optically active area. When the VOC is more polar – like ethanol – interactions with the IL and gelatine chains predominate, not fully disrupting the LC's radial configuration, while promoting a conformational rearrangement with the hybrid gel[8].
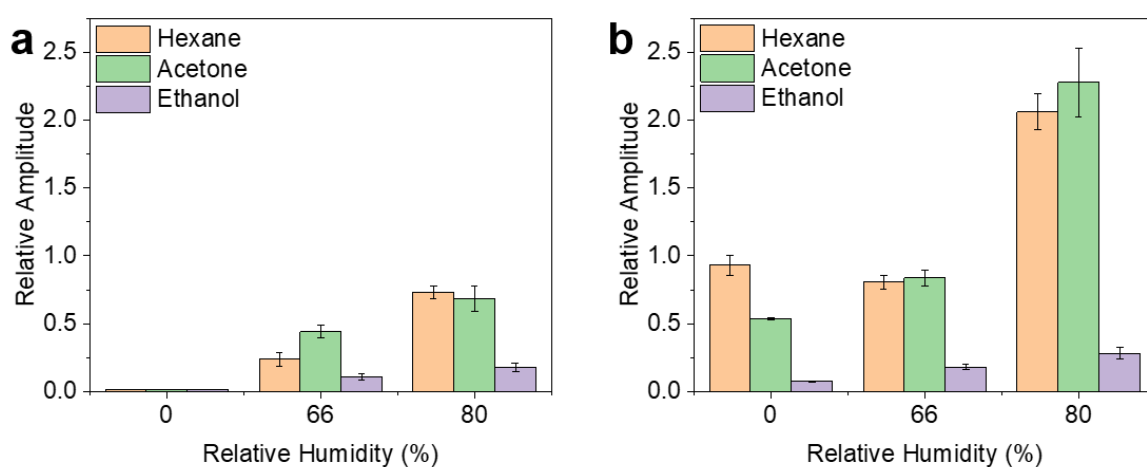
Figure 3.117- Optical signal's relative amplitude for the average humidity tested for each VOC: hexane (orange), acetone (green), ethanol (purple). Results for hybrid gel films containing [BMIM][DCA] IL (a) and [BMIM][Cl] IL (b).
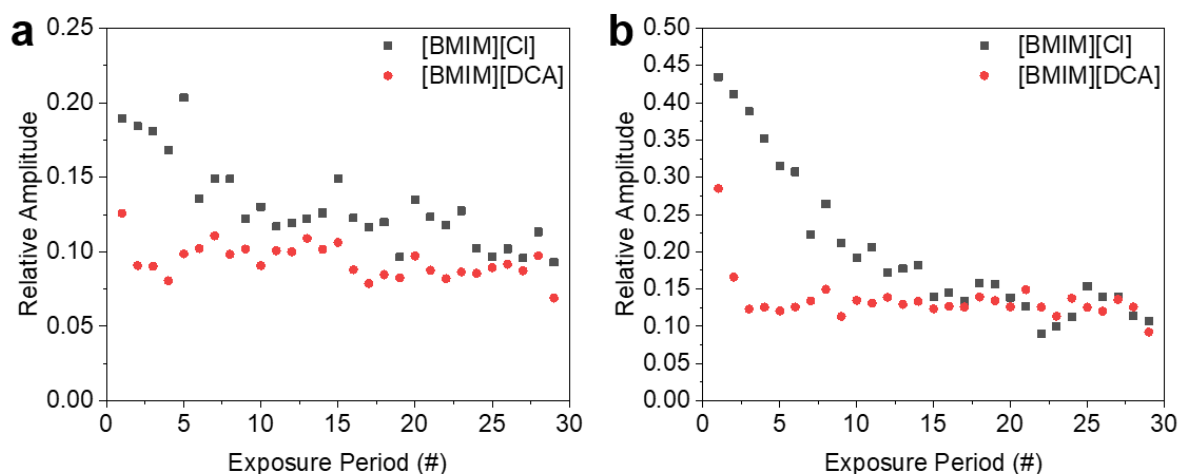
Figure 3.116- Variation of relative amplitude, per exposure period, of the optical signal exposed to ethanol – for hybrid gel films made with [BMIM][Cl] IL (grey) and [BMIM][DCA] IL (red). Humidity generated with: (a) NaCl supersaturated solutions, ~65 %; (b) distilled water, ~80 %.

Often, highly polar solvents tend to have reduced responses on gas sensors, when sampled under high relative humidity, due to the competition between VOCs and water molecules for the same reactive

sites[26,60]. Yet, a detectable optical response is provided by both hybrid gel film types, for the tested VOC concentration.

Despite the increase in relative amplitude being less noticeable for ethanol than for other VOCs (Fig. 3.16a-b), this is mainly due to the distinct interactions that take place within the hybrid gel films with distinct polarity VOCs and not as much to water-VOC competition.

3.4.   Conclusions

A gas delivery system, comprising inorganic salt solutions, bubbled with nitrogen gas for generating controlled relative humidity values, was assembled. The effect of humidity on hybrid gel films' optical response and morphology was thus studied. A fixed bed of molecular sieves was tested for removing the humidity from the carrier stream. Finally, three different VOCs were sampled to the e-nose under distinct relative humidity levels in the carrier stream.

Five different relative humidity levels, from ~20 to 80 %, were generated, using four supersaturated salt solutions and distilled water. Two hybrid gel films' formulations were tested, comprising one of two ILs ([BMIM][DCA] or [BMIM][Cl]), plus a negative control gel (without IL).

Films containing [BMIM][DCA] evinced high responsiveness towards humidity – with the ability to repeatedly capture and lose water – as seen by the fast kinetics and reversibility of their optical signal. The visible differences between the POM images of the gel thin film at the end of either exposure or recovery periods justify the observed optical signal, clarifying its reversibility. The optical signal's relative amplitude correlates linearly with the relative humidity level, with a satisfactory fit (R^2~0.98).

Films containing [BMIM][Cl] present a much less intense and slower optical response to humidity, with little to no stabilization, or response during the recovery period, suggesting a more diffusion limited mass-transfer regime and the capacity to retain water. The optical signal's relative amplitude has a quadratic correlation with the gradient between room and generated relative humidity. Despite the good fit (~0.99), further studies are needed to confirm this behaviour. Comparing with the control gel's response to a fixed value of relative humidity, the presence of [BMIM][Cl] alters the waveform of the optical signal and the ability to reach a steady state. The addition of [BMIM][DCA] results in a higher amplitude and an opposite response, with faster kinetics and loss of optically active area upon drying. The obtained results thus aid in the understanding of the films sensitivity to humidity.

The molecular sieves' efficiency to capture humidity was tested by exposing a fixed bed of these sieves to nitrogen gas humidified in distilled water (~85 % relative humidity) and measuring the relative humidity of the nitrogen gas afterwards. An effective removal of the total exposed humidity was achieved, with a stable reading of 0 % relative humidity at the outlet for nearly 30 seconds, after which a slight growth occurs, reaching ~7.0 % by the end of the remainder 30 seconds of experiment. Depending on the humidity present in the carrier stream, the molecular sieves may saturate with faster or slower rates, theoretically allowing dry conditions for six 5 seconds' exposure periods in the most humid conditions. Further, the retention of smaller VOCs (< 4Å) may accelerate its saturation.

For the combined study of VOCs and humidity sampled to the e-nose, the VOCs were chosen with an increased degree of polarity –hexane, acetone and ethanol – to assess their different interactions with the humidity and the hybrid gel films. Higher relative humidity translates in a higher amplitude of the optical response – often saturating for the less polar VOCs. The more polar VOCs affect the stability of the humidity profile throughout time, probably due to stronger water-VOC molecules' interactions. Accordingly, hybrid gel films containing [BMIM][DCA] suffer drifts in the baseline, while for [BMIM][Cl], it has a visible effect on the relative amplitude. The analysis of the relative amplitude is limited by the saturation of the optical response, not allowing to conclude about the real influence of humidity.

In the future, analytical techniques – Karl Fischer titration, rheology test and determination of films' thickness – should be conducted to allow a deeper understanding of the hybrid gel films' properties containing the studied ILs. The concept of relative humidity gradient must be validated, and its mathematical characterization optimized. Mean grey values of POM images of the films' exposed area should be determined to precisely compare the differences in optically active area under several humidity conditions. Further, it is planned to test molecular sieves more selective towards water, by reducing their pore size, validate its humidity removal potential using ambient air and on a respective carrier stream containing VOCs, and explore its application in sensing VOCs from bacterial culture media, in which humidity is of common presence[13].

Regarding the study of the drift effects caused by humidity, a wider range of VOCs should be tested, with the need to be sampled under more diluted conditions in the carrier stream, correlate the findings with the individual effect of humidity and fully characterize the occurring drifts.

4. Characterization and optimization of the e-nose's odorant delivery system

4.1. Introduction

An odorant delivery system is the component of an e-nose responsible for sampling a gaseous mixture to the sensing chamber containing the gas sensors. It is important for this delivery system to be capable of generating samples of known concentrations in a wide range, so that the study of the e-nose sensitivity and limit of detection to a variety of gas analytes can be made – relevant parameters defining the equipment performance.

A gas delivery system meeting the above criteria is exemplified in Figure 4.1, providing the means to manipulate and quantify the concentration of VOCs fed to the e-nose.

Generally, the dilution of the target analyte stream is done by mixing it with a dilution gas, both at known flow rates. Thus, depending on the desired concentration range, one or more dilution stages may be adopted, i.e. the use of more than one stream of dilution gas[88].
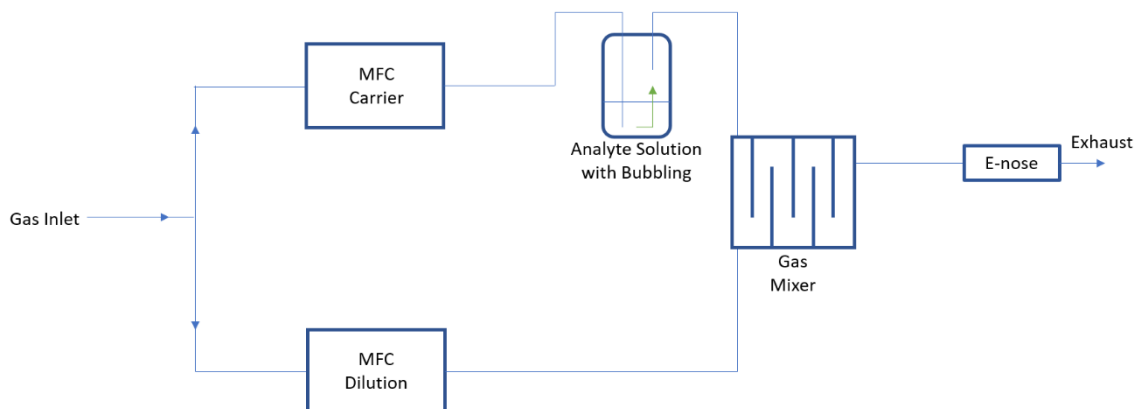
Figure 4.1- Generic block diagram of a gas delivery system. The upper mass flow controller (MFC Carrier) carries the analyte gas in the stream, while the lower one (MFC Dilution) is, generally, used for diluting the analyte gas until a desired concentration is achieved. Sometimes a gas mixer is employed for homogenizing the gas mixture, prior to be fed to the e-nose[1,3,4].

Distinct gas delivery apparatus arrangements have been described (Table 4.1). Most of them employ mass flow controllers for direct reading of the flow rates of carrier and dilution gas, and bubbling systems for mixing the analyte gas with the dilution stream[45,89]. The techniques used for quantifying the target analyte in the stream pass by adopting mathematical models, under the principle of saturating the carrier gas with the gas analyte through bubbling in a solution of analyte[73]. For a precise measurement of the concentrations calculated with this method, analytical methods can be used[45,46,90].

When the analytical methodology is applied, the gas mixture is usually sampled for gas chromatography combined with mass spectrometry (MS) or flame ionization detector (FID), thus providing a quantitative

and qualitative reading of the amount of analytes in the stream[57,3]: Nevertheless, this is a rather time-consuming technique, of high cost and requiring skilled handling[26,71].

Table 4.1- Methods of quantification and delivery of a gas analyte to e-noses.

Quantification Method	Analyte Delivery System	References
Mathematical	MFCs + Bubbler + Valve system/gas mixer	45,46,66,89,90
Mechanical	MFCs + Gas analyte pressurized bottles + valve system	91
Mechanical/Mathematical	MFCs + Bubbler + Gas Mixer + Valve system	23
FID	MFCs + Vacuum Pump + Multi-port valves	57
SPME	MFCs + Bubblers + Gas Mixer	92
GC-MS	N/A	93
GC-MS/FID	N/A	3
N/A	MFCs + Valve system	71

A combination of both mathematical and analytical procedures to quantify the complex gas stream is desired, as analytical methods provide the required validation, or optimization, of the mathematical estimation. When the gas stream contains only an individual VOC, quantification through mass-spectrometry (MS)[94] is straightforward and enough for the purpose of performing a VOC sensitivity analysis.

In the Biomolecular Engineering Lab, hybrid gel thin films' responsivity to VOCs is assessed with a standard e-nose experiment, which consists of exposing the films to individual VOCs diluted in a stream of ambient air. For that, the odorant delivery system currently installed at the inlet of the e-nose flushes ambient air through the headspace of a chamber containing a saturated atmosphere with the VOC, which then enters the e-nose and interacts with the gels. However, the VOC concentrations in the inlet stream have not been quantified yet. On the other hand, for the future characterization of the e-nose, namely regarding VOC sensitivity and limits of detection, there is the need of a dedicated odorant delivery system able to generate controlled VOC concentrations at the e-nose's inlet.

In this work, the concentrations of VOC sampled to the in-house built e-nose in a standard experiment were estimated – without the use of hybrid gel films to obtain the VOCs response – providing the preliminary results for advancing towards a VOC sensitivity analysis. The amount of each VOC in the carrier stream was calculated through the rate of evaporation and the gas-liquid equilibrium in the sample chamber. A VOC dilution system was designed, for future implementation of a VOC sensitivity study, using nitrogen as carrier and diluting gas. The system includes a VOC sampling stage and a dilution stage, controlled by 2 MFCs. A chamber for generation of controlled relative humidity is also included, as well an automated monitorization of flowrate stability. These main features constitute the system required for performing a quantification and sensitivity study of the e-nose towards a range of VOCs.

4.2. Materials and Methods

4.2.1. Chemicals

The organic solvents diethyl ether (99.8 %), isopropanol (99.5 %) and ethanol (99.8 %) were purchased from Sigma-Aldrich (Portugal). N-Hexane (99.2 %), ethyl acetate (99.9 %) and toluene (99.9 %) were purchased from Fisher Chemical (Portugal). Acetone (99.5 %) was purchased from Honeywell (Portugal). Dichloromethane (99.8 %) was purchased from VWR Chemicals (Portugal). All solvents were used has purchased.

4.2.2. Materials

Glass vials with an approximate volume of 27 cm^3, inlet and outlet channels with an external diameter of 6.45 mm (Fig. 3.1) and a lid with inside cover of Teflon were homemade. Silicon tubes of 4x6 mm diameter were used. A thermal plate (VMS-C7, VWR Advanced) was used. Two air pumps (Air 550R Plus, Sera, Borsigstr, Germany) were used for sampling. An Arduino Due was used for controlling the pumps and for the data acquisition. A temperature & humidity sensor (HTU21D-F, Adafruit, New York, USA) was used for measuring room conditions. A mass flow controller (MC-5SCCM-D/5M, 5IN, Alicat Scientific Inc.) was employed. Compressed nitrogen gas (UN 1066, Air Liquide, Portugal) was used as feed to the mass flow controller. Silicon tubes of 4x6 mm diameter were used.

4.2.3. Software

Tailor-made python script (python 3.6, alicat library 0.2.2) developed in the Biomolecular Eng. Lab (by Cláudia Alves) was custom-made to program the mass flow controller operation and obtain the reading of the gas flowrate. *Excel* software was used for all mathematical operations, recurring to the *Solver* tool when appropriate.

4.2.4. Estimation of VOC concentrations fed to the e-nose with the current odorant delivery system

4.2.4.1. Odorant Delivery System

To simulate the conditions of a standard e-nose experiment, the apparatus represented in Figure 4.2 was assembled. The silicon tubing, corresponding to the inlet and outlet streams of the exposure course, had an approximate internal volume of 8.7 cm^3. In total, the apparatus had a volume of about 35.7 cm^3, not accounting for the volume of the recovery course. A sample of solvent (Table 4.2) was placed in a tailor-made glass vial and included in the apparatus schematized in figure 4.2. The solvent temperature was equilibrated to 23 - 24 ºC (Table 4.2) for 15 minutes in a pre-heated water bath. The pumps provided ambient air from the laboratory to the system as carrier gas, at an approximate flowrate of 3.000 slpm. Due to pressure drop throughout the equipment, the flowrate at the exhaust line of the exposure pump was measured as 1.820 slpm. The VOC was expelled through contact of the air stream

from the exposition pump with the glass vial's headspace during the exposure cycle. During the recovery cycle, no air passed through the vial. Exposure (5 s) / recovery (25 s) cycles were alternated during 100 min to 360 min, depending on the solvent (Table 4.2), using an Arduino Due programmed to automatically switch the air pumps on or off.
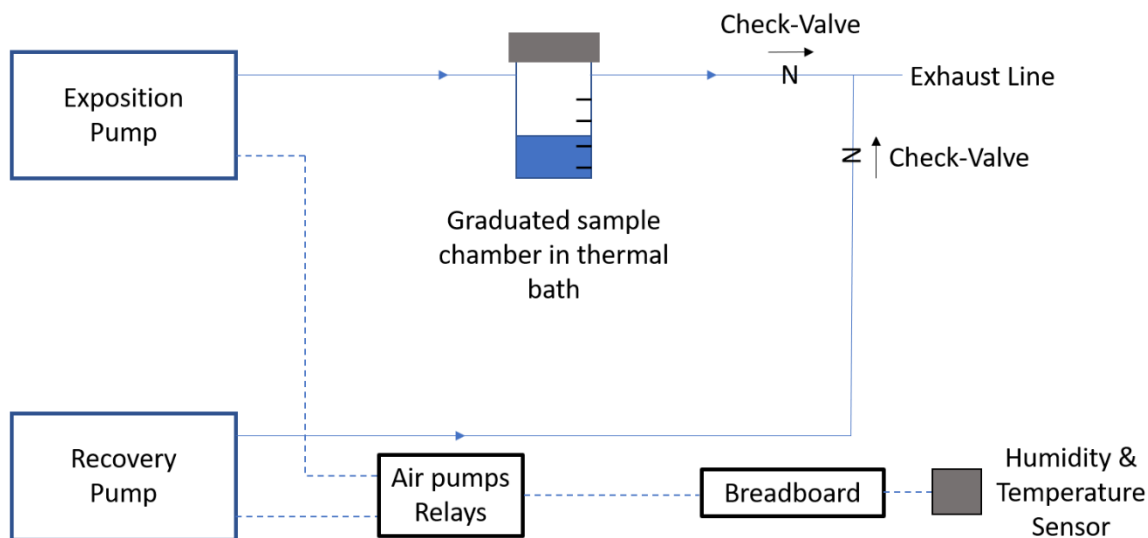
Figure 4.2- Assembled apparatus for quantifying the VOCs sampled to the e-nose.

Table 4.2- List of VOCs analysed and their experimental conditions.

	Organic Solvent	Temperature (ºC)	Volume (mL)	Duration (min)
	Diethyl Ether	24	15	100
	n-Hexane	24	18	310
	Ethyl Acetate	24	20	360
Non- Halogenated	Acetone	24	20	360
	Toluene	24	18	240
	Ethanol	22	20	240
	Isopropanol	24	20	240
Halogenated	Dichloromethane	23	20	240

4.2.4.2. Equilibrium Measurements

To estimate the amount of solvent loss by evaporation throughout time, the total solvent volume was divided in several reference points, measured using a ruler (Fig. 4.3). The initial height of the solvent in the vial was considered as the first equilibrium; the subsequent equilibria were equidistantly measured until the experiment reached its set duration (Table 4.2). For characterizing each equilibrium, the

solution's height and temperature, and the elapsed time since the previous equilibrium were registered. The ambient air pressure, temperature and relative humidity (Eq. 4.1) were measured using a temperature and humidity sensor installed in the laboratory, to provide the necessary data for extracting the absolute humidity (Kg_{H_2O}/m^3) from tabulated values[95].

$$Relative\ Humidity\ (\%) = \frac{P_{H_2O}}{P^*_{H_2O}} \times 100\ \%$$
(eq. 4.1)

where P_{H_2O} and $P^*_{H_2O}$ correspond to the partial and saturated vapour pressures of water respectively, for a fixed temperature.
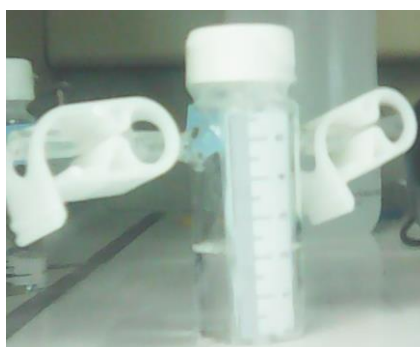
Figure 4.3- VOC sampled chamber with imprinted ruler.

The rationale of the method was based in the principle that, for a given decrease in solvent's height in the vial, a correspondent volume was evaporated (Fig. 4.4).
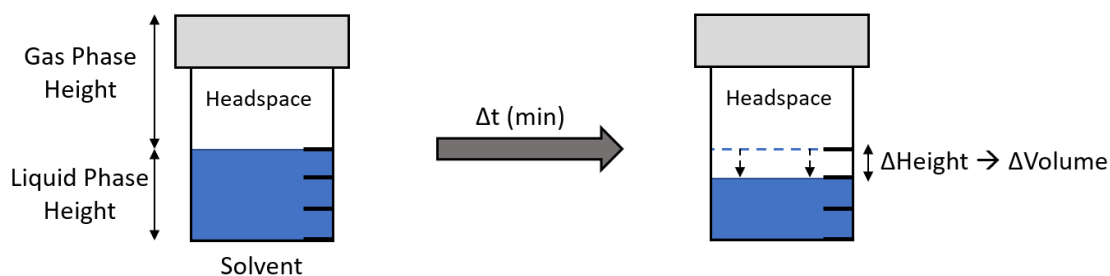
Figure 4.4- Measurement of solvent's volume loss throughout time.

4.2.4.3. Thermodynamics Characterization

For characterizing the equilibrium conditions in each reference point, the liquid and vapour phases were both taken into analysis. It was assumed, for calculation purposes, a binary system water-VOC, defined by the solvents' purity – thus regarding the solvent as a solution, that new equilibria were established by the end of the recovery periods and that the totality of the evaporated solvent was expelled during the exposure periods, given that the carrier gas flowrate (50 mL/s) is enough to push the headspace

49

volume of the solvent's chamber (≤ 27 mL). For characterizing the equilibrium in the liquid phase, the total mass (Eq. 4.2) and molar quantity of solvent and water (Eq. 4.3 – 4.4) were calculated:

$$mass_{VOC}(g) = Volume\ (mL) \times Purity\% \left(\frac{v}{v}\right) \times \rho \left(\frac{g}{mL}\right) \tag{eq. 4.2}$$

$$n_{VOC}(mol) = \frac{mass_{VOC}(g)}{Molar\ Mass_{VOC} \left(\frac{g}{mol}\right)} \tag{eq. 4.3}$$

$$n_{H_2O}(mol) = Volume\ (mL) \times \frac{1 - Purity\ \% \left(\frac{v}{v}\right)}{Molar\ Mass_{H_2O} \left(\frac{g}{mol}\right)} \tag{eq. 4.4}$$

in which ρ corresponds to the solvent's volumetric mass density under NPT conditions.

Therein, the solvent's and water liquid molar fractions, x_{VOC} & x_{H_2O}, were obtained (Eq. 4.5):

$$Molar\ Fraction = \frac{Moles_i}{Total\ moles}, i = organic\ solvent, water \tag{eq. 4.5}$$

By estimating the volume of solvent evaporated between equilibria (Eq. 4.6), the total mass and molar quantity of evaporated solvent and water were similarly calculated through Equations 4.2 – 4.4, accounting for the change in volume. By dividing the amount of evaporated solvent by the total duration of the exposure periods between equilibria (Eq. 4.7), an approximate volatilization rate was obtained (Eq. 4.8). It was thus assumed that the volatilization rate remained constant during the entire exposure period.

$$Volume_{Evaporated}(mL) = \pi \times (r - 2e)^2 \times (\Delta h - e) \tag{eq. 4.6}$$

where r represents the vial radius, e the wall's thickness and Δh the difference in liquid's height between reference points.

$$Total\ Exposition\ Time\ (s) = \frac{\Delta t\ (s)}{30 \left(\frac{s}{cycle}\right)} \times 5 \left(\frac{s}{exposition\ cycle}\right) \tag{eq. 4.7}$$

where Δt represents the time elapsed between reference points, thus giving the total number of cycles when divided by the latter's total duration (i.e. considering one cycle equal to one exposition and one recovery cycle).

$$Volatilization\ Rate \left(\frac{mL}{s}\right) = \frac{Volume_{Evaporated\ (mL)}}{Total\ Exposition\ Time\ (s)} \tag{eq. 4.8}$$

For characterizing the equilibria in the gas phase, the vapour pressure of the solvents was calculated using the Antoine Equation (Eq. 4.9):

$$Antoine\ Equation: P^*_{Solvent} = 10^{A - \frac{B}{C+T}}, P(bar), T(^oC) \tag{eq. 4.9}$$

where the coefficients *A*, *B* and *C* were obtained through tabulated values[95] (Table 4.3), specific for each solvent at a given temperature range. *T* represents the solvent's temperature.

Table 4.3- Listed VOCs' Antoine's constants and heat capacities.

ANTOINE'S CONSTANTS	$(C_2H_5)_2O$	C_6H_{14}	C_3H_8O	C_2H_5OH	CH_2Cl_2	$C_4H_8O_2$	C_3H_6O	C_7H_8
				SOLVENTS				
A	6.96559	4.00091	5.24268	4.92365	4.07622	4.21248	4.35647	4.0854
B	1071.54	1171.17	1580.92	1410.46	1070.07	1238.15	1277.03	1348.77
C	227.774	224.408	219.61	208.514	223.24	217.205	237.23	219.976
HEAT CAPACITY (CAL/G.K)	0.556	0.735	1.054	1.375	0.746	0.719	1.091	0.687

The vapour pressure of water was taken from tabulated values[95] at room temperature and the water bath's temperature (Table 4.4). The solutions' water and solvent partial pressures were calculated using Raoult's Law (Eq. 4.10):

$$Raoult's\ Law: P_i = x_i \times P_i^* \ (bar), i = Solvent, water \tag{eq. 4.10}$$

It was assumed that the vial's headspace was only exposed to the ambient humidity after the first exposure cycle, thus for the first equilibrium, water vapour pressure was only the one from the solution (Eq. 4.10). For the subsequent equilibria, the water vapour coming from the carrier gas (Eq. 4.11) was accounted for the total pressure of the mixture (Eq. 4.12):

$$Ideal\ Gas\ Law: P_{H_2O\ carrier}(bar) = \frac{n_{H_2O\ (mol)} \times R\left(L.\frac{bar}{mol.K}\right) \times T\ (K)}{Volume\ (mL)} \tag{eq. 4.11}$$

where $n_{H_2O}(mol)$ was determined through the absolute humidity and carrier gas flowrate (Eq. 4.13), *T* corresponds to the temperature of the gas mixture and *R* to the ideal gas constant (Table 4.4).

$$Dalton's\ Law: P_{Total}(bar) = P_{H_2O\ Solution} + P_{H_2O\ Carrier} + P_{Solvent} \tag{eq. 4.12}$$

$$n_{H_2O}(mol) = \frac{Absolute\ Humidity\left(\frac{g_{H_2O}}{mL}\right) \times Carrier\ Gas\ Flowrate\left(\frac{mL}{s}\right) \times Exposition\ Cycle\ Duration(s)}{Molar\ Mass_{H_2O}\left(\frac{g}{mol}\right)} \tag{eq. 4.13}$$

Since the mixture of gas from the solution and from the air (carrier gas) may be at different temperatures, the temperature of the resulting mixture (Eq. 4.14) was calculated to allow summing partial pressures (Eq. 4.12):

$$\begin{cases} \boldsymbol{Q_{Carrier}}\left(\frac{\boldsymbol{cal}}{\boldsymbol{s}}\right) = mass_{carrier}\left(\frac{g}{s}\right) \times cp_{carrier}\left(\frac{cal}{g.K}\right) \times (\boldsymbol{T_{Mixture}} - T_{initial\ carrier})(K) \\ \boldsymbol{Q_{Solution}}\left(\frac{\boldsymbol{cal}}{\boldsymbol{s}}\right) = mass_{solution}\left(\frac{g}{s}\right) \times cp_{solution} \times (\boldsymbol{T_{Mixture}} - T_{initial\ solution})(K) \end{cases} \tag{eq. 4.14}$$

where $mass_{carrier}$ represents the flowrate of carrier gas, $mass_{solution}$ the average value of the solvent's volatilization rate, measured at each equilibrium, *Q* the sensible heat and *cp* the heat capacity of the

solvent or of the external air (Tables 4.3 – 4.4), obtained through tabulated values. Establishing $|Q_{Carrier}| = |Q_{Solution}|$, the temperature of the mixture was calculated. It was observed that the temperature of the mixture always approached that of the external conditions, given the high ratio of flowrate to volatilized volume.

The resulting gas molar fractions y_{VOC} & y_{H_2O} were further calculated (Eq. 4.15):

$$y_i = \frac{P_i(bar)}{P_{Total}(bar)}, i = Solvent, water \tag{eq. 4.15}$$

Thus, with the above steps completed, the total molar quantity of the gas mixture in each equilibrium was determined (Eq. 4.16):

$$Total\ moles = \frac{P_{Total}(bar) \times Volume_{Headspace}(mL)}{R\left(L.\frac{bar}{mol.K}\right) \times T_{Solution}\ (K)} \tag{eq. 4.16}$$

from there, it was further possible to estimate the total moles and mass of solvent in equilibrium in the gas phase of the sample chamber (Eq. 4.17 – 4.18):

$$Solvent_{moles}(mol) = Total\ moles \times y_{Solvent} \tag{eq. 4.17}$$

$$Solvent_{mass}(g) = Solvent_{moles} \times Molar\ Mass_{Solvent}\left(\frac{g}{mol}\right) \tag{eq. 4.18}$$

For converting the liquid phase rate of volatilized volume onto the gas phase, the latter was calculated (Eq. 4.19)

$$Volume_{gas\ phase\ volatilization\ rate}\left(\frac{L}{s}\right) = \frac{n_{VOC}(mol/s) \times R\left(L.\frac{bar}{mol.K}\right) \times T_{Mixture}\ (K)}{P_{VOC}(bar)} \tag{eq. 4.19}$$

where n_{voc} are the moles of evaporated solvent from the liquid phase and P_{voc} the solvent's partial pressure.

Similarly, to obtain the amount of equilibrated solvent in volumetric units, Equation 4.19 was employed, but accounting for the correspondent moles (Eq. 4.17). Finally, for estimating the concentrations of volatiles fed to the e-nose, both the volatilization rate and volatile in equilibrium (Eq. 4.19) were separately divided by the carrier gas flowrate at the e-nose inlet (Eq. 4.20).

$$Volatile\ Concentration\ \%\left(\frac{v}{v}\right) = \frac{V_{VOC}(\mu L/s)}{V_{VOC}(L/s) + V_{Carrier\ Gas}(L/s)} \times 10^{-4} \tag{eq. 4.20}$$

Table 4.4- Other constants used for thermodynamics characterization.

Ideal Gas Constant, R (L.atm/mol.K)	0.08206
Heat Capacity$_{air}$ (cal/g.K)	0.445
Water vapour pressure$_{Room\ Conditions}$ (bar, 20 ºC)	0.02275
Water vapour pressure$_{Solution}$ (bar, 24 ºC)	0.02912

4.2.5. Operational characterization of a mass flow controller

A mass flow controller (MFC) was connected to a bottle of compressed nitrogen using silicone tubing (Fig. 4.5a). Gas leaks were checked with a mixture of water and soap and mitigated by tightening the joints with proper PTFE insulation (Fig. 4.5b-c).
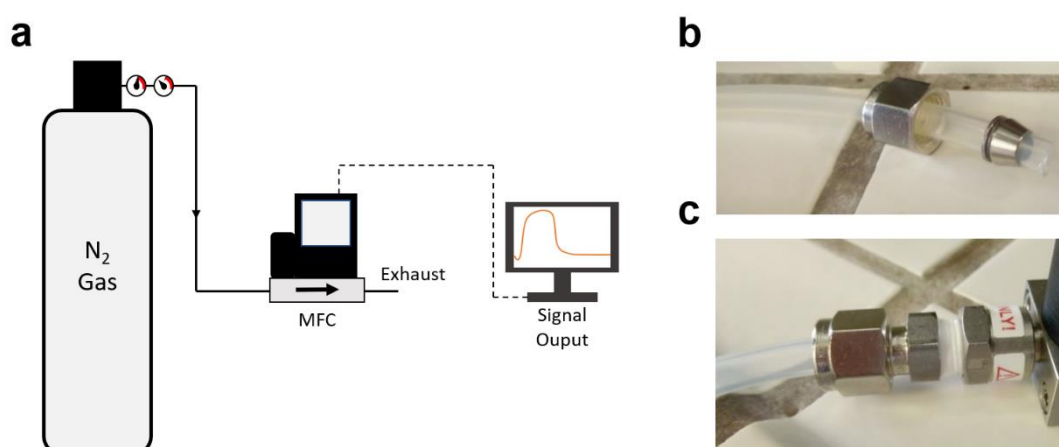
Figure 4.5- (a) Experimental apparatus for analysing MFC's output data; (b-c) connection of silicon tubing to the MFC.

The operation of the MFC was studied by quantifying several features of the flow rate profiles generated for a range of different combinations of nitrogen flow rates (0.125, 0.250, 0.500, 1.250, 2.500, 5.000 sccm) and nitrogen pressures (0.5, 1.0, 1.5, 2.0 bar). Each nitrogen pressure was tested for each flow rate, defined as the setpoint on the MFC.

Prior to starting the assay, the MFC setpoint was manually set to 0.000 sccm and the MFC was adjusted for measuring nitrogen gas.

An in-house made Python script was used to further program the MFC setpoints, to switch between exposure (MFC ON) and recovery periods (MFC OFF) and to register the generated flow rate profiles. Exposure and recovery periods were set at 5 and 25 seconds respectively. At the start of each exposure period, the MFC setpoint was automatically switched from 0.000 sccm to the specified flowrate (setpoint) and, inversely, at the start of each recovery cycle, back to 0.000 sccm.

Output flow rate profiles were registered for five exposure/recovery periods (Fig. 4.6) to each nitrogen pressure and flowrate setpoint. Average values and corresponding standard deviations of the lag times (required time for flowrate stabilization) in exposure/recovery periods and maximum/minimum values of

the error signal (difference between the setpoint and measured flow rate) in exposure period were calculated and represented as a percentage (Eq. 4.21).

$$Fluctuation\ Error\ (\%) = \frac{|Setpoint - Extreme|(sccm)}{Setpoint\ (sccm)} \times 100\ \% \qquad (eq.\ 4.21)$$

where *Extreme* is defined as the average maximum (Fig. 4.6b) or minimum values (Fig. 4.6c) of the error signal.
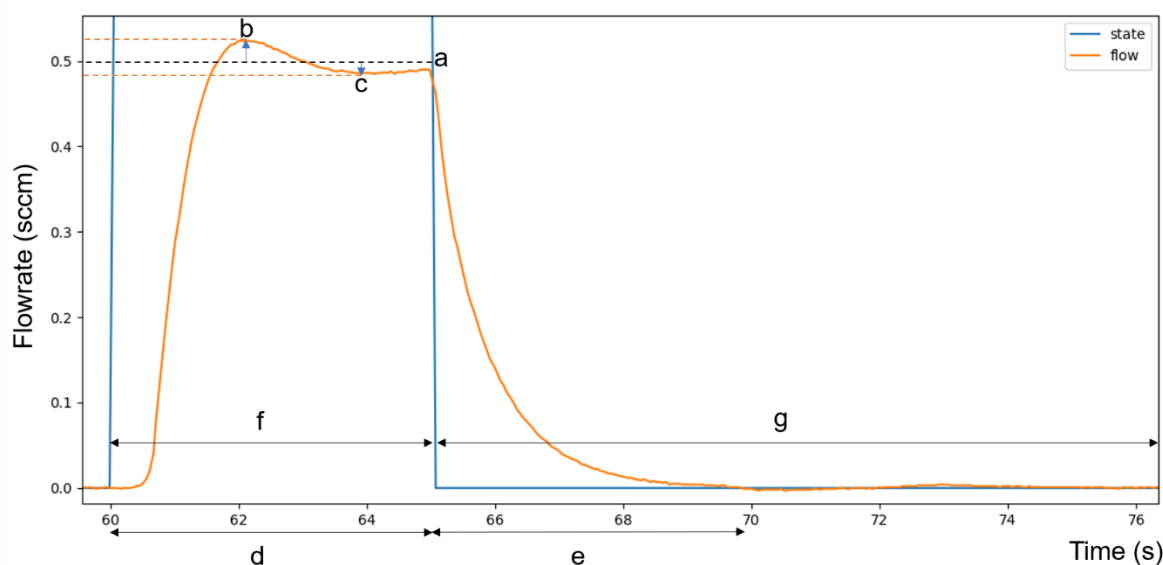
Figure 4.6- Output data of the mass flow controller, showing the profile of the generated flow rate with time (orange). From the profile, the following features were extracted: (a) setpoint; (b) difference between maximum error and setpoint; (c) difference between minimum error and setpoint; (d) lag time in exposure period; (e) lag time in recovery period; (f) exposure period; (g) recovery period.

4.2.6. Plan and design of an optimized VOC delivery system

Having in consideration the operational characteristics of the mass flow controllers and the needs regarding e-nose characterization towards VOC sensitivity and limits of detection, an apparatus for generation and delivery of controlled concentrations of VOCs to the e-nose was planned and ordered to Paralab.

4.3. Results and Discussion

4.3.1. Estimation of VOC concentrations fed to the e-nose with the current odorant delivery system

With the current odorant delivery system, ambient air – sampled as carrier gas – pushes the VOC accumulated in the headspace of the sample chamber at the start of each exposure period. In the

remainder duration of the exposure, it is the VOC resulting from solvent evaporation that mixes in with the air and is sampled into the e-nose.

To characterize the conditions under which the VOCs are sent to the e-nose, two different contributions were considered for calculating the VOCs concentrations (Fig. 4.7), one resulting from the gas-liquid equilibrium, established in the chamber headspace during the recovery period – corresponding to the concentration sampled in an initial pulse of carrier gas (~1 second) at the start of each exposure (pulsed VOC) (Fig. 4.7a) – and another originating from the amount of VOC evaporated throughout exposure (steady VOC) (Fig. 4.7b).
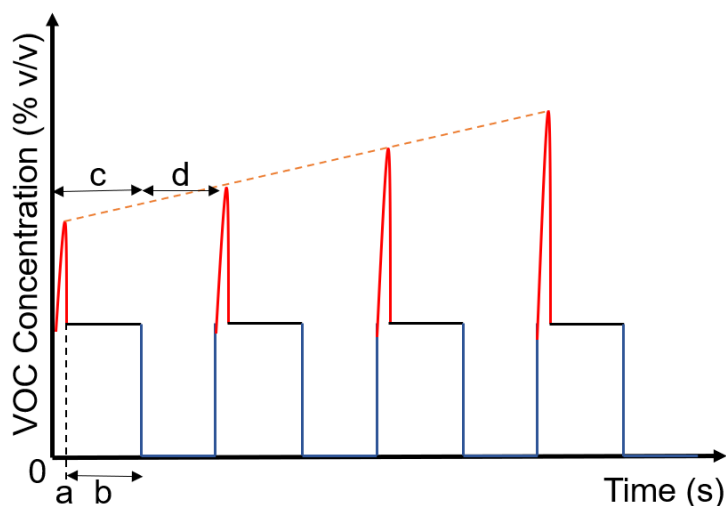
Figure 4.7- VOC concentration profile at the e-nose inlet; (a) first pulse of VOC (~1 second); (b) steady VOC concentration; (c) exposure period; (d) recovery period.

The steady VOC concentration shows a stable profile (Fig. 4.8a-f), varying between 10 to 20 % (v/v) for the generality of solvents, but for diethyl ether and dichloromethane (Fig. 4.8a, e) it shows a slight decline through time. The pulsed VOC concentration grows steadily with time, from about 20 to 40 % (v/v) depending on the solvent (Fig. 4.8a-c, e-f), except for ethanol (Fig. 4.8d), maintaining a fixed value at about 25 % (v/v). The stated growth is related with the loss of liquid solvent due to evaporation, as a larger headspace volume results in a higher gas phase equilibrium composition. Accordingly, for ethyl acetate and ethanol – the solvents with the lowest vapour pressures (Table 4.5) – that phenomenon is less emphasized (Fig 4.8c-d), as less solvent is lost through evaporation. Similarly, a decrease in the equilibrium composition of acetone is registered, after a 5 mL refill was performed at 2 h (Fig 4.8f).

The pulsed VOC concentrations are generally higher than the steady VOC concentrations, which suggests that the e-nose receives a concentrated pulse of VOCs at the immediate start of each exposure, which becomes progressively more concentrated as time elapses. In future, it should be studied whether the hybrid gels response to VOCs is affected by these initial pulses.
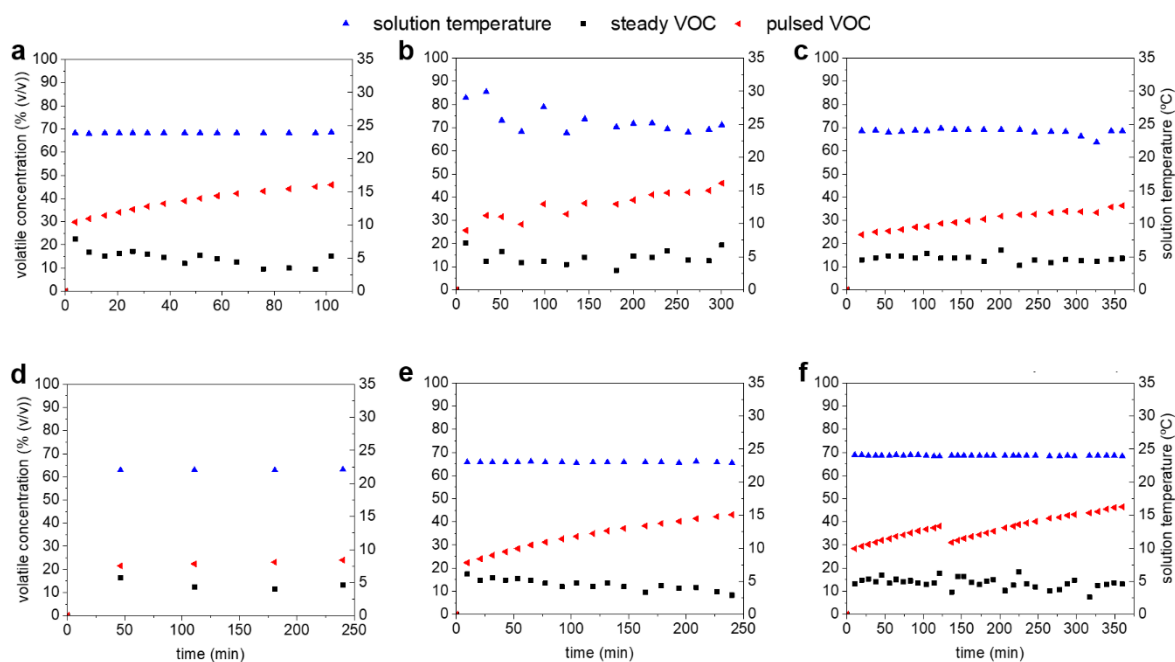
Figure 4.8- Profiles of VOC concentration sampled to the e-nose throughout time, split between steady VOC concentration (black) and pulsed VOC concentration (red). Solvent temperature (blue) is also shown. (a) diethyl ether; (b) hexane; (c) ethyl acetate; (d) ethanol; (e) dichloromethane; (f) acetone.

The solvent's temperature fluctuations have a direct impact on the equilibrium concentration (pulsed VOC), visible for hexane and dichloromethane (Fig. 4.8b-c), where an analogous fluctuation is observed for hexane (Fig. 4.8b), and a similar decrease occurs at about the 300-minute mark for dichloromethane (Fig. 4.8c). For the remainder solvents (Fig. 4.8a, c-f), a constant temperature translates into a linear increase of the pulsed VOC concentration.

Due to slow evaporation rates, the reference points for ethanol (Fig. 4.8d) are comparably farther away – as a larger amount of time elapses between measurements. Similar results are obtained for toluene and isopropanol (Appendix V, Fig. A10a-b).

Table 4.5- Average vapour pressures of the tested VOCs at the respective operating temperatures.

Solvents	Ethanol	Ethyl Acetate	Hexane	Acetone	Dichloromethane	Diethyl Ether
Chemical Formula	C_2H_5OH	$C_4H_8O_2$	C_6H_{14}	C_3H_6O	CH_2Cl_2	$(C_2H_5)_2O$
Vapour Pressure (bar)	0.06	0.12	0.19	0.29	0.53	0.66

The results show that it is possible to estimate the VOC composition of the carrier stream fed to the in-house built e-nose during the standard experiments carried out in the Laboratory in the daily routine to test the responsivity of hybrid gels. The currently detected VOC concentrations are thus within 10% and 40% (Table 4.6) and correspond to the currently known detection capabilities of the gels, as no other conditions have been tested yet.

Comparing the currently detected VOC concentrations with those tested for the same VOCs in other works, it is seen that the hybrid gel films currently detect VOC concentrations several orders of

magnitude higher (about 10^5-10^6 parts-per-million) than those tested in other works (at the sub-ppm range[40]) (Table 4.6). Thus, the hybrid gel films are likely to be working under saturation of VOCs[46,89] and their effective limits of detection and sensitivity are still unknown.

Table 4.6- Comparison between average VOC concentrations detected with the proprietary hybrid gel films and the limits of detection of other types of gas sensors.

VOC	Detected VOC Concentrations				
	Hybrid Gel Films[8]		IL-Polymer[23]	Functionalized Carbon Nanorods[40]	Microring Resonator[43]
	Pulsed VOC	Steady VOC			
Ethanol	23%	13%	0.50%	0.4 ppm	-
Acetone	37%	15%	-	0.4 ppm	0.1 ppm
Isopropanol	26%	14%	-	0.4 ppm	-
Toluene	33%	12%	-	0.4 ppm	20 ppm
Diethyl Ether	39%	15%	-	0.4 ppm	-
N-Hexane	37%	14%	-	-	-
Dichloromethane	34%	13%	0.50%	-	-
Ethyl Acetate	30%	14%	-	-	-

The presence of humidity in the carrier stream has a quantitative impact on the VOC composition of the gas phase, as a higher molar fraction of water results in the lowering of the molar fraction of VOC in the binary mixture, in accordance with previously reported works[76]. For concentrations as high as tenths of percent-per-volume, the impact of humidity may be of little importance from a quantitative point of view, but as VOC concentrations are further diluted, the presence of humidity may become a serious interferent[76], diluting the VOCs below what is anticipated[71]. Moreover, it remains uncertain whether higher or lower values of relative humidity – compared to those at the days of the experiments (~45 – 65 %) – may change the rate at which solvents evaporate, as carrier gas passes through the sample chamber's headspace.

4.3.2.   Operational characterization of a mass flow controller

With the current gas delivery system, the VOC concentration profile in the exposure period fluctuates and is restricted to high values (tenths of percent-per-volume), due to the fixed carrier gas flowrate. To optimally evaluate the e-nose response to VOCs, the delivery system must be able to generate constant and more diluted VOC concentrations in successive step-changes (Fig. 4.9), so that the response time, sensitivity and limits of detection of the e-nose can be characterized.
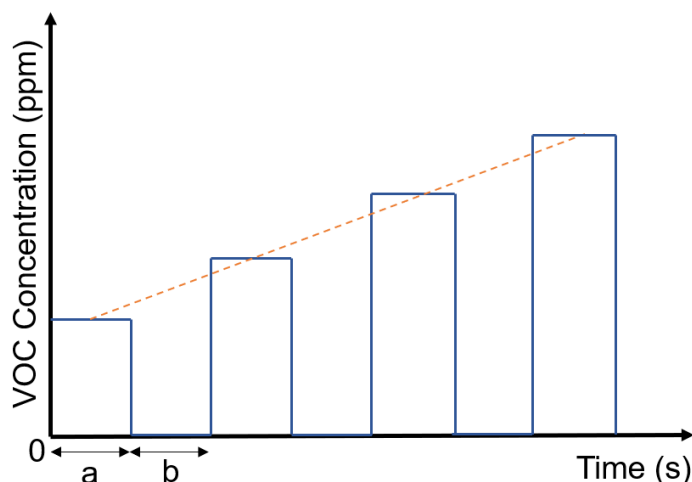
Figure 4.9- Ideal VOC concentration profile at the e-nose inlet; (a) exposure period; (b) recovery period.

An experimental apparatus to assess the sensitivity of hybrid gel films towards varying concentrations of VOCs can be schematized as represented in Fig. 4.10. VOCs are provided to the e-nose through the carrier stream of MFC I which is bubbled through the sample chamber. The stream of MFC II dilutes the VOC concentration until the desired value, upon mixture of both currents. The exposure and recovery periods are defined by alternately setting the MFC I ON or OFF, with MFC II remaining ON, on a fixed setpoint.

To ensure a controlled VOC concentration reaching the e-nose inlet, the MFC I performance must be characterized. Since the responsivity of the MFC is not immediate, a lag time is expected to occur at the start of each exposure/recovery period[96],which may reflect in the e-nose response. Moreover, during the lag time, the flow rate may fluctuate, which also has an impact on the e-nose response.

Therefore, it is important to characterize the MFC I lag time and error signal, to define the operational conditions that minimize this response delay and fluctuation. To that end, the lag time and error signal after a step-change of the flow rate setpoint of MFC I were measured. Several set points and nitrogen pressures were tested, based on the range required to generate VOC concentrations from 10^6 down to 10^0 ppm[46], with the pressures made available by the laboratory equipment.
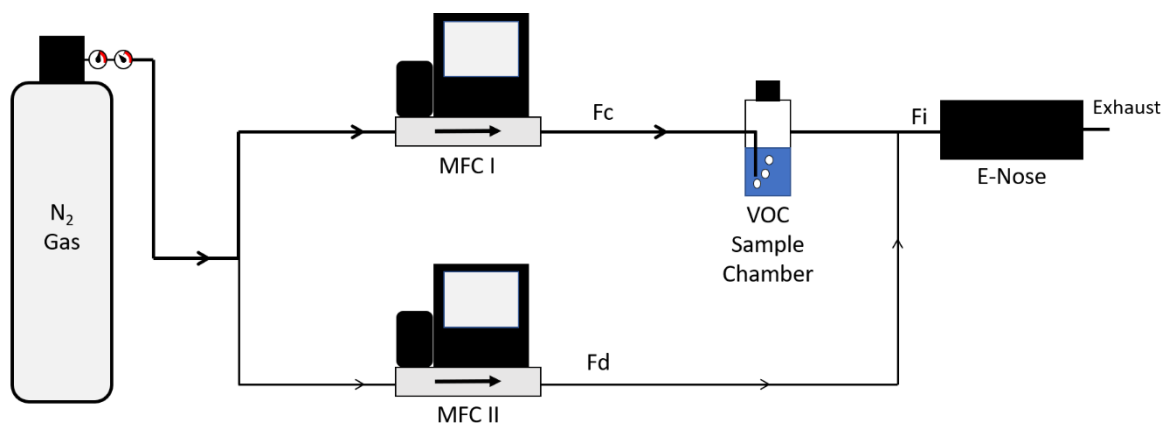
Figure 4.10- Arrangement of the suggested apparatus for varying VOC concentrations. The exposure course is highlighted in bold. Fc, flowrate of the carrier stream; Fd, flowrate of the dilution stream; Fi, flowrate of the inlet stream, resulting from the mixture of streams Fc and Fd.

The reading accuracy (eq. 4.22)[96] of the MFC I was assessed, for pressures from 0.5 to 1.0 bar, being estimated as $\pm\ 1\ \%$ from the setpoint.

$$Reading\ accuracy\ (\pm\%) = \frac{Deviation\ (sccm)}{Setpoint\ (sccm)} \times 100\ \%$$ (eq. 4.22)

4.3.2.1. Analysis of MFC lag time

Regarding the lag time to a setpoint in the exposure period (Fig. 4.11a) , some differences are noticed for the range of tested flow rates. Particularly, for the highest flow rate setpoint (5.000 sccm), a remarkable increase in lag time (about 1.5 seconds) is observed from 0.5 to 2.0 bar. For intermediate flow rates (1.250 - 2.500sccm), no changes occur. Regardless of the nitrogen pressure, the lag time is reduced the higher the set point. For the lower flow rate setpoints (0.125 – 0.500 sccm) – expected for generating 10^0 to 10^1 ppm of VOCs – a higher nitrogen pressure offers a lower lag time, not registered in the tested exposure duration (5 s) for pressures below 2.0 (0.125 sccm) or 1.0 bar (0.250 sccm).

Regarding the lag time to 0 sccm starting from different setpoints (Fig. 4.11b), a less notable dependence upon varying pressures is noticed for the different flowrates. In general, independently of the pressure, the lower the setpoint, the lower becomes the lag time, ranging between 4 s and 9 s. Additionally, with increased pressure, the lag time approaches a linear relationship with the setpoints, becoming obvious at 2.0 bar ($R^2 = 0.89$).
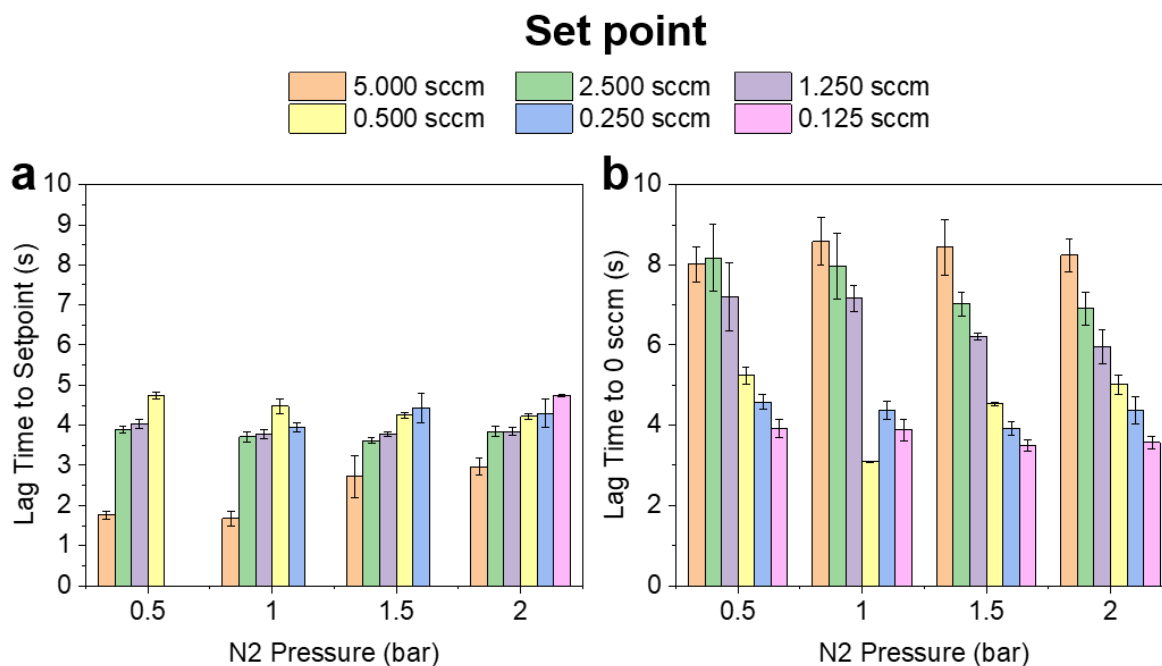
Figure 4.11- Mass flow controller lag time for different flow rate setpoints and varying nitrogen pressures. (a) Lag time after a step change from 0 sccm to a given setpoint; (b) Lag time after a step change from a given setpoint to 0 sccm. Absent bars indicate unregistered flow rate stabilization to setpoint;

Given the short duration of the exposure period in standard e-nose experiments (5 s), the lag times measured after a step change in setpoint (Fig. 4.11a) may affect the controlled VOC concentration fed to the e-nose, as it constitutes ~80 % of the exposure period. Nevertheless, the works that employed similar VOC sampling systems for gas sensors did not address this topic[23,45,66,71,89], possibly due to the longer exposure periods.

The lag time for the setpoint of 0 sccm at the start of each recovery period (Fig. 4.11b), is of less concern compared to what applies for exposure, as it represents only ~23 % of the recovery period.

4.3.2.2. Analysis of MFC setpoint fluctuation error

For inferring how far away the flowrate deviates from the setpoint, an analysis of the error signal – the difference between the setpoint flow rate and the measured flow rate[96] – was conducted through a discreet analysis, regarding only the maximum (positive fluctuation) and minimum value (negative fluctuation) of the error signal.

An integral calculation of the total error signal would have been more accurate, providing the total flowrate that deviates from the setpoint, however, in the scope of the present analysis, the current data was enough for extracting the required conclusions.

Remarkable differences are noticed between the higher (Fig, 4.12a-c) and lower (Fig. 4.12d-f) ranges of flow rate setpoints, particularly regarding the magnitude of the fluctuation and its dependence on nitrogen pressure.

For the higher flow rate setpoints and maximum operating pressure (2.0 bar), the positive/negative fluctuations are below (Fig, 4.12a-b) or close to (Fig, 4.12c) the reading accuracy of the MFC (1 %).

Regarding the lower flow rate setpoints (Fig, 4.12d-f), increasing the nitrogen pressure results in a growth of the positive fluctuation, to about 15 % (Fig, 4.12e) or 25 % (Fig, 4.12f) at 2.0 bar, except for 0.500 sccm (Fig, 4.12d), remaining closer to the MFC reading accuracy. A similar dependence is observed for the negative fluctuations, though in a smaller extent (Fig, 4.12d-f).

The instability of the flow rate as the setpoint becomes lower may be associated to it being farther away from the mass flow controller's designed setpoint (5.000 sccm).
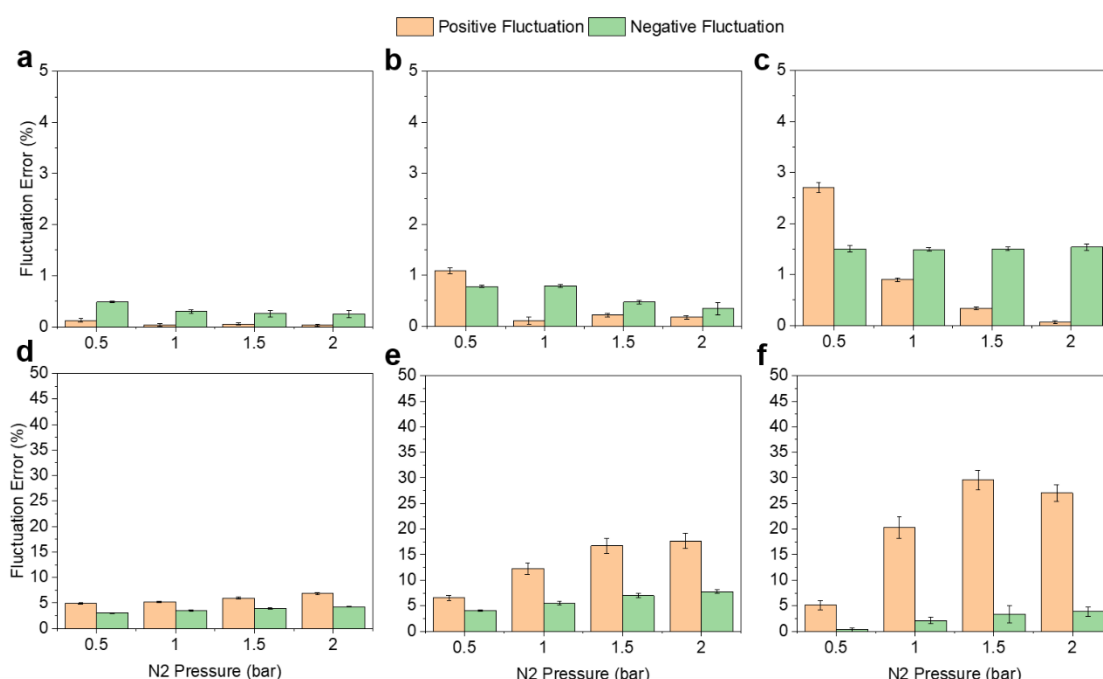
Figure 4.12- MFC positive fluctuation (orange) and negative fluctuation (green) errors during the lag time in exposure period, for varying nitrogen pressures and several setpoints: (a) 5.000 sccm, (b) 2.500 sccm (c) 1.250 sccm, (d) 0.500 sccm, (e) 0.250 sccm, (f) 0.125 sccm.

Evaluating the data on the lag time and the error combined, it is possible to conclude that the best operating nitrogen pressure for the range of tested setpoints is of 2.0 bar, because it reduces the positive/negative fluctuations of the higher flow rates and the lag time of the lower flow rates.

To compensate for the increased fluctuations in the lower flow rates, which could hinder the e-nose response to more diluted VOC concentrations, the exposure period could be extended until a stabilized flowrate, and thus a constant VOC concentration, was achieved.

The MFC functions under a proportional, integral plus derivative (PID) action[96] for correcting the flow rate to the setpoint, so a second approach could be the optimization of the individual P, I and D parameters, which however is ideally done by the MFC manufacturers[97].

The limitations of the MFC performance were thus addressed by implementation of a control system in an optimized gas delivery system, to mitigate both the lag time and the positive/negative fluctuations.

4.3.3. Proposed design for an optimized controllable VOC delivery system for the e-nose

Considering the need for generating VOC concentrations in the ppm range and the functional limitations of the carrier mass flow controller (MC-5SCCM-D/5M, 5IN, Alicat Scientific Inc.) to alternate between setpoints, an optimized version of the afore-mentioned VOC delivery apparatus (Fig. 4.10) was planned in collaboration with Paralab (Fig. 4.13).

To compensate for the limitations of the carrier mass flow controller (Fig. 4.13, no. 2), a two-way solenoid valve (Fig. 4.13, no. 4) was adapted at its outlet. Its purpose is to switch the carrier stream onto an exhaust line for five seconds, the duration of the lag time, thus preventing an unintended flow rate to be fed to the VOC sample chamber (Fig. 4.13, no. 6). After the setpoint is reached, the valve switches back to the main stream, towards its intended course.

At the outlet of the dilution mass flow controller (MC-5SLPM-D/5M, 5IN, Alicat Scientific Inc.) (Fig. 4.13, no. 1) a glass vial was installed (Fig. 4.13, no. 5), to provide the possibility of generating controlled levels of relative humidity, through bubbling of supersaturated salt solutions. This assembly would allow to evaluate the e-nose response to known VOC concentrations under different humidity conditions.

Two check-valves (Fig. 4.13, no. 3) were installed at the outlet of each glass vial to avoid backflow and allow mixing of the carrier and dilution streams, prior to be fed to the e-nose, at the outlet of the apparatus.

The glass vial containing the volatile sample (Fig. 4.13, no. 6) is installed in the lower stage of the apparatus to enable the easy installation of a thermal bath for maintaining the sample under fixed temperatures, which would not be possible if the sample was to be positioned in the upper stage.

The tubing (6 mm) and adaptors are made of stainless-steel. Check valves and nuts are made in Teflon. The high quality material prevents the condensation of water vapour and adsorption of VOCs in the equipment[2,88]. The assembled system is installed in a portable stainless-steel support.
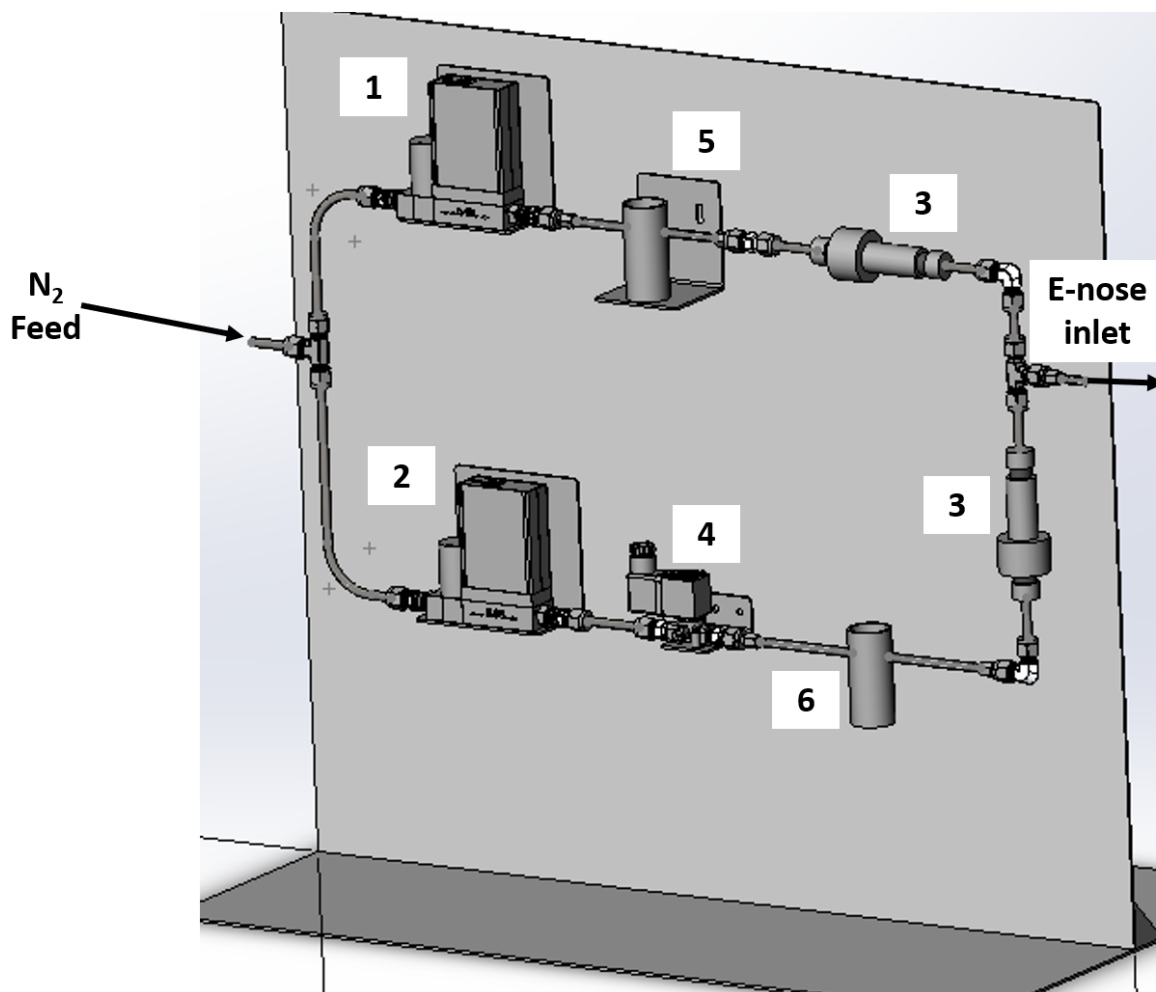
Figure 4.13- Proposed VOC delivery system, suitable for an e-nose sensitivity study. (1) dilution MFC (MFC II); (2) carrier MFC (MFC I); (3) check-valves; (4) two-way solenoid valve; (5) supersaturated salt solution; (6) solvent chamber. Three-dimensional design was provided by Paralab.

Comparing the presently proposed system with previous works[45,46,89,92], some similarities are found regarding the key features of a VOC delivery system, namely the use of mass flow controllers for manipulation of the carrier flowrate (nitrogen[23,91], argon[89], purified[92] or dry air[46]) to generate a range of different VOC concentrations, either with a single[45,89] or multiple[46,92] dilution stages. The use of a second, or vials in series, for generating a desired humidity allows for a wider range of analysis possibilities – a similar approach to a previous work that bubbled water at the outlet of the MFC[92],but limited to a fixed relative humidity of 45 %.

A similar approach for stabilizing the carrier stream was employed[46], in which a three-way valve switches the VOC carrier stream to an exhaust line for one minute, before being sampled to the detection chamber for a period of two minutes. With the proposed apparatus, a period of 5 seconds is expected to be enough to stabilize the carrier stream.

Overall, in other works, exposure and recovery periods have a duration of two to three minutes each[23,46,89] to which the short lag time of the carrier MFC is of minor relevance.

Gas mixers are often employed before the inlet of the e-nose or sensing chamber for homogenising the gasses[23,45,89,92], yet similar results are obtained for an immediate mixture of the multiple streams[46,91].

Once the apparatus is made available, the e-nose sensitivity should be studied by progressively diluting the sampling stream below the presently sensed VOC concentrations, allowing for a correlation between the hybrid gel films' response and the generated concentrations, and for the determination of the several LODs. Farther, the manipulation of the relative humidity should be accessed to accurately determine its impact on the responses to different VOCs.

4.3.4. Analytical & mathematical approaches towards VOC quantification

For precisely determining the concentrations of VOCs sampled to the e-nose with the proposed VOC delivery system, either a mathematical or an analytical approach may be implemented.

The mathematical methodology is based upon the thermodynamics principle of saturation of the carrier gas with the gaseous VOC in the sample chamber[23], usually done through bubbling of the liquid solvent[2], being dependent upon the components of the gas mixture and whether humidity is present[66], and on the vapour pressures of each[45,46]. The analytical technique, would consist of directly quantifying the sampling stream at the e-nose inlet using a mass-spectrometry device[94], allowing for a precise quantification of the present VOCs.

Ideally, both methods should be applied, thus validating the mathematical approach through the more precise MS quantification technique.

4.4. Conclusions

The concentrations of eight VOCs currently sampled to the in-house built e-nose in standard experiments were estimated and an optimized VOC delivery system was proposed for producing more diluted and controlled VOC concentrations.

The calculation of the VOC concentrations was based on approximate rates of solvent evaporation from a sample chamber and on the application of thermodynamic principles. VOC concentrations resulting from the gas-liquid phase equilibria and from the evaporated VOCs during exposure to an ambient air stream were simultaneously considered. As the volume of the sample chamber´s headspace increases, the VOC concentration resulting from gas-liquid phase equilibrium grows linearly from ~20 to 40 % (v/v), depending on the total time span and tested VOC. The VOC concentration derived from solvent evaporation during exposure is constant throughout time, between ~10 to 20 % (v/v) for the generality of tested VOCs. The temperature has a direct effect on these parameters, as it influences the VOC's vapour pressure. Under the present conditions, the array of hybrid gel films housed in the e-nose is likely sensing VOCs under saturated conditions, when compared to the generality of works[46,89].

The planning of the optimized VOC delivery system started by performing a process control study of the carrier mass flow controller to determine its lag time, fluctuation error and the optimal operating nitrogen pressure, for a range of flow rate setpoints. Higher nitrogen pressures were found to stabilize all flow rates after a certain lag time. For the lower flow rates (0.125 – 0.500 sccm) a lag time between 4 s and 5 s was measured at 2.0 bar, while for the higher flow rates (1.125 – 5.000 sccm), a slightly lower lag time (3 s - 4 s) was measured at the same pressure. The lag time from the setpoint to 0 sccm reduces the lower the flow rate. The fluctuation error was low for the higher flow rates (~0 – 3 %) and nearly mitigated with increasing pressure, while for the lower flow rates it became more significant (~5 – 30 %), increasing with increasing pressure, and with a bigger impact the smaller the setpoint.

To compensate for the detected carrier MFC limitations, an automated two-way valve was added to the VOC delivery system, to direct the carrier stream to an exhaust line until stabilization of the flowrate is achieved. The use of stainless steel and Teflon in the tubing of the proposed apparatus mitigates gas leaks, and prevents humidity condensation and VOC adsorption in the tubing[2,88]. The addition of a second glass chamber for inorganic salt solutions will allow to generate fixed relative humidity levels. In future, the proposed optimized VOC delivery system will provide controlled conditions for the characterization of the e-nose regarding its response time, sensitivity and limits of detection towards VOCs as it enables the generation of diluted VOC concentrations (10^0 – 10^6 ppm) and their delivery as step variations to the e-nose, with precise control of the flowrate. Further on, it is intended to explore its potentiality to perform an in-depth cross study on the hybrid gel films, combining different VOCs' dilutions, sampled under different relative humidity conditions.

5. Concluding remarks and future perspectives

The present work is integrated in the process development of new hybrid gel film gas sensors and of an in-house built e-nose at the Biomolecular Engineering Lab. The first part aimed towards developing a controlled relative humidity system and studying the effect of humidity on the response of hybrid gel films. In the second part, the current VOC delivery system of the e-nose was characterized, and an optimized apparatus was planned, aimed towards the precise control of the VOC concentrations sampled into the e-nose and the study of the e-nose sensitivity and limits of detection.

The effect of relative humidity on proprietary hybrid gel films, composed by 5CB, one of [BMIM][DCA] or [BMIM][Cl] and gelatine was investigated through their optical response in an in-house built e-nose and through POM. Supersaturated inorganic salt solutions were used for generating four levels of relative humidity (25, 36, 50 and 65 %), and distilled water for 80 %. Nitrogen gas was bubbled through these solutions, using an MFC, and sampled into the e-nose, housing the array of sensitive gel films. A method for removing the humidity in the sampling stream using a fixed-bed of molecular sieves was investigated and a preliminary cross-study of the hybrid gel films' optical response to three selected VOCs – hexane, acetone and ethanol – under different relative humidity environments was performed.

It was found that the change in the hybrid gel films' IL anion confers distinctive responses towards humidity. Films containing [BMIM][DCA] were highly responsive to humidity changes, quickly achieving stable-state response that is reversible, increasing its optically active area for higher humidity levels and becoming inoperable at conditions of 0 % relative humidity. The relative amplitude of optical response of these films has shown a strong linear correlation with the sampled relative humidity. Films with [BMIM][Cl] were not as responsive, hardly achieving stabilization and suggesting irreversible conditions over time. The waveform features of these films' optical response were evaluated as a function of the relative humidity gradient between the sample and room conditions. The film's response became weaker the lower the gradient, with hardly any visible relative amplitude for null and negative gradients. For positive gradients, the film's signal increased with humidity and decreased upon drying, with a relative amplitude restricted to small variations. Further work is however needed to determine a mathematical description of the correlation between humidity and the film's responses.

Future work is required to assess the hybrid gel films properties through analytical techniques – Karl Fischer titration, rheology and thickness tests – to help understanding mass-transfer phenomena of water in the hybrid gels and validate the relative humidity gradient concept, based on the water diffusion properties and water-retention capability evinced by films containing [BMIM][Cl]. Mean grey values of the POM images should be obtained to more precisely compare the optically active area of the hybrid gel films, after exposed to different humidity environments.

The molecular sieves (4Å, 8-12 mesh size) provided an efficient removal of the humidity in the nitrogen gas sampling stream, however for a limited time (30 seconds for 85 % relative humidity sampled), until saturation started to occur. Hereafter, molecular sieves of smaller size and more selective towards water molecules (3Å, 4-8 mesh size) should be tested, possibly providing a longer period of humidity

control, as more sieves may be housed in a similar fixed-bed. Further, their efficiency should be tested with ambient air and in humidity removal from the headspace of complex VOCs containing gas-mixtures.

When mixed with a humidified nitrogen stream, VOCs with increased polarity were found to affect the controlled relative humidity profile and the optical response of the hybrid gel films. Films containing [BMIM][DCA] evinced a baseline drift – increasing when humidity decreased and vice-versa – while films with [BMIM][Cl] suffered changes in the optical-response's relative amplitude – reducing with the decrease of humidity. The less polar VOCs most always saturated the optical response, and, for 0 % relative humidity, the films containing [BMIM][DCA] shown no response whatsoever. Overall, the increased relative humidity lowered the optical signal baseline for films with [BMIM][DCA] and heightened the response's relative amplitude for both studied films. The optimal operational conditions for sensing VOCs with films containing [BMIM][DCA] seem to be at the maximum relative humidity, while for films with [BMIM][Cl], the most favourable conditions are at 0 % relative humidity, where a response is still visible without the interference of humidity. In the future, more VOCs should be tested, further diluted in the sampling stream to avoid saturation of the optical response, thus aiding in the assessment of the humidity's drift effect – possibly drawing a correlation between the humidified VOC's response and the sampled relative humidity – and relating it to the previous findings of its isolated influence.

In the second part of this work, the VOC delivery system currently installed in the Laboratory's e-nose was characterized regarding the concentrations of eight VOCs usually fed to the e-nose for quality assessment of the VOCs concentration profile. An optimized gas delivery system for generating known diluted VOC concentrations using MFCs was proposed and approved, for which effect a process control study on the lag time and fluctuation error of the carrier MFC was conducted, for a range of setpoints (0.125 – 5.000 sccm) and operating nitrogen pressures (0.5 – 2.0 bar).

Regarding the current VOC delivery system, it was found that the VOCs concentrations fed to the e-nose have one contribution from VOC generated in the gas-liquid phase equilibria and another contribution from the VOC evaporation by the carrier stream. The contribution of gas-liquids phase equilibria grows in a linear tendency with time, generally ranging from about 20% to 40 % (v/v), as the headspace volume of the sample chamber increases, due to solvent evaporation. The contribution of VOC evaporation by the carrier stream is constant (10% to 20 % (v/v)). These thresholds suggest that the hybrid gel films are sensing VOCs in concentrations above the ideal, when compared to the significantly lower detecting capabilities of other works – in the range of ppm to sub-ppm.

The nitrogen pressure of 2.0 bar overall optimized the MFC's lag time and fluctuation error, however increasing the fluctuation for the lower setpoints (0.125 – 0.500 sccm). These limitations were assessed by insertion of a two-way automated valve on the proposed apparatus, directing the flowrate to an exhaust line until stabilization. A second glass chamber was further added in the dilution stream, for generating desired levels of relative humidity through bubbling of supersaturated inorganic salt solutions. In the future, the planned apparatus potential should be explored for studying the correlation

of the hybrid gel films' optical-response with known VOCs concentrations and for the determination of the response-times and of the correspondent LODs. Further, it should be used to perform a comprehensive study of the humidity drift effect on the films' optical response to several VOCs, manipulating both the VOCs concentration and the level of relative humidity.

6. Bibliography

1. Gardner, J. W. & Bartlett, P. N. A brief history of electronic noses. *Sensors Actuators B. Chem.* (1994). doi:10.1016/0925-4005(94)87085-3

2. Pearce, T. C., Schiffman, S. S., Nagle, H. T. & Gardner, J. W. *Handbook of Machine Olfaction - Electronic Nose Technology*. (Wiley-VCH, 2002). doi:10.1002/3527601597

3. De Blas, M., Navazo, M., Alonso, L., Durana, N. & Iza, J. Automatic on-line monitoring of atmospheric volatile organic compounds: Gas chromatography-mass spectrometry and gas chromatography-flame ionization detection as complementary systems. *Sci. Total Environ.* **409,** 5459–5469 (2011). doi: 10.1016/j.scitotenv.2011.08.072

4. Wilson, A. D. & Baietto, M. Advances in electronic-nose technologies developed for biomedical applications. *Sensors* **11,** 1105–1176 (2011). doi: 10.3390/s110101105

5. Fallis, A. . *Volatile Organic Compounds in the Atmosphere. J. Chem. Inf. Model.* **53,** (2013). doi: 10.1017/CBO9781107415324.004

6. Hong-Geller, E. & Adikari, S. Volatile Organic Compound and Metabolite Signatures as Pathogen Identifiers and Biomarkers of Infectious Disease. *Biosensing Technol. Detect. Pathog. - A Prospect. W. Rapid Anal.* (2018). doi:10.5772/intechopen.72398

7. Korotcenkov, G. *Handbook of Gas Sensor Materials.* **1,** (Springer New York, 2014). doi: 10.1007/978-1-4614-7388-6

8. Hussain, A. *et al.* Tunable Gas Sensing Gels by Cooperative Assembly. *Adv. Funct. Mater.* **27,** 1–9 (2017). doi: 10.1002/adfm.201700803

9. Hierlemann, A. & Gutierrez-Osuna, R. Higher-order chemical sensing. *Chem. Rev.* **108,** 563–613 (2008). doi: 10.1021/cr068116m

10. Wilson, A. D. Diverse applications of electronic-nose technologies in agriculture and forestry. *Sensors (Switzerland)* (2013). doi:10.3390/s130202295

11. Zhang, S. *et al.* Spoiling and formaldehyde-containing detections in octopus with an E-nose. *Food Chem.* (2009). doi:10.1016/j.foodchem.2008.08.090

12. Yu, H., Wang, J., Yao, C., Zhang, H. & Yu, Y. Quality grade identification of green tea using E-nose by CA and ANN. *LWT - Food Sci. Technol.* (2008). doi:10.1016/j.lwt.2007.08.018

13. Schiffman, S. S., Wyrick, D. W., Gutierrez-Osuna, R. & Nagle, H. T. Effectiveness of an Electronic Nose for Monitoring Bacterial and Fungal Growth. *Proc. 7th Int. Symp. Olfaction Electron. Nose* 20–24 (2000).

14. Yang, J. S. & Swager, T. M. Fluorescent porous polymer films as TNT chemosensors: Electronic and structural effects. *J. Am. Chem. Soc.* **120,** 11864–11873 (1998). doi: 10.1021/ja982293q

15. Gibson, T. D. *et al.* Detection and simultaneous identification of microorganisms from headspace samples using an electronic nose. *Sensors Actuators B Chem.* **44,** 413–422 (1997). doi: 10.1016/S0925-4005(97)00235-9

16. Tait, E., Perry, J. D., Stanforth, S. P. & Dean, J. R. Identification of Volatile Organic Compounds Produced by Bacteria Using HS-SPME-GC – MS. 363–373 (2014). doi:10.1093/chromsci/bmt042

17. Cho, S.-Y. *et al.* High-Resolution p-Type Metal Oxide Semiconductor Nanowire Array as an Ultrasensitive Sensor for Volatile Organic Compounds. *Nano Lett.* (2016). doi:10.1021/acs.nanolett.6b01713

18. Gibson, T. D. *et al.* Detection and simultaneous identification of microorganisms from headspace samples using an electronic nose. *Sensors Actuators B Chem.* **44,** 413–422 (1997). doi: 10.1016/S0925-4005(97)00235-9

19. Holmberg, M. *et al.* Bacteria classification based on feature. **12,** 319–324 (1998). doi: 10.1023/A:1008862617082

20. Gardner, J. W., Craven, M., Dow, C. & Hines, E. L. The prediction of bacteria type and culture growth phase by an electronic nose with a multi-layer perceptron network. *Meas. Sci. Technol.* **9,** 120–127 (1998). doi: 10.1088/0957-0233/9/1/016

21. Sánchez, M., Guirado, R. & Rincón, M. E. Multiwalled carbon nanotubes embedded in sol–gel derived

TiO2 matrices and their use as room temperature gas sensors. *J. Mater. Sci. Mater. Electron.* (2007). doi:10.1007/s10854-007-9144-5

22. Chen, Y., Zhu, C. & Wang, T. The enhanced ethanol sensing properties of multi-walled carbon nanotubes / SnO 2 core/shell nanostructures. *Nanotechnology* (2006). doi:10.1088/0957-4484/17/12/033

23. Hou, K. Y., Rehman, A. & Zeng, X. Study of ionic liquid immobilization on polyvinyl ferrocene substrates for gas sensor arrays. *Langmuir* (2011). doi:10.1021/la104191n

24. Si, P., Mortensen, J., Komolov, A., Denborg, J. & Møller, P. J. Polymer coated quartz crystal microbalance sensors for detection of volatile organic compounds in gas mixtures. *Anal. Chim. Acta* (2007). doi:10.1016/j.aca.2007.06.050

25. Nurjuliana, M., Che Man, Y. B., Mat Hashim, D. & Mohamed, A. K. S. Rapid identification of pork for halal authentication using the electronic nose and gas chromatography mass spectrometer with headspace analyzer. *Meat Sci.* (2011). doi:10.1016/j.meatsci.2011.02.022

26. Hao, H. C., Chiangn, M. C. & Yao, D. J. Detection of hazardous vapors including mixture in different conditions using surface acoustic wave device array. in *9th IEEE International Conference on Nano/Micro Engineered and Molecular Systems, IEEE-NEMS 2014* (2014). doi:10.1109/NEMS.2014.6908754

27. Kakuda, D. Y. *Headspace Analysis of Food and Flavors, Theory and Practice. Trends in Food Science & Technology* **12,** (2001). doi: 10.1016/S0924-2244(02)00017-1

28. Narasimman, S. *et al.* Fabrication of ZnO thin film based VOC sensor. in *Springer Proceedings in Physics* (2017). doi:10.1007/978-3-319-44890-9_39

29. Sakai, G., Matsunaga, N., Shimanoe, K. & Yamazoe, N. Theory of gas-diffusion controlled sensitivity for thin ® lm semiconductor gas sensor. **80,** 125–131 (2001). doi: 10.1016/S0925-4005(01)00890-5

30. Rivera, D., Alam, M. K., Davis, C. E. & Ho, C. K. Characterization of the ability of polymeric chemiresistor arrays to quantitate trichloroethylene using partial least squares (PLS): Effects of experimental design, humidity, and temperature. *Sensors Actuators, B Chem.* **92,** 110–120 (2003). doi: 10.1016/S0925-4005(03)00122-9

31. Hossein-Babaei, F. & Ghafarinia, V. Compensation for the drift-like terms caused by environmental fluctuations in the responses of chemoresistive gas sensors. *Sensors Actuators, B Chem.* **143,** 641–648 (2010). doi: 10.1016/j.snb.2009.10.006

32. Hajmirzaheydarali, M. & Ghafarinia, V. A smart gas sensor insensitive to humidity and temperature variations. *IOP Conf. Ser. Mater. Sci. Eng.* **17,** (2011). doi: 10.1088/1757-899X/17/1/012047

33. Wongchoosuk, C., Lutz, M. & Kerdcharoen, T. Detection and classification of human body odor using an electronic nose. *Sensors* **9,** 7234–7249 (2009). doi: 10.3390/s90907234

34. Ghanbarian, M., Zeinali, S. & Mostafavi, A. A novel MIL-53(Cr-Fe)/Ag/CNT nanocomposite based resistive sensor for sensing of volatile organic compounds. *Sensors Actuators, B Chem.* **267,** 381–391 (2018). doi: 10.1016/j.snb.2018.02.138

35. Spinelle, L., Aleixandre, M. & Gerboles, M. *Protocol of evaluation and calibration of low- cost gas sensors for the monitoring of air pollution.* (2013). doi:10.2788/9916

36. Wei, P. *et al.* Impact Analysis of Temperature and Humidity Conditions on Electrochemical Sensor Response in Ambient Air Quality Monitoring. *Sensors* **18,** 59 (2018). doi: 10.3390/s18020059

37. Zhang, H., Lin, L., Liu, D., Chen, Q. & Wu, J. Optical nose based on porous silicon photonic crystal infiltrated with ionic liquids. *Anal. Chim. Acta* (2017). doi:10.1016/j.aca.2016.11.053

38. Zevenbergen, M. A. G., Wouters, D., Dam, V. A. T., Brongersma, S. H. & Crego-Calama, M. Ionic-liquid based electrochemical ethylene sensor. in *Proceedings of IEEE Sensors* (2011). doi:10.1109/ICSENS.2011.6126964

39. Hyodo, T. *et al.* Adsorption/combustion-type VOC sensors employing mesoporous γ-alumina co-loaded with noble-metal and oxide. *Sensors Actuators, B Chem.* (2015). doi:10.1016/j.snb.2015.06.065

40. Tripathi, K. M. *et al.* Green carbon nanostructured quantum resistive sensors to detect volatile biomarkers. *Sustain. Mater. Technol.* **16,** 1–11 (2018). doi: 10.1016/j.susmat.2018.01.001

41. Herberger, S., Herold, M., Ulmer, H., Burdack-Freitag, A. & Mayer, F. Detection of human effluents by a MOS gas sensor in correlation to VOC quantification by GC/MS. *Build. Environ.* (2010). doi:10.1016/j.buildenv.2010.05.005

42. Leidinger, M. *et al.* Highly sensitive benzene detection with MOS gas sensors. in *Proceedings Sensor 2017* (2017). doi: 10.5162/sensor2017/A4.3

43. Fu, D. *et al.* Polymer coated silicon microring device for the detection of sub-ppm volatile organic compounds. *Sensors Actuators, B Chem.* **257,** 136–142 (2018). doi: 10.1016/j.snb.2017.10.166

44. Herberger, S., Herold, M., Ulmer, H., Burdack-Freitag, A. & Mayer, F. Detection of human effluents by a MOS gas sensor in correlation to VOC quantification by GC/MS. *Build. Environ.* **45,** 2430–2439 (2010). doi: 10.1016/j.buildenv.2010.05.005

45. Lai, Y.-T., Kuo, J.-C. & Yang, Y.-J. A novel gas sensor using polymer-dispersed liquid crystal doped with carbon nanotubes. *Sensors Actuators A Phys.* **215,** 83–88 (2014). doi: 10.1016/j.sna.2013.12.021

46. Kim, Y. S., Ha, S. C., Yang, H. & Kim, Y. T. Gas sensor measurement system capable of sampling volatile organic compounds (VOCs) in wide concentration range. *Sensors Actuators, B Chem.* **122,** 211–218 (2007). doi: 10.1016/j.snb.2006.05.023

47. Hands, P. J. W., Laughlin, P. J. & Bloor, D. Metal-polymer composite sensors for volatile organic compounds: Part 1. Flow-through chemi-resistors. *Sensors Actuators, B Chem.* (2012). doi:10.1016/j.snb.2011.12.016

48. Wei, C., Dai, L., Roy, A. & Tolle, T. B. Multifunctional chemical vapor sensors of aligned carbon nanotube and polymer composites. *J. Am. Chem. Soc.* (2006). doi:10.1021/ja0570335

49. Santhanam, K. S. V, Sangoi, R. & Fuller, L. A chemical sensor for chloromethanes using a nanocomposite of multiwalled carbon nanotubes with poly(3-methylthiophene). *Sensors Actuators, B Chem.* (2005). doi:10.1016/j.snb.2004.09.034

50. Kuberský, P., Syrový, T., Hamáček, A., Nešpůrek, S. & Syrová, L. Towards a fully printed electrochemical NO2sensor on a flexible substrate using ionic liquid based polymer electrolyte. *Sensors Actuators, B Chem.* **209,** 1084–1090 (2015). doi: 10.1016/j.snb.2014.12.116

51. Zhang, H., Lin, L., Liu, D., Chen, Q. & Wu, J. Optical nose based on porous silicon photonic crystal infiltrated with ionic liquids. *Anal. Chim. Acta* **953,** 71–78 (2017). doi: 10.1016/j.aca.2016.11.053

52. Maity, D., Rajavel, K. & Kumar, R. T. R. Polyvinyl alcohol wrapped multiwall carbon nanotube (MWCNTs) network on fabrics for wearable room temperature ethanol sensor. *Sensors Actuators, B Chem.* (2018). doi:10.1016/j.snb.2018.01.152

53. Wongchoosuk, C., Wisitsoraat, A., Tuantranont, A. & Kerdcharoen, T. Portable electronic nose based on carbon nanotube-SnO2 gas sensors and its application for detection of methanol contamination in whiskeys. *Sensors Actuators, B Chem.* (2010). doi:10.1016/j.snb.2010.03.072

54. Malik, R. *et al.* A low temperature, highly sensitive and fast response toluene gas sensor based on In(III)-SnO 2 loaded cubic mesoporous graphitic carbon nitride. *Sensors Actuators B Chem.* (2018). doi:10.1016/j.snb.2017.09.193

55. Wang, Q. *et al.* Hydrothermal synthesis of hierarchical CoO/SnO2nanostructures for ethanol gas sensor. *J. Colloid Interface Sci.* **513,** 760–766 (2018). doi: 10.1016/j.jcis.2017.11.073

56. Carolina Pádua, A., Palma, S., Gruber, J., Gamboa, H. & Roque, A. C. Design and Evolution of an Opto-electronic Device for VOCs Detection. *Proc. 11th Int. Jt. Conf. Biomed. Eng. Syst. Technol.* **1,** 48–55 (2018). doi: 10.5220/0006558100480055

57. Cho, S. M., Kim, Y. J., Heo, G. S. & Shin, S. M. Two-step preconcentration for analysis of exhaled gas of human breath with electronic nose. *Sensors Actuators, B Chem.* **117,** 50–57 (2006). doi: 10.1093/jjco/hyi213

58. Branco, L. C. *et al.* Physico-Chemical Properties of Task-Specific Ionic Liquids. doi: 10.5772/15560

59. Mumyakmaz, B., Özmen, A., Ebeoğlu, M. A., Taşaltin, C. & Gürol, I. A study on the development of a compensation method for humidity effect in QCM sensor responses. *Sensors Actuators, B Chem.* **147,** 277–282 (2010). doi: 10.1016/j.snb.2010.03.019

60. Ippolito, S. J. *et al.* Layered WO3/ZnO/36° LiTaO3SAW gas sensor sensitive towards ethanol vapour and humidity. *Sensors Actuators, B Chem.* (2006). doi:10.1016/j.snb.2005.12.050

61. Xiao, X. *et al.* Polysquaraines: Novel humidity sensor materials with ultra-high sensitivity and good reversibility. *Sensors Actuators, B Chem.* **255,** 1147–1152 (2018). doi: 10.1016/j.snb.2017.04.069

62. Greenspan, L. Humidity fixed points of binary saturated aqueous solutions. *J. Res. Natl. Bur. Stand. Sect.*

A Phys. Chem. **81A,** 89 (1977). doi: 10.6028/jres.081A.011

63. Paknahad, M., Bachhal, J. S. & Hoorfar, M. Diffusion-based humidity control membrane for microfluidic-based gas detectors. *Anal. Chim. Acta* **1021,** 103–112 (2018). doi: 10.1016/j.aca.2018.03.021

64. Quincot, G., Azenha, M., Barros, J. & Faria, R. Use of salt solutions for assuring constant relative humidity conditions in contained environments. 33 (2011).

65. Young, J. F. Humidity control in the laboratory using salt solutions-a review. *J. Appl. Chem.* **17,** 241–245 (2007). doi: 10.1002/jctb.5010170901

66. De Wit, M., Vanneste, E., Geise, H. J. & Nagels, L. J. Chemiresistive sensors of electrically conducting poly(2,5-thienylene vinylene) and copolymers: Their responses to nine organic vapours. *Sensors Actuators, B Chem.* **50,** 164–172 (1998). doi: 10.1016/S0925-4005(98)00227-5

67. Ruminski, A. M., Moore, M. M. & Sailor, M. J. Humidity-compensating sensor for volatile organic compounds using stacked porous silicon photonic crystals. *Adv. Funct. Mater.* (2008). doi:10.1002/adfm.200701494

68. Nenova, Z. & Dimchev, G. Compensation of the impact of disturbing factors on gas sensor characteristics. *Acta Polytech. Hungarica* **10,** 97–111 (2013).

69. Wan, H., Yin, H., Lin, L., Zeng, X. & Mason, A. J. Miniaturized planar room temperature ionic liquid electrochemical gas sensor for rapid multiple gas pollutants monitoring. *Sensors Actuators, B Chem.* **255,** 638–646 (2018). doi: 10.1016/j.snb.2017.08.109

70. Blasioli, S. *et al.* Electronic nose as an innovative tool for the diagnosis of grapevine crown gall. *Anal. Chim. Acta* (2010). doi:10.1016/j.aca.2010.02.017

71. Chang, J. E. *et al.* Analysis of volatile organic compounds in exhaled breath for lung cancer diagnosis using a sensor system. *Sensors Actuators, B Chem.* **255,** 800–807 (2018). doi: 10.1016/j.snb.2017.08.057

72. Srinivasan, S., Gander, R. E., Member, S. & Wood, H. C. *Artificial Neural Networks.* **39,** (1992). doi: 10.1007/978-3-319-43162-8

73. Hersee, S. D. & Ballingall, J. M. The operation of metalorganic bubblers at reduced pressure. *J. Vac. Sci. Technol. A Vacuum, Surfaces, Film.* **8,** 800–804 (1990). doi: 10.1116/1.576921

74. Morgan, D., Ferguson, L. & Scovazzo, P. Diffusivities of gases in room-temperature ionic Liquids: Data and correlations obtained using a lag-time technique. *Ind. Eng. Chem. Res.* **44,** 4815–4823 (2005). doi: 10.1021/ie048825v

75. Huddleston, J. G. *et al.* Characterization and comparison of hydrophilic and hydrophobic room temperature ionic liquids incorporating the imidazolium cation. *Green Chem.* (2001). doi:10.1039/b103275p

76. Id, A. C. *et al.* Potential Applications and Limitations of Electronic Nose Devices for Plant Disease Diagnosis. *Sensors* **17,** 2596 (2017). doi: 10.3390/s17112596

77. Cao, Y., Chen, Y., Sun, X., Zhang, Z. & Mu, T. Water sorption in ionic liquids: Kinetics, mechanisms and hydrophilicity. *Phys. Chem. Chem. Phys.* **14,** 12252–12262 (2012). doi: 10.1039/c2cp41798g

78. Brandt, A. Ionic liquid pretreatment of lignocellulosic biomass. (2011).

79. Cao, Y., Chen, Y., Wang, X. & Mu, T. Predicting the hygroscopicity of imidazolium-based ILs varying in anion by hydrogen-bonding basicity and acidity. *RSC Adv.* **4,** 5169–5176 (2014). doi: 10.1039/c3ra44464c

80. Brandt, A. *et al.* Ionic liquid pretreatment of lignocellulosic biomass with ionic liquid-water mixtures. *Green Chem.* **13,** 2489–2499 (2011). doi: 10.1039/c1gc15374a

81. Anderson, J. L., Ding, J., Welton, T. & Armstrong, D. W. Characterizing ionic liquids on the basis of multiple solvation interactions. *J. Am. Chem. Soc.* (2002). doi:10.1021/ja028156h

82. Sánchez, L. G., Espel, J. R., Onink, F., Meindersma, G. W. & Haan, A. B. de. Density, Viscosity, and Surface Tension of Synthesis Grade Imidazolium, Pyridinium, and Pyrrolidinium Based Room Temperature Ionic Liquids. *J. Chem. Eng. Data* **54,** 2803–2812 (2009). doi: 10.1021/je800710p

83. Mchale, G. *et al.* Density - Viscosity Product of Small-Volume Ionic Liquid Samples Using Quartz Crystal Impedance Analysis. *Ann. Chem.* **80,** 5806–5811 (2008). doi: 10.1021/ac800490q

84. Seddon, K. R., Stark, A. & Torres, M.-J. Viscosity and Density of 1-Alkyl-3-methylimidazolium Ionic Liquids. 34–49 (2002). doi:10.1021/bk-2002-0819.ch004

85. Ghatee, M. H., Zare, M., Zolghadr, A. R. & Moosavi, F. Temperature dependence of viscosity and relation with the surface tension of ionic liquids. *Fluid Phase Equilib.* **291,** 188–194 (2010). doi: 10.1016/j.fluid.2010.01.010

86. Lourenço, N., Nunes, A., Duarte, C. & Vidinha, P. Ionic Liquids Gelation with Polymeric Materials: The Ion Jelly Approach. *Cdn.Intechopen.Com* (2010). doi:10.5772/24464

87. Rawat, K., Pathak, J. & Bohidar, H. B. Effect of solvent hydrophobicity on gelation kinetics and phase diagram of gelatin ionogels. *Soft Matter* **10,** 862–872 (2014). doi: 10.1039/c3sm52701h

88. Barratt, R. S. The preparation of standard gas mixtures. A review. *Analyst* **106,** 817 (1981). doi: 10.1039/an9810600817

89. Yun, S. & Kim, J. Multi-walled carbon nanotubes-cellulose paper for a chemical vapor sensor. *Sensors Actuators, B Chem.* **150,** 308–313 (2010). doi: 10.1016/j.snb.2010.06.068

90. Wang, L. C., Tang, K. T., Chiu, S. W., Yang, S. R. & Kuo, C. T. A bio-inspired two-layer multiple-walled carbon nanotube-polymer composite sensor array and a bio-inspired fast-adaptive readout circuit for a portable electronic nose. *Biosens. Bioelectron.* **26,** 4301–4307 (2011). doi: 10.1016/j.bios.2011.04.015

91. Khan, M. R. R. & Kang, S. W. A high sensitivity and wide dynamic range fiber-optic sensor for low-concentration VOC gas detection. *Sensors (Switzerland)* **14,** 23321–23336 (2014). doi: 10.3390/s141223321

92. Daneshkhah, A., Shrestha, S., Siegel, A., Varahramyan, K. & Agarwal, M. Cross-selectivity enhancement of poly(vinylidene fluoride-hexafluoropropylene)-based sensor arrays for detecting acetone and ethanol. *Sensors (Switzerland)* **17,** 1–16 (2017). doi: 10.3390/s17030595

93. Ciccioli, P. *et al.* Quantitative determination of volatile organic compounds (VOC) in milk by multiple dynamic headspace extraction and GC-MS. *Ann. Chim.* **94,** 669–678 (2004). doi: 10.1002/adic.200490084

94. Esteves, I. A. A. C. *et al.* A sensitive method approach for chromatographic analysis of gas streams in separation processes based on columns packed with an adsorbent material. *Adv. Mater. Sci. Eng.* **2016,** (2016). doi: 10.1155/2016/3216267

95. S, P., Perry, R. H., Green, D. W. & Maloney, J. O. *Chemical Engineers ' Handbook*. **27,** (McGraw-Hill Companies, 1997). doi: 10.1021/ed027p533.1

96. Dunn, W. C. *Fundamentals of Industrial Instrumentation and Process Control*. (McGraw-Hill Companies). doi:10.15713/ins.mmj.3

97. Scientific, A. Operating Manual - Precision Gas Mass Flow Controllers, MC-Series. 1–6 (2007).

Appendix

Appendix I – Relative humidity profiles during optical response assays
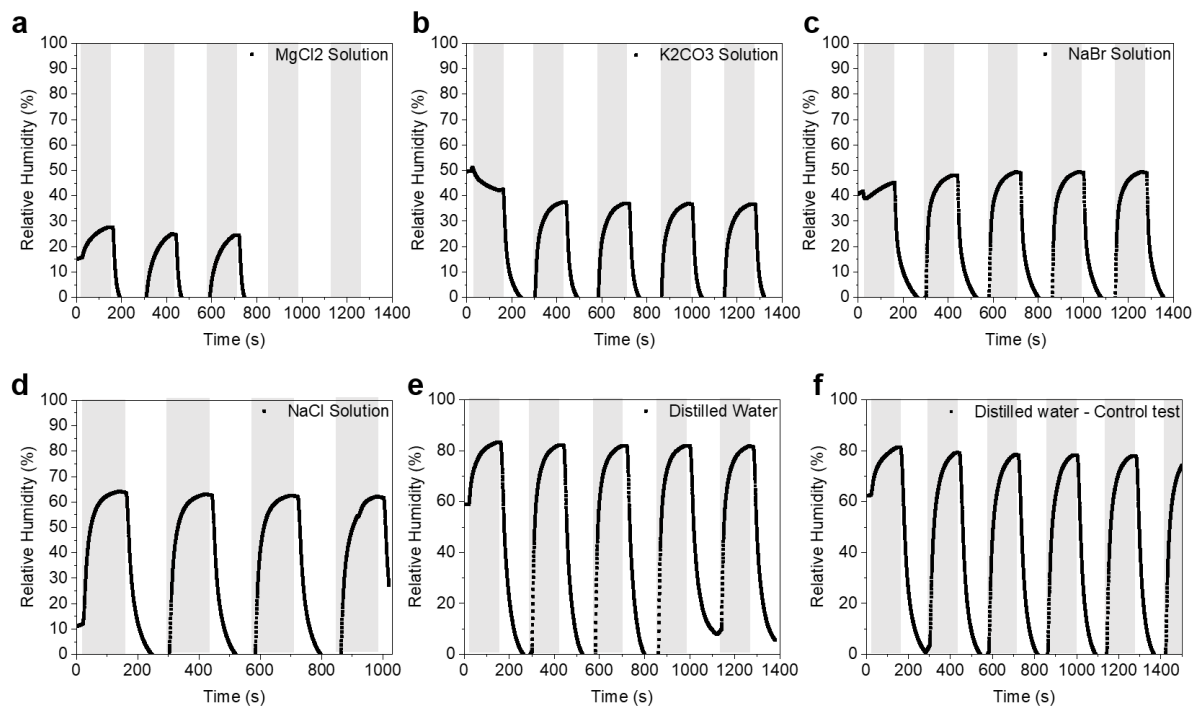

Figure A1- Relative humidity profiles during the assays for evaluating the optical signals of the hybrid gel films on the e-nose. Exposure period highlighted in grey. Correspondent generated relative humidity: (a) 25 %; (b) 36 %; (c) 50 %; (d) 65 %; (e-f) 80 %. An error in the relative humidity reading after the third exposure period occurred for the lowest generated relative humidity (a).

Appendix II – POM Images
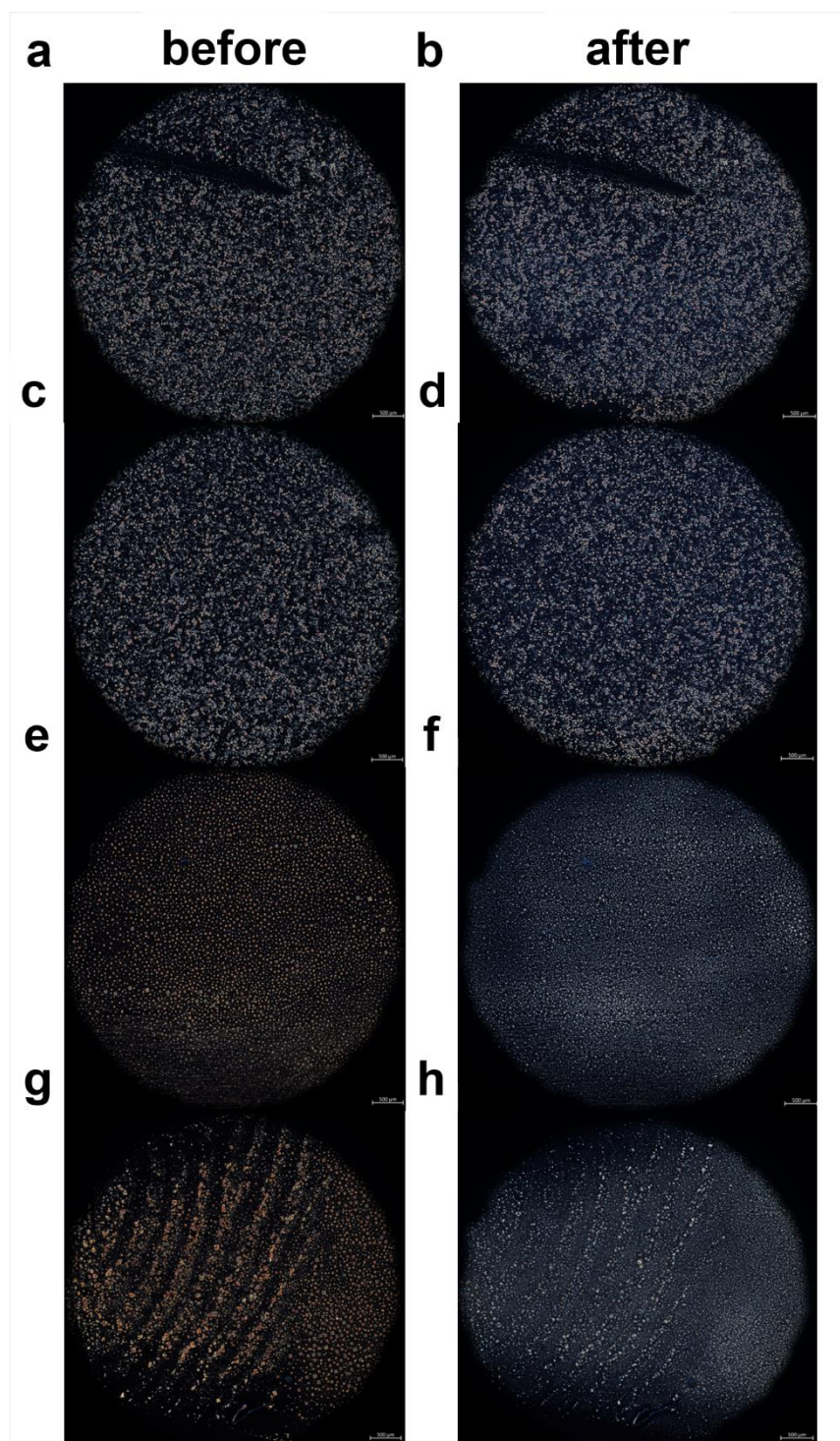
Figure A2- POM images of the hybrid gel films C28 (a-b), C29 (c-d), D47 (e-f), D48 (g-h) before (left panels) and after (right panels) exposure to ~25 % relative humidity. Experiment ended in recovery.
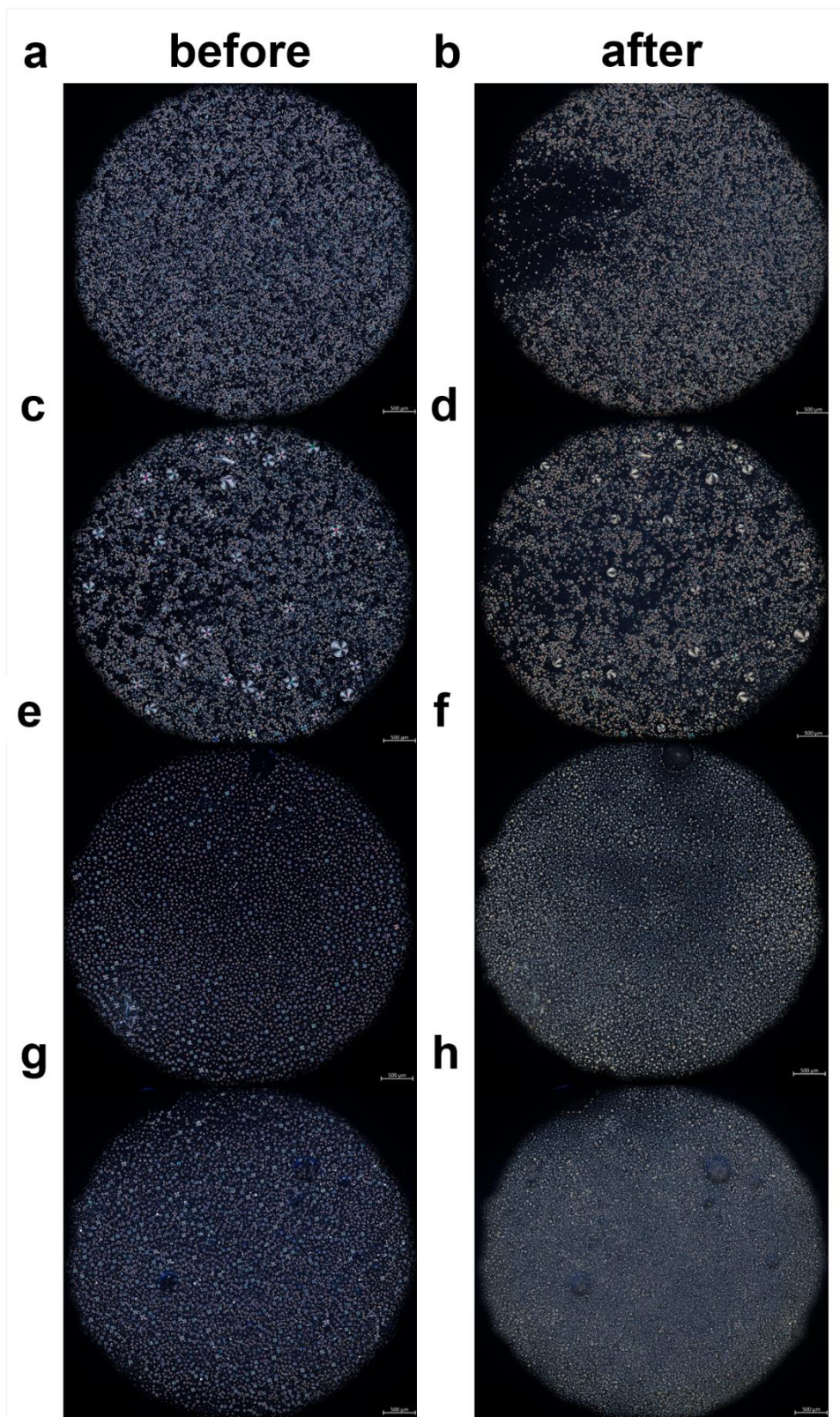
Figure A3- POM images of the hybrid gel films C31 (a-b), C32 (c-d), D44 (e-f), D50 (g-h) before (left panels) and after (right panels) exposure to ~36 % relative humidity. Experiment ended in recovery.
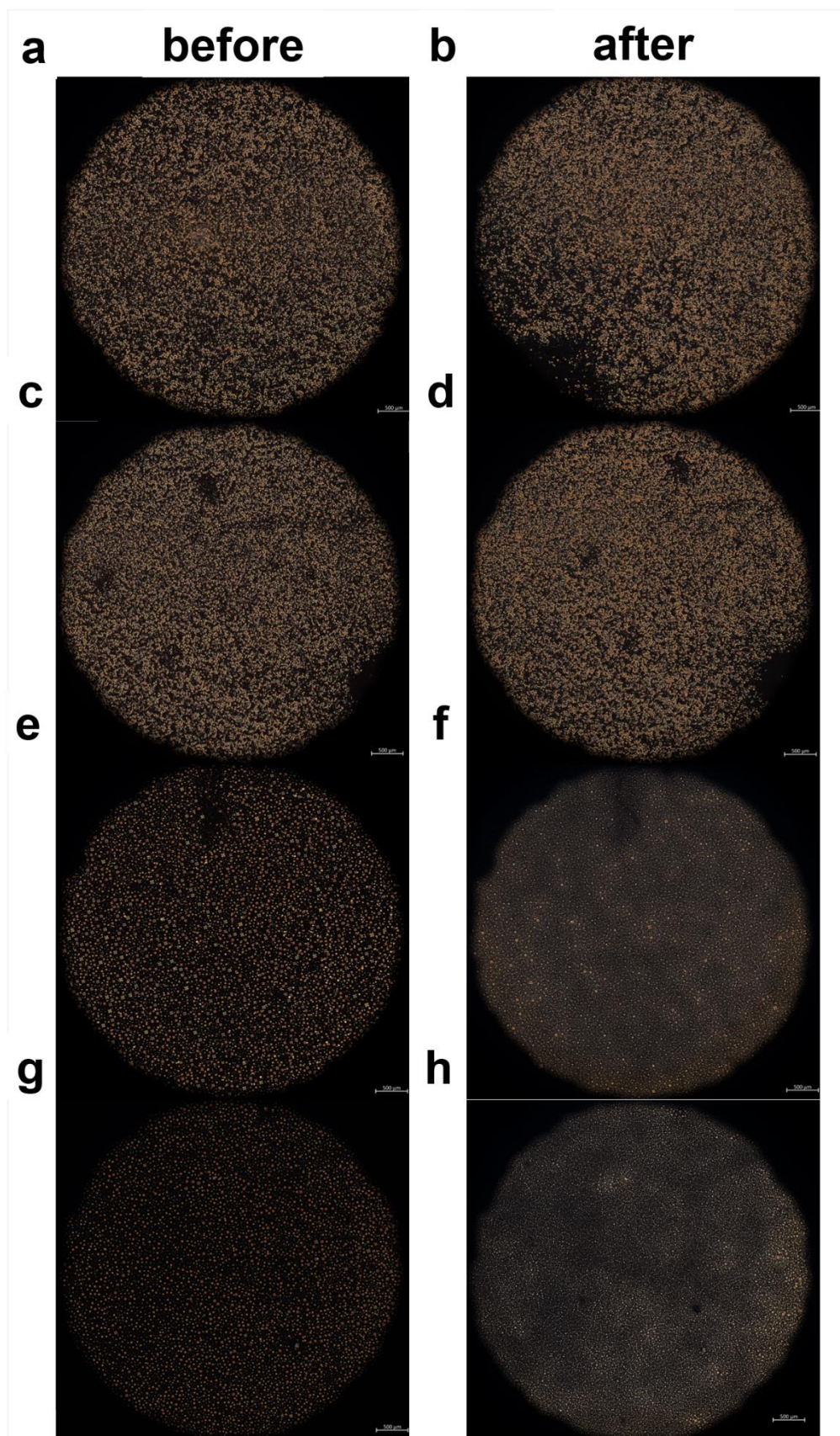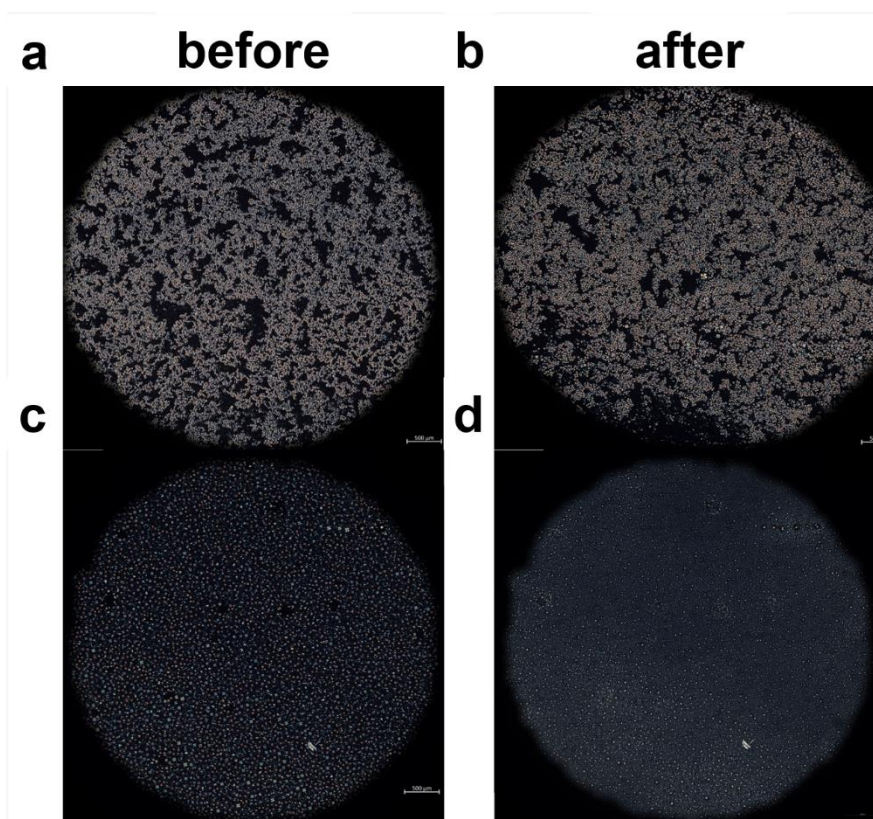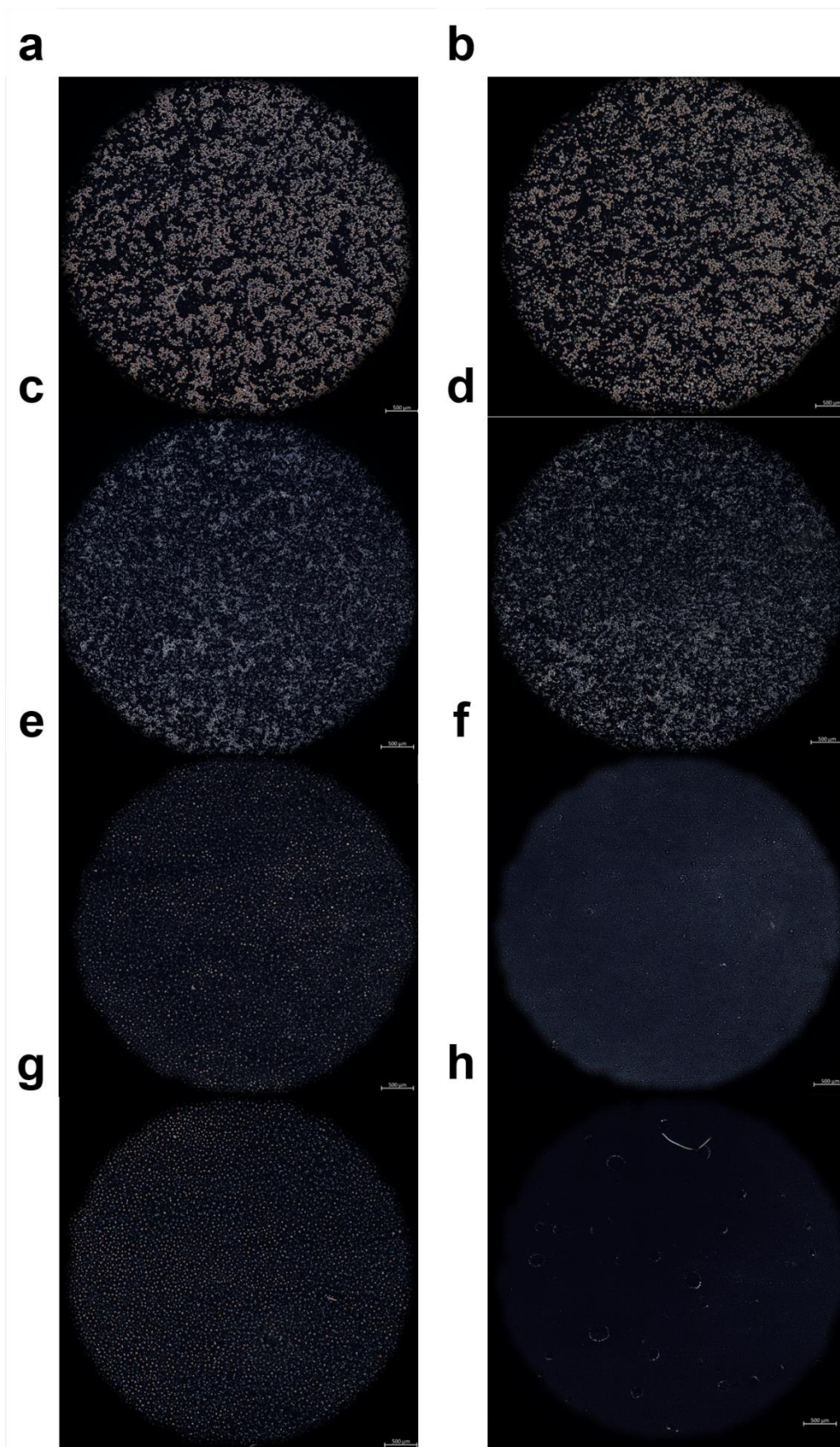
Figure A4- POM images of the hybrid gel films C36 (a-b), C37 (c-d), D52 (e-f), D53 (g-h) before (left panels) and after (right panels) exposure to ~50 % relative humidity. Experiment ended in recovery.
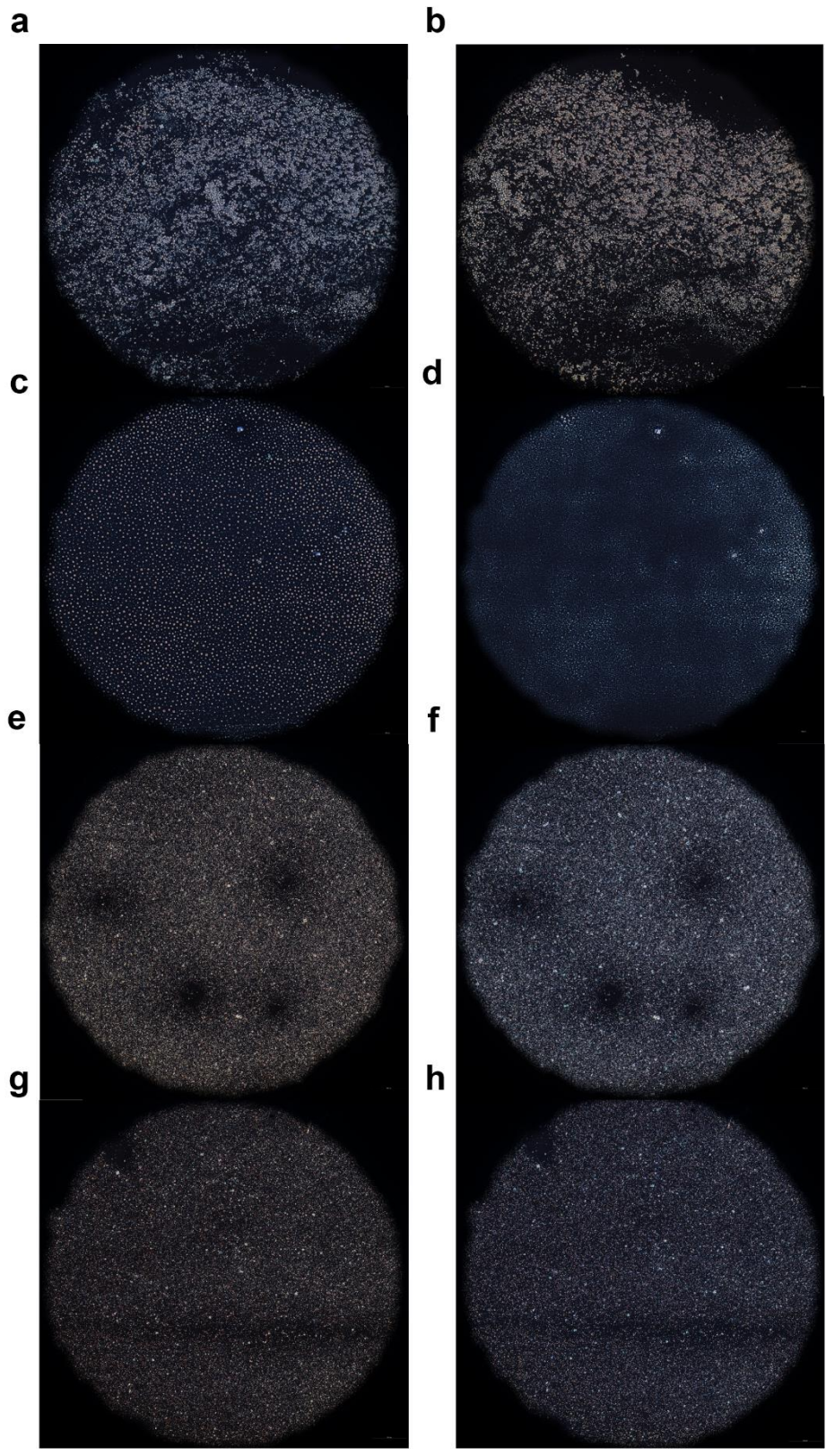
Figure A5- POM images of the hybrid gel films C15 (a-b) and D25 (c-d) before (left panels) and after (right panels) exposure to ~65 % relative humidity. Experiment ended in recovery.

Figure A6- POM images of the hybrid gel films C18 (a-b), C19 (c-d), D28 (e-f), D31 (g-h) before (left panels) and after (right panels) exposure to ~80 % relative humidity. Experiment ended in recovery.

Figure A7- POM images of the hybrid gel films C50 (a-b) D74 (c-d) CT5 (e-f) and CT6 (g-h) before (left panels) and after (right panels) exposure to ~80 % relative humidity. Experiment ended in exposure.

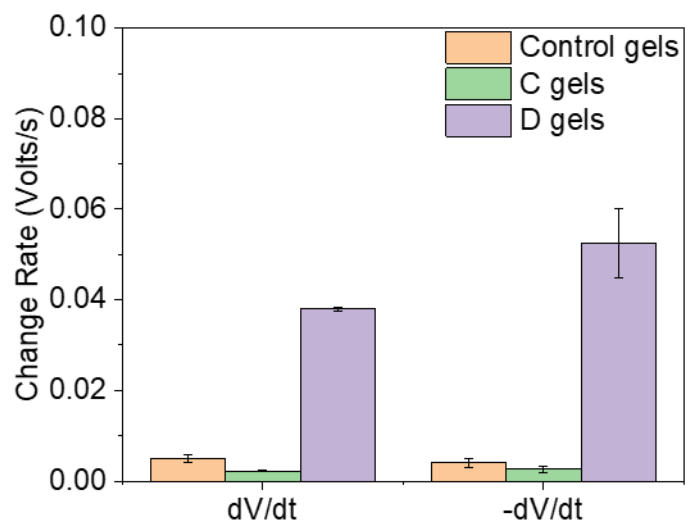# Appendix III – Negative control test hybrid gel's optical signal change rate

Figure A8- Comparison of the maximum slopes – positive (dV/dt) and negative (-dV/dt) – at the start of each period, between the negative control hybrid gel films (orange), films with [BMIM][Cl] (green) and films with [BMIM][DCA] (purple).

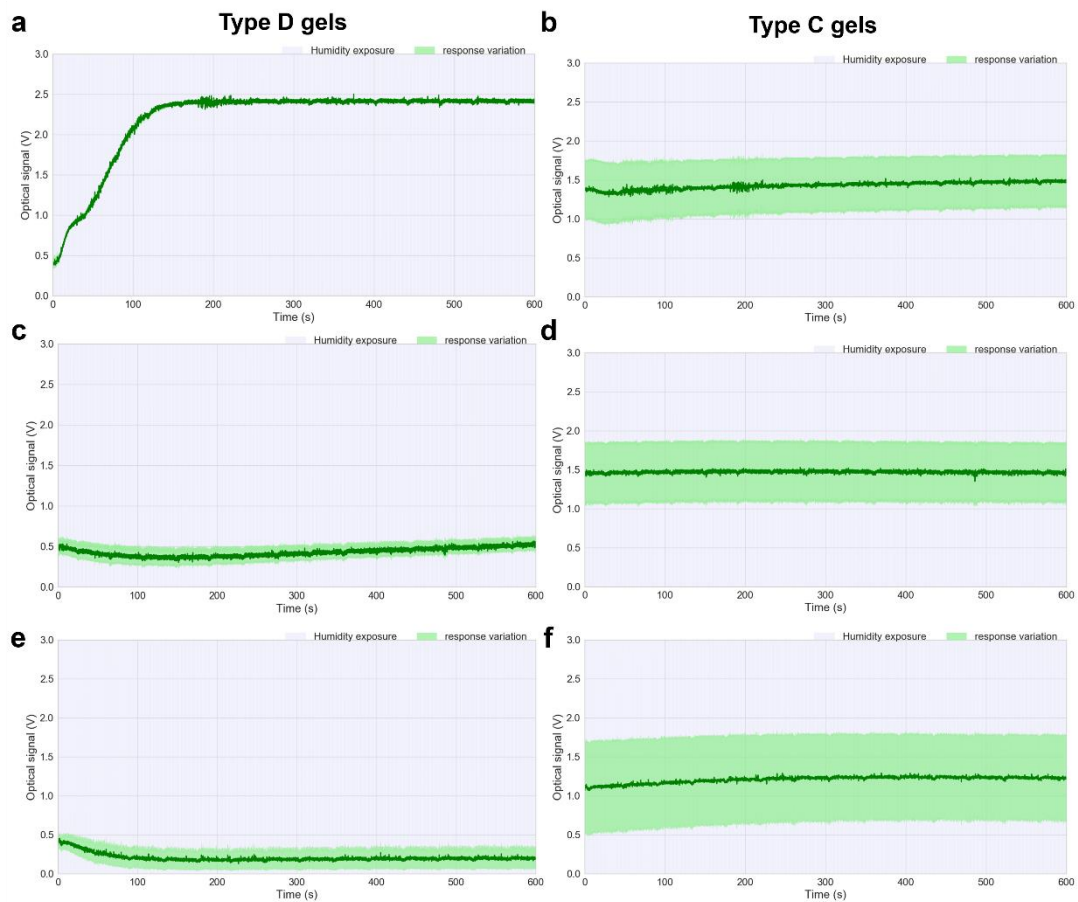# Appendix IV – Optical signal stabilization to generated relative humidity

Figure A9- Calibration of the hybrid gel films', containing [BMIM][DCA] (left panels) and [BMIM][Cl] (right panels), optical signal to the generated relative humidity – (a-b) 0%; (c-d) 65 %; (e-f) 80 % - prior to exposure to VOCs. Ambient relative humidity at the days of experiment was ~65 %.

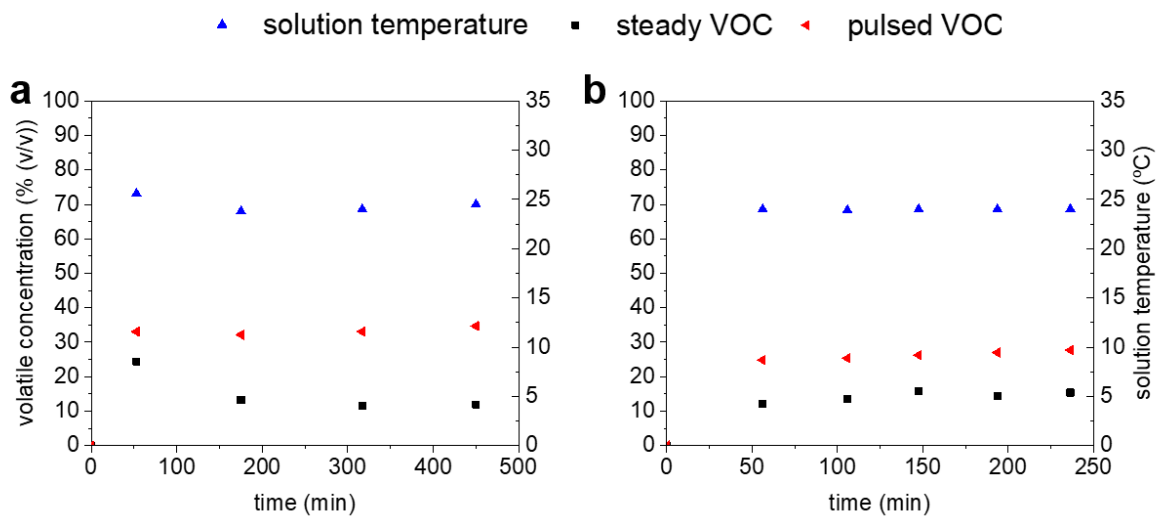# Appendix V – VOCs concentrations

Figure A10- Profiles of VOC concentration sampled to the e-nose throughout time, split between steady VOC concentration (black) and pulsed VOC concentration (red). Solvent temperature (blue) is also shown. (a) toluene; (b) isopropanol.